Department of Geological Sciences
Department of Physics and Astronomy

UNIVERSITY OF CANTERBURY
CHRISTCHURCH NEW ZEALAND

Polygonal patterned ground and ancient buried ice on Mars and in Antarctica

Michele T. Bannister

GEOL 490 Project
submitted in partial fulfilment of the requirements
for the degree of
Bachelor of Science with Combined Honours in Astronomy and Geology

2007

Frontispiece

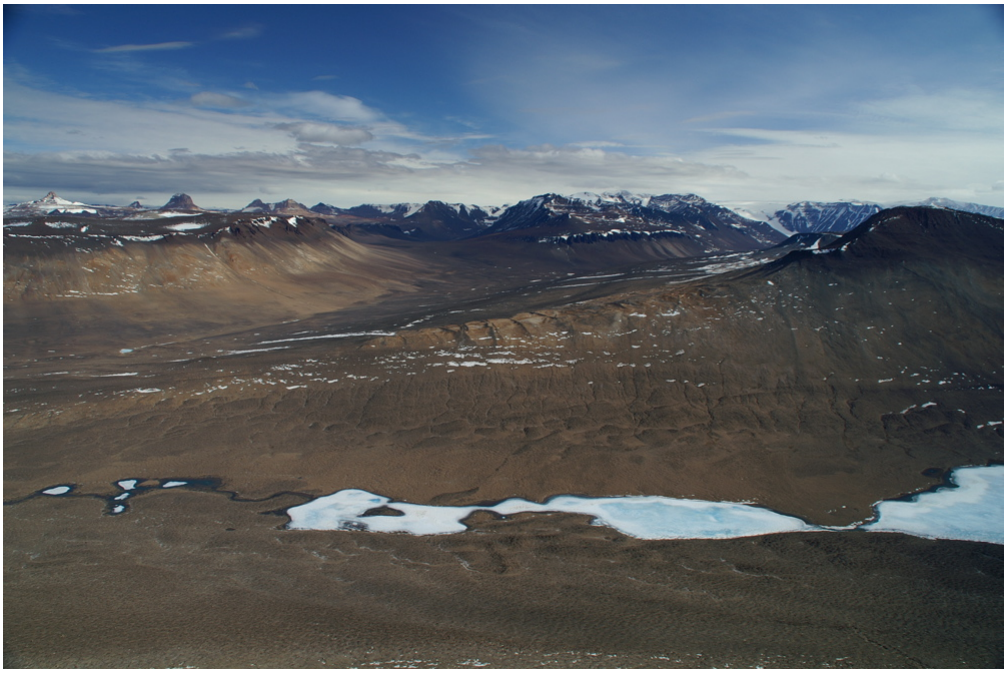

Victoria Valley, McMurdo Dry Valleys, Southern Victoria Land, Antarctica.

Beacon Valley, McMurdo Dry Valleys, Southern Victoria Land, Antarctica.

Abstract

Polygonal patterned ground and buried ice are features of the permafrost environments of Earth and Mars. A detailed understanding of these periglacial features in a terrestrial environment is necessary, as it will aid future interpretation of data provided by remote study of the features on Mars. It will also provide a reference for monitoring the effects of climate change on Earth.

In this study, the terrestrial context is provided by the examination of the subsurface physical properties of patterned ground and buried ice. The research is undertaken through ground-based geophysical methods in the Dry Valleys (Victoria Valley and Beacon Valley) of Antarctica. These are the most similar terrestrial sites to Mars. A 1.3 km transect profile across each valley was created using the methods of resistivity tomography, ground-penetrating radar, time-domain (transient) electromagnetism and a magnetic survey.

Analysis of the data found the depth of the buried massive ice in Beacon Valley to be far greater than previously thought: over a hundred metres and across a large spatial extent. Regularly spaced, vertical features of high resistivity were interpreted as connections between the ice-cemented polygon centres and the massive ice body of Beacon Valley.

Several lenses of massive ice were found in the layered permafrost sediments of Victoria Valley. The depth to the basement bedrock, inferred from the time-domain electromagnetism measurements, was over a hundred metres. This bedrock appeared to be overlain by a layer of brackish water. Regularly spaced, resistive vertical features in the near surface were interpreted as the sand wedges or cracks of the polygonal patterned ground.

Due to its successful application in Victoria Valley, it is proposed that time-domain electromagnetism would be a useful geophysical method for inclusion on a future Mars mission.

Contents

Glossary

A

active layer The top part of the ground that undergoes an annual freeze and thaw.

aggradational ice New ice layers or ice that enlarges older layers within previously frozen ground. The new ice is derived from water pulled by cryogenic suction into the thickening permafrost from above, below or the sides. Permafrost aggradation is the growth of permafrost by increase in its thickness or in extent in area.

astronomical unit The unit of distance most commonly used on a scale of stellar systems, 1.496×10^{11} m, approximately equal to the length of the semi-major axis of the orbit of Earth.

B

basal regelation Regelation at the base of a warm-based glacier or ice-rich body that had formed a film of liquid at its base to the underlying sediment or bedrock. Regelation is the refreezing of water that has been pressure-melted from ice, after the release of the pressure. Regelation also includes ice melting at a high-temperature location that refreezes at another, lower temperature, location.

C

clast lithic fragment, broken from a larger rock.

creep Slow downslope deformation of perennially frozen soil due to gravity acting on the plastic soil and ice mixture.

D

deflation Removal, typically by wind erosion, of silt and sand particles: in barren areas deflation can create stone pavements.

F

freeze-thaw weathering Water seeps into rock pores and expands on freezing into crystals, exerting a force on the structure of the rock. Repeated freeze-thaw cycles cause the rock to weaken and eventually break. Fracture is most likely along surfaces of pre-existing weakness such as foliation planes or grain boundaries in coarse-grained rocks.

G

gelifluction Cryogenic solifluction creating a slow downslope flow of soil weakened by freeze and thaw processes, caused by the development of excess pore-water pressure in the active layer, which allows slow slippage along melting layers of segregation ice. It results from shearing within the active layer. Gelifluction implies the presence of permafrost.

H

high-centred polygon Large unsorted polygons with centres elevated above the boundaries. At the boundaries ice wedges occur, which are often inactive or decaying.

I

ice wedge A wedge-shaped deposit of foliated ice. It is formed from the repeated freezing of ground water, gravitationally drawn into a fissure opened by contraction of the ground in response to intense lowering of the soil temperature. They typically form in polygonal arrays. Ice wedges can express themselves on the surface, as a network of cracks, or lie concealed beneath a top layer of soil.

K

K-index A quantifiable measure of the amount of disturbance in the Earth's magnetic field, as measured by the maximum variation in the horizontal component of the local magnetic field over a three-hour interval. It is given as an integer from 0 to 9, with calm geomagnetic weather at 1 and geomagnetic storms ≥ 5.

kettle holes The sinkholes formed by meltout of ice blocks left behind in sediment by a glacier. May also form in the top surface of a glacier with a heavy sediment load. Often seen in moraines adjacent to a glacier.

L

laccolith A mushroom-shaped intrusion of material.

low-centred polygon Large unsorted polygons with centres below the bounding ridges formed by soil warped upwards by active ice wedges.

M

moraine An accumulation of unconsolidated, angular debris material left by a glacier. Lateral moraines lie alongside the glacier, terminal moraines at its snout. Hummocky moraine is an area of moraine material forming small irregular mounds and depressions.

P

patterned ground Microtopography creating regular patterns, ranging in size from a few centimetres to several metres. May involve sorting of clasts, changes in elevation, soil composition, and vegetation.

pedogenesis The process of soil formation.

periglacial Conditions, processes and landforms associated with cold, non-glacial environments. This area of study is also termed geocryology.

permafrost The thermal condition existing in a material when its temperature is below the freezing point of water (Hughes, 1973). An operational definition for permafrost ground is that it remains at or below 0°C for at least two consecutive years, so that the depth of freezing in winter exceeds the depth of thawing in summer. Permafrost does not include seasonal frost that occasionally survives over a summer. The term was first coined by Simeon W. Muller (1945). Alpine permafrost is found at high altitudes in middle to low-latitude regions.

permafrost table The top of the permafrost layer.

polygonal patterned ground Closed, multi-sided, roughly equidimensional features, bounded by curvilinear sides. Some sides may be irregular.

pore ice Ice formed from water present in soil pores.

R

rock glacier A lobate or tongue-shaped body of debris that moves downslope by deformation of contained interstitial ice and ice lenses. The slope of the toe of an active rock glacier is near the angle of repose of the unfrozen material forming the rock glacier.

S

sand wedge Wedge-shaped sand deposits with a vertical fabric that results from sand entering the voids formed by polygonal contraction cracks.

segregation ice Ice formed from water drawn into position by cryogenic suction.

solifluction Slow downslope movement of the top layer of wet, unfrozen soil.

sorted circles A patterned ground form that is equidimensional in several directions, with a dominantly circular outline. Sorted circles have a border of stones, while nonsorted circles lack the border.

sorted step Step-like form of patterned ground, with a fine-grained area of bare ground bordered downslope by stones. Found only on shallow, 5-15° slopes.

sorted stripes Patterned ground with a striped appearance. Sorted stripes alternate strips of stones and finer material. Nonsorted stripes are due to parallel strips of vegetation-covered ground and intervening strips of relatively bare ground. Both are oriented down the steepest slope available.

stress The external force per unit area on a material that is resisted by the strength of the material, if the material is in equilibrium with the force. Stress in the plane of a cross-section is shear stress, while that perpendicular to a cross-section is normal stress, either compressive or tensile.

T

thermokarst Topographic depressions resulting from the thawing of ground ice.

V

ventifact A rock that has been shaped by the abrasive action of fine wind-borne grit. Ventifacts may have striations, grooves, facets, or polishing. Undisturbed ancient ventifacts can provide information about the prevailing wind direction in an area.

Chapter 1

Introduction

This study makes a comparison between the polygonal patterned ground and buried ice of the Dry Valleys of Antarctica and that of Mars.

In perennially frozen ground, vertical ice or sand wedge wedges often form in cracks in the subsurface. These cracks are generated by thermoelastic stresses from rapid cooling. The networks of cracks form a variety of patterns, including sorted circles, polygons, sorted stepped terraces of discrete shapes and parallel sorted stripes down slopes (Washburn, 1956). In the cold and arid glacial Dry Valleys of Antarctica, these polygons occur on many valley floors (Berg and Black, 1966).

Patterned ground occurs in areas of permafrost, such as in Antarctica, the Arctic and Scandinavia (Svensson et al., 1967). A fragile signature of the present climate and the palæoclimate, it is a common feature of the polar regions on both Earth and Mars.

Ice remnants, buried within the subsurface, are a feature of some areas of terrestrial permafrost, including those with patterned ground. Such permafrost and massive ground ice have been found to be patchy but widespread on Mars (Bandfield, 2007).

Geophysical methods can be used to obtain detailed information about the physical properties of the ground. The data can then be interpreted to determine the underlying geological structures, possibly allowing interpretation of their history. The underlying structure of polygonal patterned ground has had minimal examination with geophysical methods. The spatial extent and depth of subsurface massive ice bodies in the Dry Valleys of Antarctica has also received little study. Such data may provide insights into polygon structure and formation processes, and the influence of buried ice. This information can then be extended to the polygons of Mars.

This chapter begins with the rationale for a comparison between the patterned ground and buried ice of the Dry Valleys of Antarctica and that of Mars (§ 1.1). The current understanding of polygonal patterned ground, particularly that in the Dry Valleys, is discussed with reference to its morphology, evolution and the theoretical understanding of its formation (§ 1.2). Buried massive ice is considered in § 1.3. Finally, the objectives for this research (§ 1.4) and the outline of the study (§ 1.5) are presented.

1.1 Relevance for analysis with planetary science

"Deciphering the geologic history of Mars is today one of the most important problems in space science" according to Malin and Edgett (2000b). The ice-free regions of Antarctica have been identified for more than three decades as the best terrestrial analogue for the geological features of Mars related to permafrost, including patterned ground (Morris et al., 1972). Analogue studies have a well-developed history in planetary science, as prior to landers such as Viking they were the only possible method of investigation. Antarctica-Mars analogue studies are well established in the literature, for example Morris et al. (1972); Berkley and Drake (1981); Gibson et al. (1983); Dickinson and Rosen (2003).

There were early suggestions that permafrost and associated microtopographic features such as polygons were present on Mars (Wade and de Wys, 1968). Tentative identifications were made of periglacial features, based on morphologic comparisons with terrestrial analogs, from Viking and to a lesser extent Mariner imagery (Belcher et al., 1971; Carr and Schaber, 1977; Lucchitta, 1981; Rossbacher and Judson, 1981).

Fine scale features in the size range of terrestrial polygons were not detectable until high-resolution images were made of the planet's surface in the 1990s. These were primarily taken by the Mars Orbital Camera (MOC) of the Mars Global Surveyor (MGS) orbiter, which mapped Mars for seven years to a resolution of $4-5$ m. The Mars Orbital Laser Altimeter (MOLA) on MGS, the High Resolution Stereo Camera (HRSC) on the Mars Express orbiter and the Thermal Infrared Mapping Spectrometer (THEMIS) on the Mars Reconnaissance Orbiter have also been valuable in identifying and visualizing features. These data have allowed the informed speculation generated by Viking's imagery to move to a firmer base. The MOC imagery confirmed the presence of polygons on Mars similar in size to those seen on Earth (Mangold, 2005).

The polygons seen on Mars come in several size ranges. Massive polygons, 5–10 km and up to 20 km across, are seen in the mid-latitudes of the northern hemisphere, on Acidalia, Elysium and Utopia Planitia (Rossbacher and Judson, 1981). There is a distinct transition in scale to sub-kilometer-scale polygons, 50-300 metres in diameter. The final scale transition is to polygons in the same 15–30 m size range as the Antarctic Dry Valleys polygons. They display a range of microtopographic morphologies: depressed interiors and raised perimeters which may be with or without boulders, and raised, bouldery centres with depressed perimeters (Sletten et al., 2003). Several studies have mapped the latitude-dependent distribution of Martian patterned ground (Klima, 2003; Mangold, 2005), through examination of the 35,000+ MOC images.

The processes that form polygonal patterned ground on Earth do not require liquid water, particularly for sand wedge polygon formation, and could also be an active process on Mars. All that is required for contraction crack polygons is the presence of frozen ice-cemented ground. Buried ice on Mars could be distributed throughout the regolith as segregated ice or be in massive lenses, since both forms occur on Earth. Evidence for slope-related geological structures directly related to massive ice, such as glaciers and rock glacier glaciers, is well established (Head et al., 2003; Marchant et al., 2003;

Head et al., 2005; Parsons and Head, 2005; Head et al., 2006). Martian subsurface massive ice has not yet been well investigated.

Two geophysical instruments are currently studying the subsurface of Mars. The long wavelength MARSIS subsurface sounding radar/altimeter on the Mars Express spacecraft is mapping the distribution of water and ice and the subsurface structure in the upper 0.5–5 km of crust, using centre frequencies of 1.3–5.5 MHz (Picardi et al., 2004). Its results from 2005–06 are beginning to be published (Watters et al., 2006). The Mars Reconnaissance Orbiter's Shallow Radar (SHARAD) began operation in November 2006 and has similar targets at depths of 0.1 to 1 km, although as it has a centre frequency of 20 MHz with a 10 MHz bandwidth, it will map at higher horizontal and vertical resolution (Seu et al., 2007). The two are complementary.

However, the highest lateral resolution possible at present from orbit, using SHARAD, is only 300 m (Seu et al., 2007), so high-resolution subsurface information from a Martian analogue such as the Dry Valleys of Antarctica is vital. It provides information for design and targeting of future Mars missions, and allows evaluation of the suitability of various geophysical methods for the conditions. Methods that work well in the Dry Valleys could be practically applied to Mars. Data obtained in the Dry Valleys can be used comparatively to potentially understand Martian subsurface conditions and structure in detail.

1.2 Polygonal patterned ground

1.2.1 Morphology and formation processes

The current theory of the origin of patterned ground was first detailed by Leffingwell (1919), with subsequent mathematical modelling (Lachenbruch, 1962). Its acceptance is mainly due to fieldwork such as that by Berg and Black (1966). Permafrost underlies Antarctic soils, and the active layer in the top of the permafrost thaws annually in the summer. On cooling in winter, the soil of the active layer cracks from tensile stress created by thermal contraction (Lachenbruch, 1962; Berg and Black, 1966; Pewe, 1974). The crack is filled by infalling material from the unconsolidated layer above, forming a vertical wedge (Fig. 1.1). The most common wedge filling is a composite of ice, sand and rubble (Berg and Black, 1966). In the next thermal cycle, the wedge, which is weaker than the surrounding soil, breaks on contraction and develops a crack in its centre. This fills with material and enlarges the initial crack. Continued thermal cycling continues the growth of the vertical or near-vertical crack until it may be several metres deep. From then it increases only in width (§ 1.2.3). Progressive creation of cracks occurs across the landscape, and intersecting networks of cracks of polygonal form develop into polygons with diameters of ten to thirty metres (Fig. 1.2). In very dry areas with abundant free-running sand, sand wedges develop, while in areas with high moisture and where the active layer is cemented by ice, ice ice wedges form. The origin and development of the two is very similar (Black and Berg, 1963; Sletten et al., 2003). Sand wedges are either undersaturated sand or largely composed of rubble, and may undergo some sorting. Ice wedges are formed by filling of the crack

Figure 1.1: Three ice wedges along the coast of the Tuktoyaktuk Peninsula, Northwest Territories, Canada, in very close proximity to thermal contraction polygons. From Burr et al. (2005).

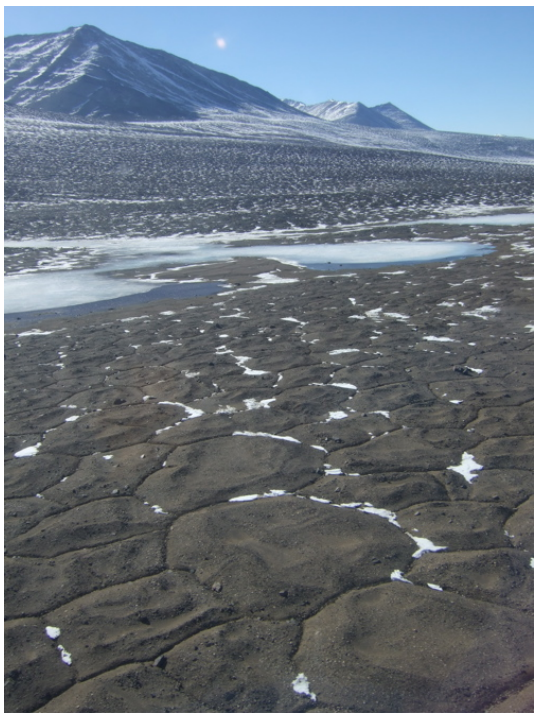

Figure 1.2: Polygonal patterned ground, Victoria Valley, from an altitude of about 120 m. The polygons are 20-30 m wide.

Figure 1.3: Triple-junction of cracks between polygons, ground level, Victoria Valley. The trough is 40 cm deep.

with hoarfrost or snowmelt water. Composite wedges with supersaturated sand or rubble, occasionally partially sorted, are also common. Since sand wedges are more typical in the cold, arid environment of Antarctica and therefore presumably also on Mars (Sletten et al., 2003), they are the main wedge type discussed in this study. However, ice wedges have received considerably more attention in the literature, probably since they are prominent in the less arid and more accessible Arctic.

The growth cycles of ice wedges are marked by their internal layering, a vertical foliation. The layers are distinguished by air bubbles or dirt. It is likely that most new water within the wedge runs down into the crack from the active layer. However, at temperatures fractionally below 0°C the thermal and hydraulic conductivities of ice exceed that of silty, frozen ground, and water can move through the ice wedge into its core (Davis, 2001). In contrast, sand wedges have horizontal foliation (Sletten et al., 2003). Five physical processes can account for most of the morphological characteristics of polygonally patterned ground (Levy et al., 2005): thermal contraction, material failure in response to structural non-thermally-induced stress, variable sublimation rates and marginal slumping. The fifth, marginal cryoturbation, produces raised rims alongside ice-wedge polygons (Berg and Black, 1966) but is minimal in the upland frozen zone of the Dry Valleys of Antarctica (Levy et al., 2005).

The surface morphology of the polygon evolves in parallel to its widening cracks. Initially, narrow cracks form in the surface, with slight slumping from the sides. As the wedge width increases, the bordering ground deforms plastically from horizontal stresses in compression perpendicular to the crack, due to the soil's expansion in summer, and is forced upwards to form a double-rimmed trough (Fig. 1.3). This trough is predominantly filled by sand, in a combination of trapped wind-blown sediments and material derived from adjoining polygons (Sletten et al., 2003), which may fill the trough entirely, in a $\sim$ 20cm layer of dry sand overlying the ice-cemented sand wedge. Sletten et al. (2003) considers that sand may be added to a depth of about 5 m, although the cemented wedge is 5–10% ice. Contraction of the permafrost layer in winter re-opens the cracks, allowing the sand to sift down into them, and may produce small collapse craters aligned along the cracks (Morris et al., 1972). As small quantities of fines easily fall deeper into the crack, rough sorting means that the trough may concentrate clasts in sizes up to cobbles and small boulders. However, increasing the insulation over wedges can cause them to become inactive (Davis, 2001).

The centres of the polygons generally concentrate fines and æolian sand. Typical Dry Valleys sand wedge polygons, such as those in Taylor, Wright and lower Beacon Valley, have an ice-cemented centre with $\sim$ 10% ice, overlain by 20-50 cm of dry soil sediments (Sletten et al., 2003). Field observations show the icy centres have stronger cementing than the wedges (Sletten et al., 2003).

Aggradation or net surface inflation must occur as mass is added to the polygon system through the cracks, if the ratio of recycling material to accumulation from æolian sources is small (Sletten et al., 2003).

The upthrust rims increase in height above the troughs and polygon centres with age (Morris et al., 1972). Convection models have been proposed (Sletten et al., 2003), in a complex form of cryoturbation. The rims are thought to eventually fold back over on themselves (Sletten et al., 2003),

inferred from excavations that show an upwards warp in frozen soil layers adjacent to the crack (Péwé, 1959), and the ramparts may coalesce. Similar warping may occur within the wedge if it deforms more easily than the frozen soil layers. Deformation of the permafrost that extends into the centre of the polygon has been observed in Arctic ice-wedge polygons (Mackay, 2000). This convection may lead to a transition from a bowl-shaped, high-sided and low-centred polygon to a high-centred polygon with increasing age.

In humid climates, high-centred polygons can form indirectly from degradation of low-centred polygons due to an increase in the seasonal thaw depth. This thaw settlement causes marginal slumping from melting in the top of the wedge, particularly in ice wedges, and preferential settlement at wedge edges (French, 1996). Inactivity can also lead to the production of a depression over the wedge and a high-centre polygon (Davis, 2001).

Alternatively, in cold dry climates, high-centred polygons may form directly as "sublimation" polygons (Marchant et al., 2002). In central Beacon Valley in the Dry Valleys of Antarctica, polygons with diameters of $9-35$ m, surrounded by troughs 1.2–3.0 m deep (Marchant et al., 2002) are present in massive ground ice that is overlain by a half-metre lag of boulders and sublimation till. The cracks are filled by coarse, porous gravel and cobbles sifted by passive sorting into the cracks. In the polygon centres, unsorted fine-grained sediment gathers, while the ice-cemented centre is $\sim 90\%$ ice (Sletten et al., 2003). It is postulated that the openwork structure in the cracks allows increased rates of sublimation from the ice, while the fine sediments in the polygon centres are much less permeable, leading to high-centred polygons (Marchant et al., 2002).

The Mullins rock glacier, several kilometres distant, at the southern end of Beacon Valley, also has "sublimation" polygons on its active lobes (Marchant et al., 2002). It is thought that radial fractures in the upper surface of the rock glacier due to structural stresses associated with its viscous flow are deepened by sublimation (Levy et al., 2005).

The formation of patterned ground is favoured by a water-rich active zone at least tens of centimetres and up to several metres thick. If the thickness of the active layer is in the expected range, the thermal conditions of permafrost are in approximate equilibrium with the present climatic conditions (Haeberli, 1985). This water-rich condition makes flood plains and ice-cored moraines particularly favourable environments. Patterned ground is also found on upland rock benches, sloping valley walls, and bedrock surfaces in the Dry Valleys (Morris et al., 1972). There do not seem to have been investigations of how the depth to bedrock influences the formation or surface expression of patterned ground. Morris et al. (1972) mentions that it occurred in places where there visually appeared to be very thin soil overlying bedrock. Additionally, patterned ground is not present where the soil has a dry upper part thicker than 1–2 m, due to the need for ice content to give the soil tensile strength. Morris et al. (1972) gives as an example the Insel Drift of the McKelvey Valley, Antarctica, with a surface of glacial sediments but no meltwater streams and all fallen snow removed by sublimation.

1.2.2 Rate of evolution and age

The size of wedges and the amount of adjacent ground deformation is a function of their age. The rate of evolution of patterned ground has been deduced by two methods: rate of crack growth, as measured through the separation of rods placed either side of numerous cracks as a function of time, and deformation of the ground surface by patterned ground on areas of known exposure.

Initial propagation of the cracks and interconnection to form a network can occur within decades or a century (Sletten et al., 2003). In a study of ice-wedge formation in an experimentally drained Canadian lake-bed, formation occurred within 12 years (Mackay and Burn, 2002). The relief of stress by fracturing within nearby wedges can assist the growth of others, or slow the network's growth (Davis, 2001). The rate of crack development is moderately well understood through some forty-five years of measurement of rod spacings (Berg and Black, 1966; Black, 1973, 1982; Malin and Rawine, 1995; Sletten et al., 2003). The rate of growth of the cracks is 0.1–1.8 mm yr^{-1}, inferred from wedge width measurements on surfaces of known age to be quite steady with time (Sletten et al., 2003). Reworking of the geomorphic surface by complex soil turbation in the convection model has a time scale given by the ratio of the size of the polygon to the wedge growth rate. This time scale, simplistically $\sim$ 10m/ $\sim$ 1mm $yr^{-1} = 10^4$ years (Sletten et al., 2003), is quite short. Notable evolutionary changes in the microtopography, mean polygon size and mean crack intersection angle are thought to be on time scales of 10^3 to 10^6 years (Sletten et al., 2003).

The measured and inferred ages of Antarctic patterned ground varies throughout the Dry Valleys. Sletten et al. (2003) suggest that different areas in the Dry Valleys show different stages of development of the patterned ground. The initial orthogonal network proposed by Lachenbruch (1962) can be seen on coastal surfaces in isostatic rebound of 1 to 2×10^3 years age (by GPS measurements) in New Harbour, Lower Taylor Valley, and on surfaces of similar age at the Hobbs Glacier delta (Sletten et al., 2003). These orthogonal polygons have little microtopography.

Whether the rate of pattern evolution on Mars is similar to that of Earth is not known. This evolution rate has implications for the interpretation of surface ages, such as the observation by Malin and Edgett (2000a) of an unpatterned debris fan surrounded by patterned ground, which they inferred to have a "recent" origin. However, patterned ground in the early orthogonal stage and without significant microrelief might not be visible in satellite images (Sletten et al., 2003).

1.2.3 Technical properties

Thermal contraction polygons are produced by repeated, rapid decreases in the subzero temperature of ice-rich ground, which cause differential shrinkage in the ground that produce internal tensile stresses. Cracks are produced, and stresses relieved, by the ground's tensile strength being exceeded. The scale of the cracking is dependent on the tensile strength, though ground that is ice-cemented and frozen has increased tensile strength. The model of Lachenbruch (1962) treats permafrost ground as a Maxwellian viscoelastic solid, responding to thermal contraction on short time scales by accumulation of elastic stress. This stress relaxes viscously over longer intervals.

The initial cracks open abruptly, to widths of 3–20 mm at the ground surface. They taper downwards, since the stress is reduced at depth, and propagate down into the active layer and permafrost below, until stopped by the gradually increasing compression force from the overburden in combination with the tensile strength of the substrate. They do not then subsequently increase in depth, but only in width. This cracking relieves stress normal to its plane.

The stress relief provided at increasing distance governs the diameter of the developing polygon (Lachenbruch, 1962). Typical terrestrial crack depths are 3 to 10 m, and the normal stress declines to a third at a distance of 3 m horizontally, and 5% at 10–20 m distant (Davis, 2001).

The calculations of Lachenbruch (1962) determined that a steady-state tensile stress maintained near 0°C could just exceed the tensile strength of frozen soil for reasonably high cooling rates. Cracking typically occurs when the near-surface ground temperature is ~ -15°C or below and rapidly falling air temperature cools the ground by another 10–15 degrees (Davis, 2001). More rapid cooling produces smaller polygons (Davis, 2001). A mean annual temperature of -7°C allows widespread wedge formation (Davis, 2001).

Intersection of the fractures forms the characteristic polygonal network, which can be categorized as orthogonal or non-orthogonal. These types are a result of formation in a material that is either non-homogenous or homogenous. In orthogonal cracking, the cracks tend to be perpendicular, producing four-sided orthogonal polygons. Non-orthogonal polygons have cracks that meet at 120°, have six sides, and form in homogenous materials. This form minimizes energy, as it releases the most strain energy per unit crack area (Lachenbruch, 1962). Formation of regular polygon patterns in two dimensions has been modelled as a consequence of crack propagation in a homogeneous material, although in spatially non-uniform material, cracking can be promoted by flaws (Hornig et al., 1996).

Most permafrost polygons are orthogonal, and secondary cracks are also typically orthogonal (Davis, 2001). If the initial cracks are curved, secondary orthogonal cracking is preferentially on the convex sides of bends (Davis, 2001). Morris et al. (1972) found that rectangular patterned ground in the Dry Valleys occurred on areas of alluvial plains associated with present drainage, while non-orthogonal patterned ground was widely developed on old moraine surfaces and alluvial-mantled hillsides.

Oriented polygonal terrain is also seen, generally in response to an oriented stress field acting on the frozen ground or to horizontal temperature gradients (Lachenbruch, 1962). For example, this occurs when the initial cracks are parallel to lake and stream shores (Davis, 2001).

Martian polygons of the largest scale are dominated by hexagonal crack networks. Small-scale polygons have both types of networks, though for example in Utopia Planitia, over 80% of the small-scale polygons display a regular random orthogonal pattern (Klima, 2003). There are also regions, commonly within large impact craters, that contain radially oriented networks of smaller-scale orthogonal-intersection polygons adjacent to, and mixed with, hexagonal polygon networks (Levy et al., 2005). Causes of the radial networks could include structural stress and thermal stress from uneven insolation created by the slope of the crater walls (Levy et al., 2005). Such an environment is

not seen on Earth, due to the lack of crater preservation that results from higher erosion rates, though the radial polygonal patterning on proximal lobes of the Mullins rock glacier, Beacon Valley has been suggested as useful for comparison (Levy et al., 2005). In this case the orientation may imply polygon development over time.

1.3 Buried massive ice

Ground ice is key to understanding important geological processes, as it is a marker for the present and palæoclimate on both Earth and Mars (Sugden et al., 1995; Head et al., 2003). Ground ice on Earth is used to reconstruct palæoclimate (French, 1996), which has also been done in the mid and polar latitudes of Mars (Seibert and Kargel, 2001; Mustard et al., 2001). The near-surface distribution of water on Mars is ice (Head et al., 2005), and ice-formed features then aid in defining the extent of the cryosphere. Ground ice is also important for determining the cycle of volatile movement and storage in the little-understood Martian hydrosphere.

The presence of water ice beneath the Martian surface is determined from the maps of the abundance of hydrogen in the regolith made by the Gamma Ray Spectrometer (GRS) on the Mars Odyssey orbiter. This water appears to be mixed into the top metre of the planet's surface. Its presence has also been used to explain observed landforms that appear very similar to periglacial/glacial formations on Earth (Lucchitta, 1981; Rossi et al., 2000), such as gelifluction of periglacial talus lobes and fretted terrain produced by the sublimation of subsurface ice. On Mars, the theoretical stability of shallow subsurface water ice is limited at the present day to latitudes above $\sim 60^{\circ}$, a prediction confirmed by the GRS observations (Head et al., 2005).

Ground ice on Mars may be derived from flooding, ground water or atmospheric water vapor. Precipitation promoted by volcanism or groundwater from subterranean aquifers could be a source of water for segregated ground ice (Burr et al., 2005). Floods could have emerged from deep aquifers via volcanotectonic fissures, as is postulated for ice-formed features in Athabasca Valles (Burr et al., 2005).

Debris aprons are one of the main ice-rich features of the Martian surface, and are seen in the mid-latitudes of Mars. They are widespread in the northern parts of Arabia Terra, and are found in the same latitude band at Acheron Fossae, north of Olympus Mons (Dickson et al., 2006). In the southern hemisphere there are great concentrations around the Hellas Basin (Pierce and Crown, 2003). Debris aprons are geomorphic features that slope gently away from scarps or highland massifs, with lobate margins and a thickness of hundreds of metres. With viscous flow features, convex profiles, and frequent areas of a fretted, honeycomb-like texture formed by pits and ridges, they are interpreted as containing an indeterminate amount of distorting ice. Since the amount of ice within the rock debris cannot be easily determined from orbital photography, their origins are debated, and models include ice-assisted rock creep, ice-rich landslides, rock glaciers and debris-covered glaciers (Head et al., 2005). Outstanding questions include the abundance of the ice during formation of the deposits and

the origin of the ice, from ground ice or groundwater, or from atmospheric frost or snow accumulation.

On Earth, buried ice masses can form in two ways. Aggradational ice lenses form by aggradation of pore water within the soil, which freezes onto a small body of ice and causes its gradual growth. Broad ground ice layers derive from atmospherically emplaced water, producing cavity or pore ice. Massive ice with a glacial origin is derived from fragments of a glacier or rock glacier left after its retreat or disintegration to become buried by sediment. Such blocks of ice can easily maintain stability in a permafrost climate, allowing insulating sediment to accumulate around them. Basal blocks in particular are likely to have surrounding sediment, though the load of rocky debris carried by the glacier on top of its main ice body provides immediate insulation to all underlying ice. The lifetime of massive ice, regardless of origin, is determined by the climate of its location. Lifetimes may be several thousand to tens of thousands of years. Ice masses in the arctic Russian permafrost have been dated to be over eighty thousand years old (Henriksen et al., 2003), and possibly as much as 250 thousand years (Ingólfsson and Lokrantz, 2003). The permafrost itself may be much older. For example, that in Siberia is at least 2 million years old, and that in the interior mountains of Antarctica may be as much as 20 million years old (Frolov, 2003).

Buried ice exists in several areas within the Dry Valleys of Antarctica. Its influence on the formation of polygonal patterned ground has had minimal discussion. Interpretation of the age and origin of buried ice can also provide constraints on the palæoenvironment (Zwartz, 2005). The thickness of permafrost in the sediments above bedrock can indicate if the permafrost is stable in the current climate (Frolov, 2003). Its subsurface topography is created by the frozen sediments, but can be locally altered by the formation of aggradational ice lenses within the permafrost. Any ice lenses underlying patterned ground may be very old — an age of 8×10^6 years was reported for buried ice remnants in Beacon Valley, Antarctica (Sugden et al., 1995), and corroborated by a minimum age of 2.3×10^6 years (Schäfer et al., 2000). Sugden et al. (1995) determined the deposition time of the ice by dating the development of the till layer at the surface through volcanic ash in polygon cracks, but the suitability of this ash as an age constraint has been subsequently debated (Ng et al., 2005). The age obtained by Schäfer et al. (2000) is from cosmogenic exposure dating of clasts embedded within the top of the till-covered ice. This age of several million years requires persistent stable polar climate conditions to avoid sublimation of the ice. It also requires a mechanism to be found that prevents sublimation.

Ng et al. (2005) note from cosmogenic ^{3}He depth profiles that the lower 80% of the till formed in the last $310 - 43 \times 10^3$ years, difficult to reconcile with the order-of-magnitude-greater ages. Sletten et al. (2003) mentions that indirect indices for surface age, including pedogenesis development and weathering of surface boulders, and also a cosmogenic isotope study (Stone et al., 2000), support a younger age. Age constraints have since centred around determination of the sublimation rate of the till-insulated ice (Schorghofer, 2005; Kowalewski et al., 2006).

Such ages still exceed the time scale of 10^4 years for convection polygon models, inferring that either polygons on buried ice behave differently from polygons on sediment bases, so that the application of the time scale is erroneous, or that the extreme surface stability of Beacon Valley postulated

has unsound assumptions.

The thickness and distribution of the ice in Beacon Valley is not known (Sugden et al., 1995; Zwartz, 2005). There is a need for profile surveys to constrain the shape of the buried bodies of ice (Zwartz, 2005). If this can be determined, it could indicate if the ice was deposited by part of the Taylor Glacier flowing southwards into the valley, or if instead it is related to the rock glaciers that flow into Beacon Valley. Aggradation has not been considered as a feasible origin for the ice at this location (Sugden et al., 1995; Schäfer et al., 2000; Ng et al., 2005). Internal topography of the ice could be influenced by its origin: formation as a single mass, or as several masses.

Aggradation of the valley surface by material accumulation may be balanced or exceeded by sublimation of the massive ice (Sletten et al., 2003). The Beacon valley floor is a surface of near-constant elevation cut by the networks of polygon troughs, with scattered large bowl-shaped depressions. Determination of the proximity of the massive ice to the surface, and whether the thickness of the lag varies across the valley floor, could help evaluate whether the sublimation is responsible for the sinkholes (R. Sletten, pers. comm., 2006).

It is interesting to consider that the 10–20 m polygons at the northern end of Beacon Valley, close to the margin of the Taylor Glacier, have the most developed sand wedges seen in the Dry Valleys. These wedges are greater than 5 m wide and old wedges extend entirely under the centres of the high-relief polygons that they delineate. The measurement sites there indicate they are active (Sletten et al., 2003). This rumpled and severely reworked surface is about five kilometres down the valley from the ancient and theoretically undisturbed Beacon Valley ice. While it is younger than the central Beacon polygons, it is still much older than the Victoria Valley polygons, from dating of analogous moraines in the adjacent Arena Valley (Brook et al., 1993). Sletten et al. (2003) infers a surface reworking time scale of 10^5 years.

1.4 Research objectives

Event K054 from the University of Canterbury was awarded eight weeks of field time in the 2006–07 austral summer to study the fragile and unique polygonal patterned ground of the Dry Valleys, McMurdo Sound, Antarctica. Two sites were visited: close to Lake Victoria in upper Victoria Valley, near the centre of the Dry Valleys, and central Beacon Valley, at higher elevation and closer to the East Antarctic Ice Sheet.

It was hypothesized that the size and shape of patterned ground on the surface would be particularly influenced by the presence of underlying permanent massive ice, and possibly also by the depth to bedrock. This was tested through creating a two-dimensional geophysical profile across each valley.

Four geophysical techniques were chosen, designed to produce complementary data relating to different physical properties of the valley floor sediments. Two-dimensional resistivity tomography and time-domain (transient) electromagnetism would determine the electrical properties of the ground. In particular, the resistivity tomography profile would show any bodies of buried massive ice, as

ice has very high resistivity and the method is most sensitive to strongly resistive zones. Ground-penetrating radar, combined with a magnetometer survey of the local magnetic field, would give a profile of the subsurface, including bedrock if that was sufficiently shallow. These methods were selected as they can reach to depths of tens to hundreds of metres, allowing detection of the base of any massive ice and possibly the top of the bedrock. Since the survey would cover a large range, the resolution would be low.

There are three primary aims for this project:

1. identify any relationship between the subsurface structure, including buried ice, and the surface expression of polygonal patterned ground at the two field sites;

2. review the current understanding of Martian polygonal patterned ground, buried ice on Mars and any relationships yet found;

3. extend relevant findings of the data analysis to Martian polygons and buried ice, and if possible provide predictions that can be tested by future Mars missions.

1.5 Study outline

The next chapter reviews the current knowledge of the geology and cryosphere of Mars. It also considers the geology of the Dry Valleys of Antarctica. The patterned ground and buried ice of Mars are considered in the context of the background information on patterned ground and buried ice of Earth reviewed in this chapter.

Chapter 3 provides the methodology for the Antarctic fieldwork that obtained the data for this comparative study. It details the use of the geophysical techniques selected, and the extent of the data collected.

Chapter 4 presents an analysis of the data collected in the Dry Valleys of Antarctica. Each geophysical data set is considered, and its results from the Victoria Valley and Beacon Valley field sites interpreted with respect to the subsurface structures and geology that could be determined. Since the suite of geophysical methods are complementary, the individual results of each method are synthesized to provide a picture of the subsurface environment of Victoria and Beacon Valleys.

Part of this study (Chapter 5) is a limited extension of the results to the patterned ground and buried ice of Mars. In conjunction with this, the applicability of the geophysical methods to Mars is extrapolated from the Antarctic fieldwork.

Finally, the results of this study and suggestions for future work are given in Chapter 6.

Chapter 2

Martian context

The formation and development of patterned ground on Mars, and the evolution and preservation of ice on Mars, can only be considered in the context of its physical and climatic environment. Patterned ground and buried ice are permafrost features, generated in the larger context of the planetary cryosphere. The cryosphere is intrinsically related to the distribution of water on the planet and to the temperature distribution across the planet. These factors are discussed in § 2.1.

Terrestrial patterned ground and buried ice were discussed in Chapter 1. Since the fieldwork of this project is terrestrial, in the Dry Valleys of Antarctica, the geology and climatic conditions of the Dry Valleys are discussed, together with the geology of the field sites (§ 2.2). This is useful for understanding of the fieldwork (Chapter 3) and important for discussion of the analysis of the data produced (Chapter 4).

The current knowledge of the patterned ground and buried ice on Mars are examined (§ 2.3) in contrast and comparison with terrestrial permafrost features. This relates to the implications of the fieldwork and the use of geophysical methods on Mars in relation to permafrost that are discussed in Chapter 5.

2.1 Geology and cryosphere of Mars

The global geology of Mars is sharply differentiated by a crustal dichotomy between the southern highlands at an elevation of ≥ 3 km and the depressed northern plains at an elevation of ≤ -2 km, a feature unique among the terrestrial planets. Martian geology has been mapped by stratigraphic relationships and by the standard dating method of crater counts on various formations (Hartmann and Neukum, 2001). Due to the absence of plate tectonics and the consequent lack of crustal recycling, the Martian geological record is up to four billion years old.

Martian geological time contains three eras, the Noachian (formation of planet–3.5×10^9 years ago), Hesperian (3.5–(3.3–2.9) $\times 10^9$ years ago, dates dependent on specific meteor fall rate model) and Amazonian (2.9×10^9 years ago until the present), which is further subdivided into the Early Amazonian and Late Amazonian. This last epoch began 300–600×10^6 years ago (Carr, 1996b;

Hartmann and Neukum, 2001). The timings of each era are based on episodes of bombardment, and on comparisons with dated Martian meteorites and to a lesser extent the lunar samples (Hartmann and Neukum, 2001). Since the early chronology of the Solar System is still under debate, the exact dates are currently poorly defined (Greeley, 1994).

Noachian surfaces, such as Noachis Terra in the southern hemisphere, are heavily cratered and severely eroded (Kieffer et al., 1992). The formation of such features as Hellas Basin and the hemispheric crustal dichotomy date to the Noachian. In the Hesperian, widespread fissure flood volcanism formed many plateau regions, including Hesperia Planum (Kieffer et al., 1992). The Tharsis volcanism began, generating associated crustal deformation that lead to the formation of Valles Marineris. Enormous fluvial outflow channels, comparable in appearance to the channelled scablands of Washington in the United States (Malin, 1976), were also created. Late-stage lava flows in the Elysium region and in the Tharsis region, including those forming Olympus Mons, continued into the Amazonian (Kieffer et al., 1992). During this time the Hellas, Argyre, and Isidis impact basins and parts of the northern plains experienced further erosional filling. In the present era, erosion from æolian processes, landslides and impacts appear to be the main geological influences (Carr, 1996b).

The current climate of Mars is arid and subzero, factors determined by its distance from the Sun (1.67 astronomical units) and the lack of a greenhouse effect due to its tenuous atmosphere. The atmosphere has a mean radius surface pressure that is ~ 6 hPa, 0.6% of terrestrial ASL pressure, but this value varies by 25% with the seasons as part of the atmosphere condenses out onto the respective polar ice cap (Tokano, 2005). It contains 10^4 times less water than the terrestrial atmosphere (Tokano, 2005), only ~ 10 μm precipitable water vapor (Carr, 1996b). The atmosphere is mostly carbon dioxide, with 0.03% in water vapor (Carr, 1996b).

Despite the thin atmosphere, the 1/3 Earth gravity of the small planet allows wind-borne particles to be up to 210 μm (Greeley and Iversen, 1985). The grain size observed in the soils by the Mars Exploration Rovers (MER), on opposite sides of the planet, is no greater than 100 μm in diameter. Active and impact-cemented dunes are observed in large dune fields, particularly in depressions formed by craters, valleys and chiasma. Sand of a medium to coarse grain size cannot be easily moved by the typical wind speeds of 2–10 ms^{-1} (7–36 km hr^{-1}) measured by the Viking landers (Carr, 1996b). Dust storms, which have winds of 17–30 ms^{-1} (61–108 km hr^{-1}) as measured by the Viking landers, may suspend particles of 0.1–0.25 μm, as well as fine to very fine sand (Greeley et al., 1992). The abundance and distribution of fine suspended dust influences atmospheric structure (Tokano, 2005).

The temperature distribution across the Martian surface varies considerably. The mean annual equatorial temperature is -60°C (Lucchitta, 1981). At the Viking I lander site in Chryse Planitia, 22.5° N, diurnal temperatures varied strongly, -89°C to -31°C, reaching as high as $+30$°C during dust storms. The Spirit and Opportunity MER rovers have also experienced temperatures between -90 and $+35$°C. The temperature variations are partly due to the planet's current comparatively large orbital eccentricity of 0.09, which causes the summer temperatures to vary by 30°C between hemispheres. The thin atmosphere means that there is a rapid response to the effects of diurnal and seasonal

variations due to solar heating (Read and Lewis, 2004). The low thermal inertia of the Martian soil also contributes to a fast temperature change.

The cryosphere extends from the upper atmosphere at 130–140 km altitude to the planet's surface and into the subsurface layers (Kuzmin, 2005), where the long-term global subzero climate has left the upper crust of the planet permanently frozen in a cryolithosphere. The thickness of the Martian permafrost shell may approach 1-2 km near the equator and up to 5 km at the poles (Kuzmin, 2005), unlike Earth where permafrost is confined to zones near the poles. On Earth the permafrost underlies just over a quarter of the land area, and penetrates up to 1.5 km into the ground (Washburn, 1973). In contrast, the massive cryolithosphere of Mars may hold most of the remaining planetary water.

Freeze-thaw cycles of freshwater are possible between 70° S and 30° N, where the temperature exceeds 0°C during the summer (Lucchitta, 1981). Groundwater on Mars is likely to be briny due to dissolved salts (Burt and Knauth, 2003), depressing its freezing point. This could modify thermal cycling so that it takes place at subzero temperatures. Such a depression of the thermal cycle matches the Martian thermal regime.

It is generally accepted that the present Martian climate does not reflect that in its past (Kieffer et al., 1992; Carr, 1996a,b). An early warm, wet period when the atmosphere was thicker is postulated by some models, based on such evidence as dendritic valley drainage systems in the southern highlands (Craddock and Howard, 2002) and neon isotope concentrations in Martian meteorites (Lal, 1993). This model suggests a progressively cooling and water-driven Mars. During the climate evolution and loss of volatiles, the mean temperature of the Martian surface must have at all times been some distance below the freezing point of water (Kuzmin, 2005). However, in early Martian history the cryosphere would have been only several hundred metres thick, as the interior heat flow was 4-5 times greater for the same climatic conditions (Carr, 1996a).

Modelling of heavy bombardment in the Noachian indicates 50–90% of the atmosphere could have been driven off (Jakosky and Phillips, 2001), although the enrichment of heavy isotopes in the Martian atmosphere (lighter isotopes are preferentially lost to the solar wind) suggests a loss of 25–90%. The layered polar ice caps contain both frozen CO_2 and H_2O (Head, 2001). Since the small reservoir of atmospheric water together with that of the polar caps cannot account for the observed fluvial and glacial surface features, and isotope ratios of $^2H/^1H$ and $^{18}O/^{16}O$ indicate some 25–50% of the original hydrosphere has been lost to space (Jakosky and Phillips, 2001), the remaining water should be below the planet's surface in the form of ice (Malin and Edgett, 2000a). The bombardment would have created a kilometres-thick impact-brecciated megaregolith, and water is probably distributed throughout this porous structure (Carr, 1996a). Though it varies locally in chemical and physical properties, the complex Martian regolith has been demonstrated to be homogenous in elemental composition on a planetary scale (Hudson et al., 2007). It is often modelled as a generic material by the JSC Mars-1 weathered submillimetre palagonite cinder-cone tephra from Mauna Kea, Hawai'i, composed of feldspar and Ti-magnetite with minor amounts of olivine, pyroxene and glass (Allen et al., 1997).

The Martian climate has also been modelled as carbon dioxide-driven and warming under the increasing solar flux with time. Carbonate rocks are absent from Martian geology, so unlike Earth, there is no sink for its carbon dioxide atmosphere. The absence of plate tectonics also prevents recycling of carbonates to release CO_2 back to the atmosphere. The lack of carbonates is a major difficulty for warm climate models that invoke a thick CO_2 atmosphere (Carr, 1996a).

The spin-axis obliquity of Mars is thought to be among the major features in its climate change. Currently it is $\sim 25^\circ$, but modelling shows that the obliquity has averaged 35° in the last tens of millions of years. The long-term, high-amplitude obliquity variation periodically increases insolation at the poles, causing sublimation of near-surface water ice deposits and their redistribution by condensation towards the tropics (Kuzmin, 2005; Head et al., 2006). When the Martian obliquity is at, or lower than, its present value, ground ice is stable in the surface regolith of both hemispheres at latitudes poleward of 45° (Kuzmin, 2005). Ice is entirely unstable in the equatorial zone, where sublimation has removed it from the regolith to depths of hundreds of metres (Kuzmin, 2005). However, ice becomes stable within the surface regolith at the equator down to depths of several tens of metres, if the obliquity is greater than 30°. Ice stability is defined by whether the mean annual temperature at a particular location is above the frost point of -75°C (Schorghofer, 2005; Hudson et al., 2007), where ice will gradually sublime and be redeposited at the poles. At mean temperatures below the frost point, permafrost below the active layer and out of reach of the annual thermal wave is stable. The ice or permafrost table will move until the mean annual vapor density above the ice is equal to that in the atmosphere, and then becomes stable (Schorghofer, 2005; Hudson et al., 2007). Liquid water stability is not possible anywhere on the Martian surface due to the low atmospheric pressure, which would cause it to immediately boil and be lost to the atmosphere.

Martian landforms and geomorphology that suggest periglacial or glacial associations are widespread (Carr and Schaber, 1977; Rossbacher and Judson, 1981; Lucchitta, 1981, 1987; Carr, 1996b; Kuzmin, 2005). They include fretted terrain, rampart craters, rock glaciers and piedmont ice glaciers, viscous debris flows, lobate debris aprons, terrain softening, and polygonal networks of patterned ground. Rampart impact craters provide buried ice excavations, and studies of them have shown that the structure of the cryolithosphere and the relative ice content within the frozen regolith have distinct zones with latitude (Kuzmin, 2005). A desiccated regolith layer exists in the equatorial region and at mid latitudes (Kuzmin, 2005).

Low to mid-latitude glacial features are not uncommon (Head et al., 2005; Parsons and Head, 2005; Head et al., 2006). They are generally taken as evidence of Late Amazonian (10–100 Ma) extensive and localized glaciation, when conditions favoured the accumulation of snow and ice in these tropical regions. The absence of convex cross-sections in the tongue-shaped lobes of observed crater-wall rock glacier flows suggests the ice of their formation is now mostly gone, which could imply that the present time is a Martian interglacial period (Marchant et al., 2003). It does appear that the current global ice distribution (Boynton et al., 2002; Feldman et al., 2002) is consistent with ice distributions predicted from models of the current climate that are in equilibrium with the climate, eg.

Schorghofer and Aharonson (2005).

One difference to Earth is that the cyclic thermal processes that create permafrost-related landforms may on Mars be dominated by orbital cycles such as eccentricity and obliquity (Milankovich cycles), rather than diurnal or annual cycles (Rossbacher and Judson, 1981; Lucchitta, 1981; Laskar et al., 2002). The Martian obliquity cycles of 125×10^3 and 1.3×10^6 years and the longitude-of-perihelion precession over 75×10^3 years can dramatically affect the subsurface temperatures and atmospheric water pressure (Chamberlain and Boynton, 2007). This would change the subsurface cooling cycle from the length of a Martian year (1.9 Earth years) to 10^5–10^6 years. It would also produce long-term changes in the stability of buried ice.

Changes in thermal conditions at the surface do not usually produce an instantaneous change in the permafrost thickness. Response is slow when compared to the frequency of changes in surface temperature, which further reduces thickness changes: it is almost insensitive to temperature variations with periods less than a century (Haeberli, 1985). This is partly due to the slowing of thermal diffusion if the permafrost is saturated or supersaturated with ice.

2.2 Geology of the Dry Valleys

The Dry Valleys of Antarctica are located on the edge of the Antarctic continent, beside the Ross Sea in South Victoria Land. Remote, desolate and unvisited except by the occasional party of scientists, the entire area is designated an Antarctic Specially Managed Area (ASMA) under the Antarctic Treaty, in which New Zealand is a major partner.

The Dry Valleys have been deglaciated and ice-free for thousands of years, due to the surrounding 4000 m mountain ranges that prevent ice flowing from the Polar Plateau to the Ross Sea. Their mean temperatures range from -15° to -30°C (Doran et al., 2002) and they have high wind velocities and near-sterile ground. They are a hyper-arid cold "polar desert" (Tedrow and Ugolini, 1966) that is unique to Earth, but represents an environment widespread on Mars (Morris et al., 1972).

There are three major valleys, the Taylor[1], Wright and Victoria, which have been glacially carved and have floors at altitudes close to sea level. They are separated by mountain ranges roughly 2000 m high, which have small lateral hanging glaciers trailing down their flanks. All these valleys drain internally to warm, saline lakes, frozen at the surface.

The Dry Valleys have had multiple glaciations, governed by three major ice systems: the Ross Ice Shelf, which can expand to extend outlet glaciers into the eastern ends of the valleys, the ice sheet of the Polar Plateau, invading from the west, and laterally flowing alpine glaciers (Denton et al., 1971). The major valleys appear to have been sculpted by outlet glaciers from the Polar Plateau, spilling over a protective basement rock rim down to the Ross Sea. They were formed earlier than 4×10^6 years ago (Denton et al., 1971).

The metamorphic-igneous basement of the Dry Valleys comprises marbles, schists, granites and

[1] Beacon Valley is one of the smaller valleys feeding into Taylor Valley at the end closest to the Plateau.

granodiorites, and is Precambrian to Lower Cambrian (McGinnis et al., 1973). It is terminated by the erosional contact of the Kukri Erosion Surface. This extensive unconformity is overlain by the Devonian to Cretaceous Beacon Supergroup, up to 1500 m of cross-bedded quartzite and sandstones. Three main intrusions of the Jurassic–Cretaceous Ferrar dolerite cut these rocks. A 400 m thick sill intrudes about 450 m below the Kukri Peneplain, a 300 m thick sill intrudes along the Kukri surface, and the younger Beacon rocks above are cut by thinner sills and dykes (Denton et al., 1971).

Some volcanic activity occurred in the Late Tertiary, after the valleys were glacially scoured. The basalts and trachytes of the McMurdo Volcanics generated volcanic ash and other material that has been incorporated into the glacial drifts in the valleys. Pliocene, Pleistocene and recent lacustrine, glacial, æolian and marine deposits are widely distributed on the valley floors (McGinnis et al., 1973).

2.2.1 Temperature, precipitation and winds

December and January are the warmest months. Between October and February mean temperatures range from -23.7°C to 0.7°C, as recorded by twenty stations in the Valleys (Bull, 1966). Mean annual air temperatures vary according to location, with Taylor Valley warmer than Wright Valley, and Victoria Valley the coldest of the three (Doran et al., 2002). Mean temperatures from year-round automated measurements made between 1986 and 2000 range from -14.8°C at Lake Hoare, Taylor Valley, to $+30.0$°C at Lake Vida, Victoria Valley (Doran et al., 2002). Inland ice-free areas are warmer than the coast in summer, and cooler in winter. Near-surface soil temperatures may reach 15°C for short periods during the day. Rock temperatures exceed air temperatures by 5–10°C, depending on rock albedo.

The diurnal temperature range crosses the melting point of ice more than thirty times a year at coastal Marble Point (Kelly and Zumberge, 1961), while twenty to sixty freeze-thaw cycles occur each year in the active layer (Black and Berg, 1963).

Less than 100 mm water equivalent of true precipitation falls annually in the Dry Valleys, all of it from snow (Doran et al., 2002). The ablation rate in the Dry Valleys considerably exceeds the precipitation, and may be up to 1000 mm per year (Doran et al., 2002). This creates an extremely arid environment. However, the Dry Valleys are not completely dry: in the austral summer shallow melt-water streams flow from the glaciers and the snow fields, and there is some free water in the active layer. The streams are frozen most of the time and flow for only a few hours each day.

Within the Dry Valleys, winds are controlled by several factors, including the local topography, the proximity of the Polar Plateau and the Ross Sea, and the time of year. They vary widely in direction and velocity. The strongest winds are during winter, when the katabatic winds, gravity-driven from the centre of the Polar Plateau, sweep through the valleys with maximum velocities that are greater than 30 ms^{-1} (108 km hr^{-1}) (Doran et al., 2002). On-shore winds from the east with mean velocities of 2.8–4.2 ms^{-1} (10–15 km hr^{-1}) tend to dominate during the summer months (Bull, 1966). Most precipitation is associated with these humid easterlies (Bull, 1966).

Winds of these strengths can move coarse sediments, abrading rocks to form ventifacts, and the

Dry Valleys appear in many places to be paved with ventifacts. The strength of the winter winds orient all ventifacts with western-facing cut and polished facets, and pebble ridges with lee slopes facing east (Bull, 1966). The pebbles on the crests can be up to 6 cm in diameter, requiring winds of 56 ms^{-1} (200 km hr^{-1}) at three metres above the surface to allow transportation (Calkin, 1964).

Armoured pavements are common, formed by winnowing of fine-grained sediment from poorly sorted glacial sediments. Removal of the sand and silt leaves a layer of coarse fragments, which protects the underlying sediment from further erosion by deflation. A key characteristic of the formation of temperate soils is chemical weathering, predominantly of feldspars to form clay minerals. However, in the Dry Valleys there is almost no chemical weathering, only the oxidization of ferrous iron to form limonite, and some secondary ferric iron-bearing minerals (Gibson et al., 1983; Dickinson and Rosen, 2003). This soil is consequently used as a common Martian analogue for chemical weathering (Dickinson and Rosen, 2003). The dominant pedogenic weathering process is physical weathering, through freeze-thaw weathering processes (Gibson et al., 1983). Though water is not present in significant quantities, soil in the active layer seasonally contains some liquid water, which is repeatedly cycled through its freezing point.

2.2.2 Victoria Valley

Victoria Valley is located between the St Johns Range and Nickell Peak, adjacent to Bull Pass, at an altitude of 400 m at Victoria Upper Lake (Chapter 3, Fig 3.1(b)). Victoria Valley is predominantly underlain by basement plutonic and metamorphic Precambrian–Ordovician rocks of the Granite Harbour Intrusives (Turnbull et al., 1994). The St Johns Range to the northeast is formed of St Johns Pluton granite and granodiorite, overlain by the Jurassic Ferrar Dolerite. Nickell Peak is part of the Koettlitz Group, specifically the gness and marble Salmon Marble Formation. Northeast-southwest trending quasi-parallel dike swarms of the Granite Harbour Intrusives cut the St Johns Range and Nickell Peak (Turnbull et al., 1994).

Four episodes of glaciation have been defined in Victoria Valley (Calkin, 1964). These have left mantles of glacial, fluvioglacial and periglacial deposits filling the valley. The Insel Drift marks the oldest episode, the Insel Glaciation some 4×10^6 years ago, formed by a strong incursion from the inland ice of the Plateau that was followed by a partial or complete glacial retreat. It is distinguished by very silty till and extensive solifluction mantling, erratic ventifacts and frost rubble on high terraces, and no moraine-related topography.

The more recent Victoria Glaciation, with incursion of alpine and Ross Sea glaciers, is divided into three episodes. Calkin (1964) notes that the younger deposits have greater relief, more diversity in rock type, less fine-grained sediment and more prominent development of patterned ground.

The Bull Drift episode thirty thousand years ago was a strong westward advance of the Upper and Lower Victoria Glaciers, covering nearly the entire valley floor. It reached to 12–20 km beyond the present day glacier positions. The Bull Drift is marked by very silty till, isolated areas of erratic boulders, localized lake deposits and associated debris fans.

The Vida Drift episode more than ten thousand years ago (Calkin, 1964) was a minor advance to 9–11 km beyond present positions. Sandy moraines, thick broad kame-outwash deposits and minor solifluction mantling are its defining deposits.

The Packard Drift may include minor readvances, but is mostly defined by the retreat of the Victoria glaciers to their present position. The character of its deposits are sandy and very bouldery drift, ice-cored moraines, and knob-and-kettle areas. Currently forming alluvial and æolian deposits are associated with the Packard Drift. The smooth surface of the former delta of the Upper Victoria Valley lake is networked by low-relief polygons. It is probably part of the Packard Drift (Turnbull et al., 1994), and has been estimated as slightly younger than twelve thousand years, based on dating of algal deposits (Kelly et al., 2002). The former delta surface is marked by a scattering of boulders (Sletten et al., 2003), and a drop line of ice-rafted boulders was observed about six kilometres down-valley from the glacier.

The polygons of Upper Victoria Valley have many right-angle and quasi-orthogonal crack joins, and the sides are curvilinear. Sletten et al. (2003) found a width of 2–3 m for the sand wedges on excavation, corresponding to a growth rate of 0.2–0.3 mm yr^{-1}. Clear troughs and distinct microtopography with raised edges have developed, and the polygons are both smaller and more even in size (15–25 m diameter) than those observed by Sletten et al. (2003) in the lower Taylor Valley (§ 1.2.2). Sletten et al. (2003) mentions that the polygon centres are undisturbed by deformation on excavation, though near the cracks there are slight upwards warps in the layered sediments (Sletten, 2006, pers. comm.). Cracks that partially subdivide polygons are frequent, indicating progressive lateral propagation of still-forming cracks, further regularizing the patterned ground. This process is expected as the network evolves (Lachenbruch, 1962). Older, inactive (Sletten et al., 2003) cracks are also present.

2.2.3 Beacon Valley

Beacon Valley is located within the Quartermain Mountains, near the peripheral Taylor Dome of the East Antarctic ice sheet (Chapter 3, Fig 3.1(c)). The valley has a mean annual air temperature of $-21.6°C$ (Schorghofer, 2005) and precipitation of less than 10 mm water equivalent per year (Sugden et al., 1995). The north-facing mouth of Beacon Valley is dammed by a lobe of the cold-based Taylor Glacier. At the head of Beacon Valley there are several hanging glaciers, and a debris-covered rock glacier that extends down-valley for several kilometres. A flattish boulder-strewn valley floor at 1300–1450 m altitude extends between the head and the mouth.

The geology in Beacon Valley is dominated by Devonian sandstones of the Taylor Group. In the surrounding mountains large sills of the Middle Jurassic Ferrar Dolerite intrude, but the igneous sills are not present below the valley floor (McElroy and Rose, 1987).

Buried ice extends under the valley floor over an area of at least 4 km^2. It has a thickness of at least 15 m, based on features such as kettle holes that change the amplitude of the surface morphology (Sugden et al., 1995). Under a surface layer of stones, a 50 cm thick layer of till overlies the buried ice. It has a thin sandy upper layer containing angular fragments of the local sandstone and dolerite,

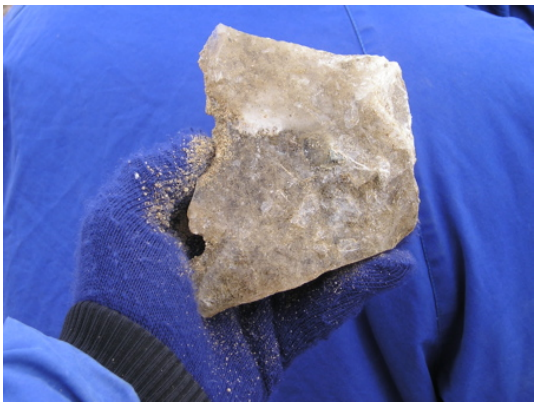

Figure 2.1: A piece of the ice buried under the field site in Beacon Valley. Excavated by R. Sletten from his existing soil and climate monitoring site. Note the lack of clarity of the ice.

over a thicker fine-grained layer of granite and glacially striated stones in a silt to clay-sized matrix (Sugden et al., 1995). This till is derived from Taylor Glacier, as it contains granite, which does not outcrop in the Beacon Valley area and is not present in the deposits of the rock glaciers (Sugden et al., 1995). The granite deposit that encompasses the till marks a former expansion of the East Antarctic outlet glaciers into the Dry Valleys. The extent of the buried ice below the granite deposit is unclear.

The buried ice is thought to be a remnant of basal glacier ice, as the ice fabric is clouded by dispersed rock debris, with alternating layers of debris-rich and clear-to-white ice. This is typical of basal regelation and debris entrainment (Sugden et al., 1995). The striated clasts suggest the glacier was sliding over its bed. The ice is "dirty", at least near the surface, and contains many salts as well as the entrained clasts (Fig. 2.1). However, it is surprising that the fabric has survived in the stagnant ice mass and that recrystallization has not occurred (van der Wateren and Hindmarsh, 1995). Sublimation has removed only the top few metres of the original ice (Sugden et al., 1995).

The soil of Beacon Valley in general is extremely salty, with the highest nitrate levels in the Dry Valleys, sufficient to prevent the growth of microbes (R. Sletten, pers. comm., 2006).

The crack intersection angles of central Beacon Valley polygons are predominantly 120°, where those of Victoria Valley are mostly 90° angles. Although the width of the trough can obscure the intersection angle, increasing uncertainty, this is likely to reflect the greater maturity of Beacon patterned ground (Sletten et al., 2003). Polygons in central Beacon have a quasi-hexagonal form, while those in Victoria are quasi-orthogonal.

2.3 Comparable geological features of Mars and Earth

2.3.1 Polygonal patterned ground

Polygonally patterned ground is a common feature of the polar regions on both planets. The polygons seen on Mars range dramatically in size, from the largest terrestrial polygons of 30–50 m to two

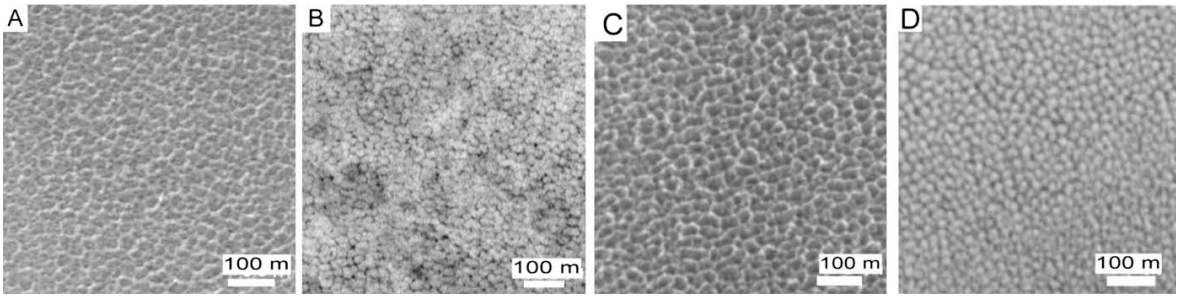

Figure 2.2: Various areas of small-scale polygonal terrain on Mars. (A) Homogeneous small polygons without apparent cracks. MOC image M02-04505, 65.7° S, 176.8° W, Ls = 162° (Ls = solar longitude). (B) Regular hexagonal patterns. MOC image M04-02503, 63.2° S, 275.4° W, Ls = 192.5°. (C) Similar to (A) in the northern hemisphere. MOC image M14-00154, 60.6° N, 2.9° W, Ls = 329.1°. (D) Hummocky terrains. MOC image M03-04266, 54.1° S, 229.5° W, Ls = 174.9°. After Mangold (2005).

orders of magnitude greater than any found on Earth. The massive polygons are up to 20 km across, and are thought to have tectonic causes (Pechmann, 1980). The polygons on scales of several hundred metres are classed as small-scale, together with those in the same size range as terrestrial polygons (Fig. 2.2). These small-scale polygons are those primarily considered for analogue with the polygons of the Dry Valleys of Antarctica. Observations from the Mars Global Surveyor Mars Orbital Camera (MOC) suggest that the polygonal ground occurs between 60 and 80 degrees of latitude, such as on southern Malea Planum (Malin Space Science Systems/NASA, 1999). It occurs on flat ground, such as crater floors or intercrater plains, and like that in the Dry Valleys is most visible when there is contrasting material filling the boundary troughs. In the Dry Valleys this is snow (Fig. 1.2), but on Mars it is bright frost, a combination of dust, CO_2 and H_2O (Wall, 1981), which condenses out of the atmosphere in the winter hemisphere (Hvidberg, 2005), or otherwise dark sand. Unlike water, carbon dioxide does not expand on freezing, so there can be no possibilities of carbon-dioxide-wedge polygons as analogues to ice wedges. Many polygon fields on both planets show a preference in orientation, usually associated with orthogonal troughs (Levy et al., 2005; Mangold, 2005). Martian polygonal patterned ground is dominated by hexagonal crack networks, associated with a variety of origins, including thermal cracking (Levy et al., 2005).

It is speculated that the lower lithostatic pressures due to the one-third Earth gravity and the higher critical viscosity of the colder, more brittle ground may cause larger versions of polygons with the same origins as those seen on Earth (Mangold, 2005). Lucchitta (1981) suggests that the absence of the vigorous and destructive fluvial erosion present on Earth may have allowed permafrost and glacial features to develop to exceptional sizes. Additionally, the Martian soil thermal regime provides different thermoelastic stresses. A semi-infinite, isotropic half space with a vertical temperature distribution dependent on seasonal variation in surface temperature has been proposed to model Martian permafrost ground (Mellon et al., 1997).

The vertical dimensions of patterned ground, useful for inferring the stage of development, can be derived from the use of two-dimensional photoclinometry (Kirk et al., 2003) and shadow mea-

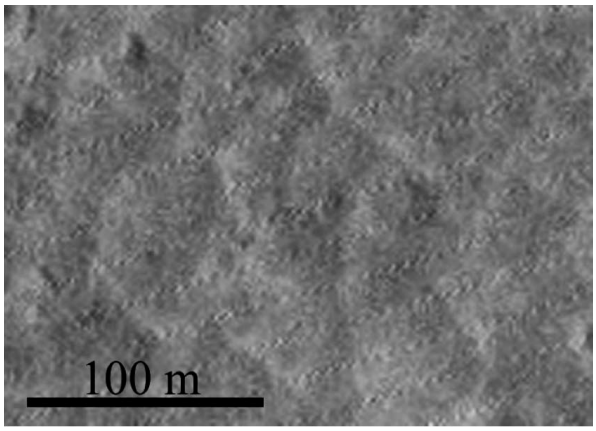

Figure 2.3: High-centred polygonal terrain in a channel floor of Athabasca Valles. The polygons have an average maximum diameter of ∼25 m and a height from trough to centre of some 0.5 to 5 m (depending on the amount of haze assumed). After Burr et al. (2005).

surements. However, photoclinometry requires assumptions about atmospheric haze and a uniform surface albedo. Consideration of specific patterned ground sites on Mars can be useful. For example, the high-centre polygonal ground in a ~ 20 km^2 area near 10° N, 204° W in Athabasca Valles, a late Amazonian outflow channel system that originates from the Cerberus Fossae, is in the terrestrial size range (Fig. 2.3). If these are ice-wedge polygons, the precipitation needed for wedge formation could be from snow, or from local precipitation initiated by volatiles from the Cerberus Plains lavas (Burr et al., 2005). This area of Mars is dusty, so the mechanisms seen on Earth where sand wedge growth is through æolian sand accumulation are possible. Sand-wedge polygons with dust wedges from æolian infill are consequently an alternative, although no high-centre sand-wedge polygons have yet been reported from Earth (Burr et al., 2005). Shallow-surface ice is scarce or absent in equatorial regions such as Athabasca Valles, so long-term preservation of the ice necessary for ice wedge formation is less likely. This suggests that Martian wedge formation could be a multi-step process, with possible secondary modification, such as debris or æolian dust infill to shift the wedge towards a sand wedge composition. It is possible that the Martian hydrosphere is active in a much more recent sense. Proposed groundwater seepage features have been observed on MOC images, overtopping patterned ground that does not show regeneration (Malin and Edgett, 2000a) (Fig. 2.4). If polygonal ground on Mars does have similar generation times to that in Antarctica, these images suggest very recent liquid water at the surface of Mars.

Alternative hypotheses of origin for Martian small-scale polygons involve tectonic processes or desiccation. While a tectonic explanation is frequently raised, it is then immediately rebutted in favour of periglacial thermal contraction polygons, which appear to better fit the current data (Lucchitta, 1981; Mellon et al., 1997; Seibert and Kargel, 2001; Mangold et al., 2002; Klima, 2003; Mangold, 2005; Burr et al., 2005). There is an absence of volcanically produced polygonal ground on Earth with the required features. Polygonal cracking of muddy sediments through desiccation is also generally

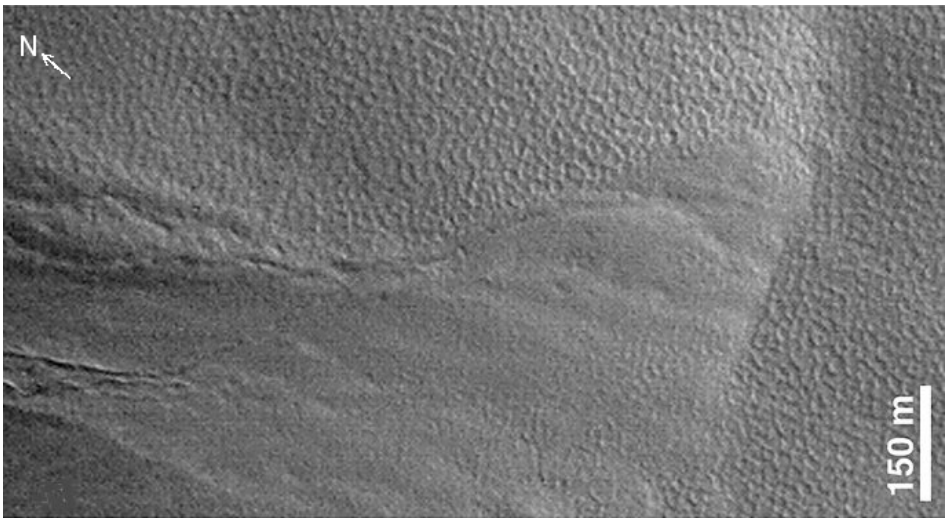

Figure 2.4: Superposition of apron material on polygonal patterned ground of similar dimensions to that in the Dry Valleys field sites. Lighting is from lower left. After Malin and Edgett (2000a).

discounted by insufficient polygon size, as such polygons do not generally reach scales larger than a few metres (Neal et al., 1968). Desiccation polygons also display little to no microtopography, and form irregular random orthogonal networks (Neal et al., 1968). However, initial periglacial polygon networks in the Dry Valleys are orthogonal, though with polygons tens of metres across, and do appear similar to those in drying mud (Sletten et al., 2003). This may simply be due to the same physical process, a homogeneous to inhomogeneous half-space placed under tensile stress, occurring in both cases (Lachenbruch, 1962).

Though patterned ground is primarily associated with permafrost, and can be indicative of continuous permafrost (Murton et al., 2000), it produces permanent microtopographic ground alteration that can remain after the removal of the permafrost. There is a strong possibility that at least some of the polygonal ground on Mars is fossil patterned ground. Many examples of fossil patterned ground can be seen on Earth. It occurs in places where permafrost conditions have ceased due to climatic change, but the ground surface has not been modified by vegetation or by geological perturbations. Fossil ice wedges, overlain with further layers of sediments, are frequently found in exposures such as road cuttings in the Arctic (Davis, 2001). Pleistocene relict sand wedges occur along the Tuktoyaktuk coastline, Northwest Territories, Canada, extending more than 10 m into massive ice (Murton and French, 1993).

French (1996) attributes a transition to high-centred degradation polygons as evidence of a periglacial landscape in collapse, following a change in climate. However, small areas of high-centred polygons may be due to thermal erosion after river avulsion.

Klima (2003) found that patterned ground in Utopia Planitia, in the northern hemisphere of Mars, appears to no longer be active. Unlike the polygons in the Martian polar regions, those in Utopia Planitia have troughs that appear deep and empty, with widespread collapse features. The regional

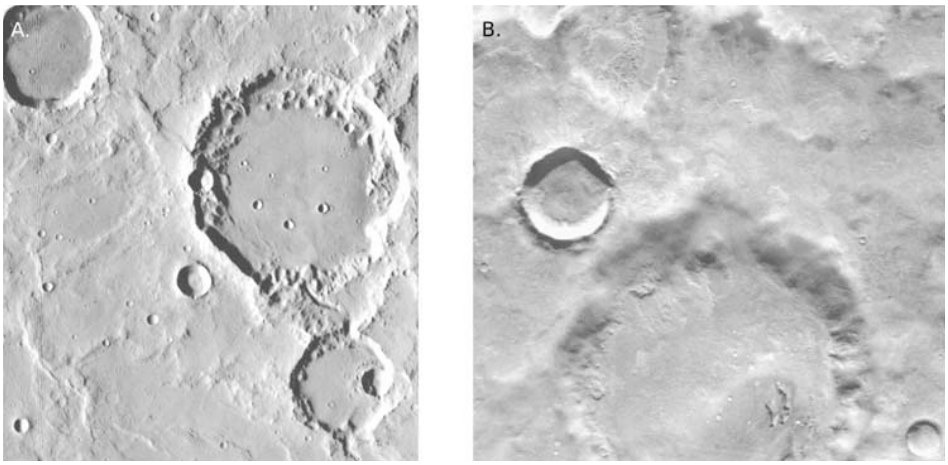

Figure 2.5: Varying degrees of ice-related terrain softening on Mars. Viking images, each 50 km wide. Image at left is near-equatorial, at 12° S. Image at right is at 49° S. From Chamberlain and Boynton (2007), after Carr (1996b).

climate has become dryer and colder with time, probably since their formation. Significantly, Mars Odyssey Gamma Ray Spectrometer observations also show the upper regolith of the area to be devoid of ground ice. Whether these polygons were originally formed by fracturing in an active layer or by sublimation-aided wedge growth in massive ice was not able to be determined (Klima, 2003). The partial patterned ground network collapses are likely to result from evaporation or sublimation of the massive ice (Klima, 2003; Burr et al., 2005).

2.3.2 Buried ice

The presence of significant amounts of near-surface ground ice above $\pm 60°$ was known several years ago from Mars Odyssey Gamma Ray Spectrometer (GRS) data (Boynton et al., 2002; Feldman et al., 2002). Its distribution could be mapped only to the 300 km per pixel resolution of the GRS composition maps, and the GRS can detect water only to its measurement depth of one metre. There is relatively little near-surface ground ice in the equatorial region (Boynton et al., 2002; Feldman et al., 2002). The distribution of ground ice on Mars has been found using Thermal Infrared Mapping Spectrometer (THEMIS) data and tends to be patchy and global in extent (Bandfield, 2007).

Several of the periglacial landforms related to the presence of buried ice (§ 2.1) only occur as the result of bodies or layers of subsurface ice. These include terrain softening, debris aprons and viscous debris flows. Mustard et al. (2001) also identifies particular areas of uncratered, smooth terrain as evidence of abundant ground ice. The regolith in areas rich in buried ice frequently exhibit terrain softening, the rounding or muting of impact features that would normally have sharp edges (Fig. 2.5) (Carr, 1996b). At equatorial latitudes, craters and fault scarps formed by heavy bombardment have little erosion and clear definition. At latitudes poleward of 30°, such features are “softened”, and the population of small craters is absent (Carr, 1996a). They are hypothetically deformed by gelifluction

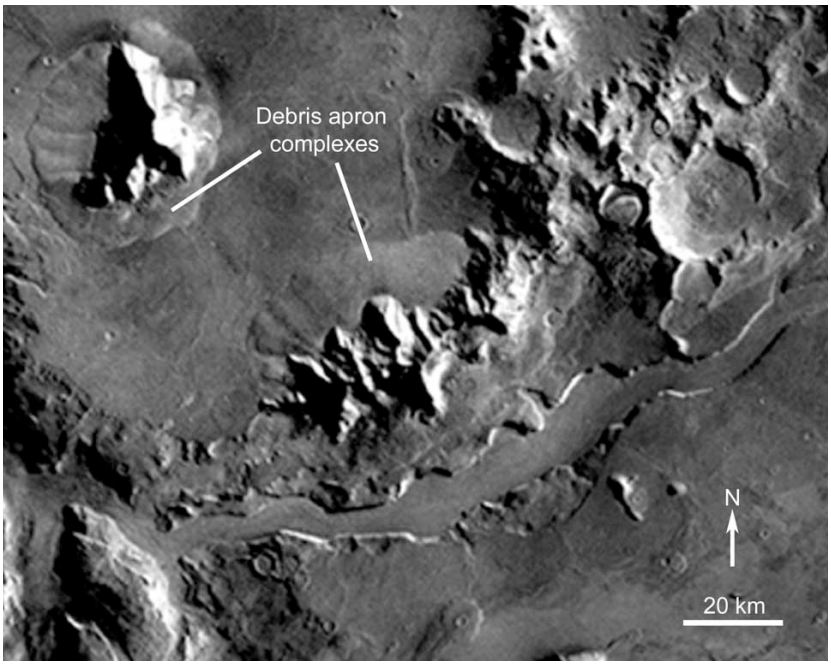

Figure 2.6: Debris apron complexes near Reull Vallis in the eastern Hellas region. Image covers 254–257° W, 40–44° S. From Pierce and Crown (2003).

of the surface material due to the subsurface ice abundant at these latitudes (Carr, 1996b). These terrain softening features appear to be without terrestrial counterparts, though it is known that ice can enhance creep rates (Carr, 1996b). The extreme forms of terrain softening, which affect the areas between high-standing massifs, and other viscous flow features that display characteristics such as compression ridges, appear to merge into the processes of lobate debris flows and debris aprons (Carr, 1996b; Milliken et al., 2003).

Debris aprons are an important expression of buried ice (Lucchitta, 1981), and are not seen on Earth. They can be divided into two forms: linear, which occur along valley walls and crater interiors, and circumferential, generally surrounding isolated massifs (Fig. 2.6) (Dickson et al., 2006). Landforms with the characteristic features of debris aprons that are confined within large valleys are termed lineated valley fills. Debris aprons can be extensive. For example, one 250 m thick lobe in the eastern Hellas region is 18 km wide, and extends 8 km outwards from the base of a 3.75 km high massif. A broad alcove in the massif is suggested as the accumulation zone for snow and ice in the deposit (Head et al., 2005). The alternating texture of fretted and plateau terrain in the lobe suggests that substantial quantities of ice remain under the debris cover, since the pits of the sublimed areas approach a depth of 100 m. As the apron has no impact craters on its surface, it must be geologically recent, although its extensive partial sublimation suggests that it is not permanently stable in the current climatic environment. Crater counts on debris aprons in the northern Deuteronilus Mensæ suggest sublimation has occurred in the last tens of millions of years up until at least the recent past (Mangold, 2003).

However, observations from Beacon Valley, Antarctica suggest that a sublimation till can insulate and protect buried glacial ice for up to several million years (Sugden et al., 1995; Schäfer et al., 2000).

Almost all aprons around the Hellas Basin show pitted, fretted terrain (Pierce and Crown, 2003). Accumulation of æolian dust can also produce smoothed areas on debris aprons as a result of the dust mantling (Mangold, 2003). The abundance of aprons apparently sourced from debris-providing alcoves in massifs suggests that the aprons originate as extremely ice-rich, debris-covered glaciers (Mangold, 2003; Head et al., 2005). Dissected mantles, in regions where ice was stable in the last 10 million years, but due to orbital forcing is no longer stable, are suggestive of layered ice-dust mantles from which the ice has sublimated (Mustard et al., 2001; Milliken et al., 2003).

Young, near-surface equatorial ground ice features do exist, such as Athabasca Valles. This area shows small-scale polygonal patterned ground and features identified as pingos in various stages of evolution (Burr et al., 2005). Pingos are ground ice features, perennial ice-cored mounds produced by injection and freezing of groundwater pressurized during freezing of the ground. The internal ice may be segregation iced or form ice laccoliths. Their origin in this case was possibly due to deposition of saturated sediments during flooding with subsequent freezing (Burr et al., 2005). A qualitative measure of thermal inertia, which can be used to distinguish fine sediments from coarse or bedrock, can be obtained by comparing day and nighttime THEMIS images that show surface thermal response (Christensen et al., 2003). On this basis the Athabasca Valles area has been described as sedimentary in origin, probably flood deposits (Burr et al., 2005). Burr et al. (2005) argue for the derivation of this ground ice from floodwater or from magmatically cycled groundwater.

Photoclinometry was used to conclude that the pingo mounds were up to 24 m high, comparable with terrestrial pingos, which can be up to 50 m high. Pingo vertical growth is driven by the pore water pressure in the sub-pingo water lens, equal to the normal force at the base of the ice core, which is proportional to gravity. At maximum growth, the force from the overburden mass, also proportional to gravity, is equal to the driving force and so the effect of gravity is nullified (Burr et al., 2005). This means pingo heights should be comparable on both planets, and therefore prevents the use of pingos for understanding the range in size of Martian patterned ground.

Rootless thermokarst cones, produced in a terrestrial environment by the partial melting of ice-rich permafrost ground to form an undulating and hummocky landscape, have been identified near the equator of Mars through morphological comparison (Lanagan et al., 2001). These cones were dated at a maximum age of 10^6 years by crater counts of the surface. Thermokarst formation on Earth requires the existence of segregation iced ice, which forms where there are aquifers through which water can percolate, and fine grained sediments that allow segregated ice to easily develop. This requirement can be satisfied on Mars as much of the highlands may be underlain by porous, unconsolidated parts of impact breccias, and æolian silt may be common (Lucchitta, 1981).

Complex heat diffusion models targeting the structure and evolution of the ice-rich regolith have been developed (Mellon et al., 1997; Kossacki et al., 2001; Helbert and Benkhoff, 2006). These calculate the thermal behaviour, energy transport and gas flux in the soil through time, until the predicted

ice table has stabilized. For example, this modelling suggests that the stable depth of ice at the equatorial location of Isidis Planitia, one of the driest places on Mars, is about 4.5 m (Helbert and Benkhoff, 2006). This matches the GRS measurements of a "dry spot" with maximum inferred water abundance of 3% wt, excluding any significant ice in the first metre of the regolith (Helbert and Benkhoff, 2006).

Ice that exists at locations where it is not in equilibrium with the current climate may simply have a transport-limiting mechanism that slows adjustment of the ice table (Hudson et al., 2007). Low diffusion coefficients have been invoked by Head et al. (2005) to explain the survival of the low-latitude glaciers and rock glaciers. The existence of a "duricrust" of the indurated upper few centimetres of soil, possibly cemented by mobile salts, has been observed at the Viking, Pathfinder and MER landing sites (Clark, 1979; Hudson et al., 2007), and it may help to impede the escape of water molecules (Hudson et al., 2007). Such a soil crust is observed in the Dry Valleys, as the salt content of the soils are similarly extreme (Clark, 1979). However, as the terrestrial atmosphere is ten thousand times more humid than the Martian atmosphere (Tokano, 2005), the need for a diffusion barrier may be lessened or be provided by other mechanisms. That the ice in parts of Antarctica and the Arctic can be stable on timescales comparable with the obliquity and other climate change cycles of Mars, at least several tens of thousands of years, is useful for comparison with Martian buried ice.

2.4 Summary

Patterned ground on Mars appears to have many similar characteristics to that on Earth, providing the possibility of terrestrial analogues. There is strong morphological evidence for its association with Martian ground ice and periglacial features. Patterned ground can form in terrestrial contexts where the sediments contain sufficient segregated ice to become ice-cemented, providing cohesion necessary for the development of tensile stress over tens of metres. This requirement is satisfied on Mars due to the planet-wide cryosphere. The similarities between the physical environments of the Dry Valleys of Antarctica and of Mars, including their aridity, strong seasonal winds and constant low temperatures, support the formation of patterned ground in an equivalent manner in both places. If the analogy with Earth holds, Martian patterned ground will be able to provide information on the Martian cryosphere.

Buried ice on Mars inhabits a polar zone, much like that on the Earth, but the Martian buried ice is part of a much more extensive cryosphere than the terrestrial one. Buried ice on Mars is responsible for features across much of the planetary surface, including terrain softening, lobate debris aprons, fretted terrain and pingos.

This chapter has introduced the physical conditions and climatic and geological variables that govern the formation, development and stability of patterned ground and buried ice on both Earth, specifically in the Dry Valleys of Antarctica, and on Mars. With this background, and the consideration given to the geology of the field sites in Victoria Valley and Beacon Valley, the fieldwork undertaken in the Dry Valleys can now be considered.

Chapter 3

Antarctic fieldwork

This chapter describes the collection of the data that forms the primary part of this study. First, the relevant previous geophysical investigations in the Dry Valleys of Antarctica are considered (§ 3.1). The extent and nature of the fieldwork is then discussed, detailing the geophysical methods used at each of the two field sites. Fieldwork in the Dry Valleys of Antarctica was conducted in Victoria Valley from November 27 to December 27, 2006, and in Beacon Valley from December 27, 2006 to January 21, 2007, as part of Event K054.

This fieldwork relates to the objectives defined in § 1.4. In Victoria Valley, this study took a transect profile across the valley to determine the depth to bedrock and the presence of any buried massive ice bodies left as relics of past glaciers and lakes (§ 3.2). In Beacon Valley, with fewer personnel, the objectives were adjusted: the spatial extent of buried massive ice was determined by the transect (§ 3.3).

The results of the investigations outlined in this chapter are presented in Chapter 4.

3.1 Previous geophysical studies in the Dry Valleys

Geophysical studies of soil, ice and rocks in the Dry Valleys of Antarctica (Fig. 3.1) began in the modern phase of Antarctic exploration, for example that of Robinson (1963). Geophysical methods are low-impact and noninvasive, especially useful in the fragile environment of the Dry Valleys Antarctic Special Protected Area (Fig. 3.1(a)). Surface geophysical studies were made before the major Dry Valleys Drilling Project in the 1970s, with reversed seismic refraction techniques and electrical resistivity methods (McGinnis et al., 1973).

The application of ground-penetrating radar (GPR) to permafrost ground has been successful in the Arctic (Leuschen et al., 2003) and mountain permafrost (Moorman et al., 2003), and surveys have been made in Antarctica (Holt et al., 2006a). Radar sounding at frequencies from tens to hundreds of MHz has been used to depths of several kilometres to study the subsurface characteristics of ice sheets on Earth (Holt et al., 2006a). GPR has previously been applied at relatively low frequencies in Beacon Valley, but produced uninformative results (R. Sletten, pers. comm., 2006).

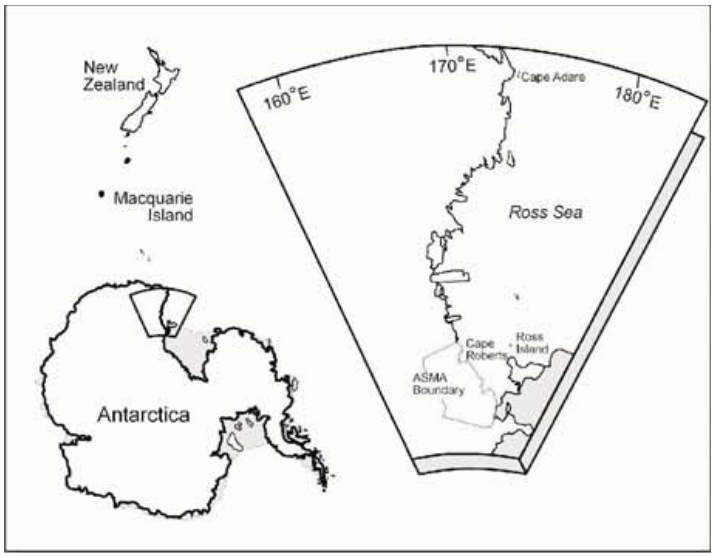

(a) Location of the McMurdo Dry Valleys ASMA relative to the Antarctic continent (Antarctica New Zealand).

(b) The Victoria Valley field site, blue dot, and transect, red line (USGS). See § 3.2.

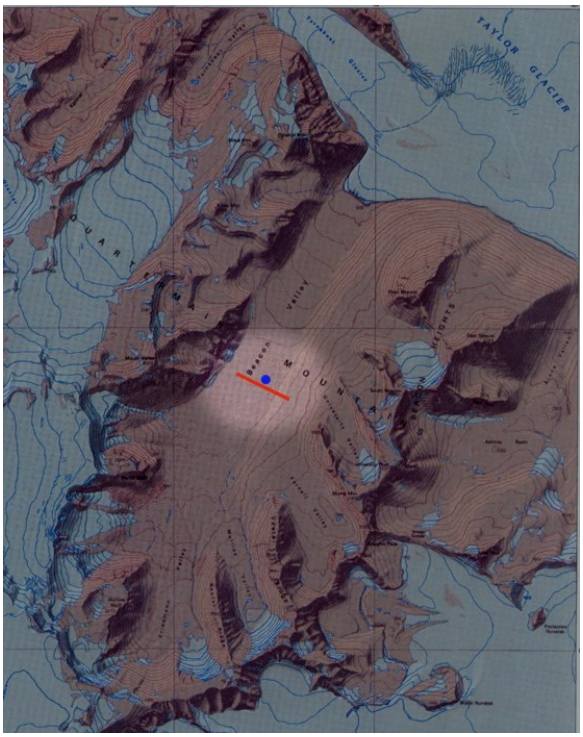

(c) The Beacon Valley field site, blue dot, and transect, red line (USGS). See § 3.3.

Figure 3.1: Location of field sites in the Dry Valleys of Antarctica.

Resistivity sounding, a related method to resistivity tomography, has been used in multiple parts of the Dry Valleys of Antarctica (McGinnis and Jensen, 1971; McGinnis et al., 1973; Guglielmin et al., 1997; Zwartz, 2005). In Victoria Valley and Beacon Valley, preliminary results exist (Zwartz, 2005), which indicated that ice, regolith and bedrock could be identified there using ground resistivity soundings. Resistivity sounding surveys around Lake Vida in Victoria Valley, and in Taylor and Wright Valleys, showed most areas to be underlain by frozen ground, which thinned near lakes. The lakes were on unfrozen sediment (McGinnis et al., 1973). Resistivity sounding has been successfully applied to buried massive ground ice in Terra Nova Bay (Guglielmin et al., 1997). Polygons also form large fields in this area (Bondesan et al., 1997).

A geomagnetic ground survey of Central Victoria Land has been made to characterize field anomalies (Bozzo and Meloni, 1992), but no detailed mapping work in small areas has been done.

It appears from the literature that time-domain electromagnetism has not been previously applied in the Dry Valleys. It has also not been applied elsewhere in Antarctica, but has been applied to permafrost ground with some success in Russia, Alaska and Northern Canada (Kozhevnikov and Antonov, 2006).

Previous seismic studies in the Dry Valleys concluded that buried ice could not be identified by seismic methods as the velocities of sound in ice and frozen ground were similar (McGinnis et al., 1973), but seismic studies on Livingston Island, in the maritime Antarctic South Shetlands island group, suggest that the method can be helpful in conjunction with other methods (Hauck et al., 2007).

In this study, electrical resistivity tomography (§ A.1), ground-penetrating radar (§ A.3), time-domain electromagnetism (§ A.2) and a magnetic survey (§ A.4) were used in Victoria Valley, and resistivity tomography and ground-penetrating radar were used in Beacon Valley.

3.2 Victoria Valley

The Victoria Valley transect ran north-east to south-west, perpendicular to the cut of the valley and approximately 7 km from Victoria Upper Glacier (Fig. 3.1(b)). It was centred a few metres from the site of the camp at S 77° 20.191', E 161° 37.216'. The transect began on the southwestern flank of the ridge of Nickell Peak (Fig. 3.2). It continued over small lateral moraines and coarse moraine material, probably of the Vida Drift (§ 2.2.2), which featured polygonal ground with raised bouldery perimeters and depressed centres. Midway down the flank, it crossed a patch of smooth, very flat, polygonal ground covered in pebble-sized clasts that was cradled between moraines. It appeared similar to other patches occurring semi-regularly along the valley flank. These patches were sheltered from the wind and each was fed by a snow-melt channel, which possibly contributed to the area's accumulation of fine sediments. The slope angle then changed gently to flatter ground, where low-relief polygons with no boulders and slightly depressed centres have developed on the former lake delta. The transect crossed the handle of a spoon-shaped depression just north-east of the camp that may be due to ground deflation. It then continued over a ridge of moraine material before traversing

Figure 3.2: The transect across Victoria Valley, looking north-east towards the St Johns Range and the camp, from the end of the resistivity line. At centre, the yellow tents of the camp beside the centre of the transect are just visible.

the frozen stream connecting two parts of Lake Victoria. On the north-east side it passed across more moraines and moved into the extensive scree slope on the southwestern flank of the St Johns Range.

3.2.1 Topographic measurements

A topographic survey was made along the transect using a tripod-mounted Nokkia optical level and a surveyor's staff. The large variation in elevation progressing down the hillside meant the tripod had to be moved frequently.

3.2.2 Resistivity tomography

Resistivity was done in two 50% overlapping sections of full 128 electrode Wenner four-string configurations, producing a subsurface profile 960 m in extent. Each section was 640 m long, and a 50% overlap was used to ensure that there would be sufficient data at moderate depths when the individual sections were merged. This meant that successive sections each extended the length of the profile by 320 m.

The top end of the resistivity line was placed low on the moraine-ridged slope at the south-west end, at S 77° 20.337', E 161° 36.172'. The resistivity line, and later the ground-penetrating radar line, were biased up onto the southwestern side of the valley as there was less scree and moraine cover over the apparent extended slope of the flank of Nickell Peak, placing the ground surface closer to bedrock. The cables were stretched to maximum extension, giving a constant spacing of 5 m between

(a) A problematic electrode.

(b) A more typical, problem-free electrode.

Figure 3.3: Examples of resistivity tomography electrodes in situ.

electrodes. This spacing had some small variation due to the undulating ground. Test runs were made to measure contact resistance, as the method requires that enough current is injected into the ground to produce a measurable voltage. Troublesome electrodes with poor contact were almost invariably those that had needed a hole in a snowdrift, up to 0.5 m deep in several cases, to be dug so that they could be placed directly in the ground, as in Fig. 3.3(a). Those over the frozen streambed also had this problem, as it was impossible to drive them more than 2 cm into the rocky bed once the ice above had been chipped away. Local water sourced from lake ice was poured over the other problem electrodes, with hot water used in the stream bed. This helped to freeze the electrodes in place. Acceptable contact resistivities were less than 300 kΩm, produced by electrodes such as in Fig. 3.3(b), while errors were shown as infinite resistivity. Testing took almost a day.

For the measurements, the current injected into the ground was set so that the three variables of current injected, on time, and off time increased systematically with increasing depth of measurement. This set low current at the surface and slightly higher current at depth where the path was longer. Measurement of the first 128-electrode section was completed in 11 hours without difficulty. However, measurement of the second 128-electrode section could not be finished due to battery problems, producing an incomplete data set.

3.2.3 Time-domain (transient) electromagnetism

Time-domain electromagnetism measurements were made using single-turn 80×80 m^2 loops laid as adjoining squares. For the maximum possible enclosed area of semi-level ground, a requirement of the method, the squares were either centred on the transect line or placed alongside it as the topography directed. Seven squares were taken, extending from the camp across to the lakeside moraines and up the hill until the moraine relief became too great, a short distance below the isolated flat polygon patch. Four squares were placed on the smooth flat polygonal ground surrounding camp, one on the rocky high-relief polygonal ground adjacent to the stream, and two on the sloping and rocky polygonal

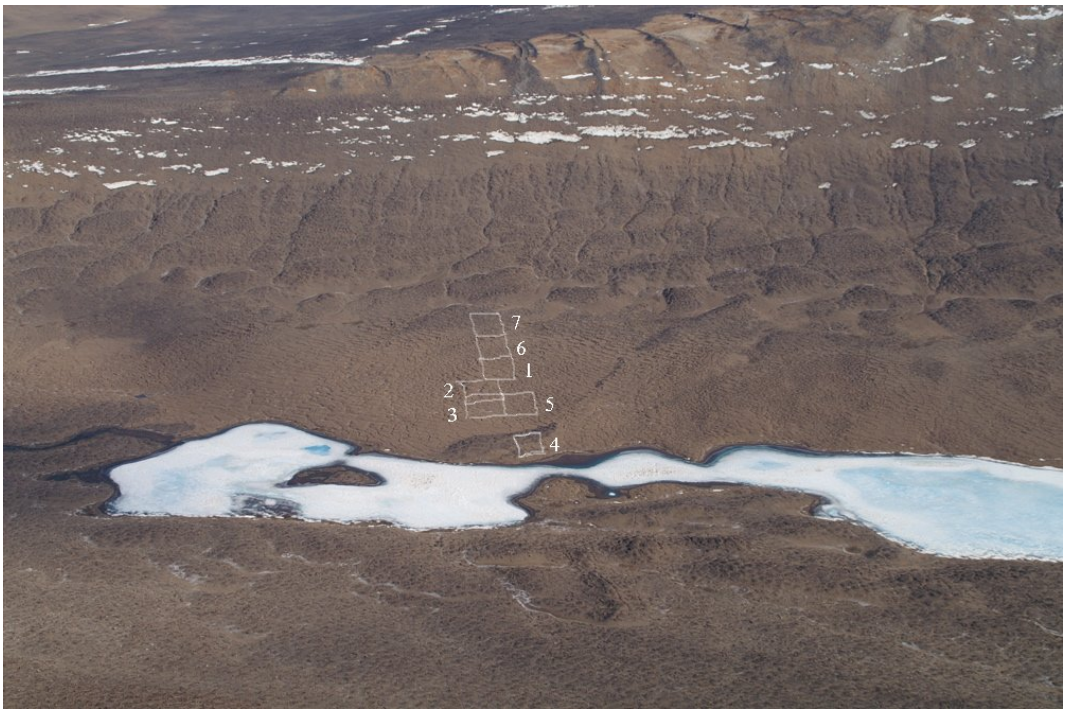

Figure 3.4: Locations of TEM measurement sites relative to the transect across Victoria Valley.

ground of increasing elevation (Fig. 3.4). Laying the loops was time-consuming, with the small trolley carrying the cable reel not ideally suited to the rocky terrain. An optical square was used to lay perpendicular sides. The current was increased from 2 A up to the near-maximum of 2.42 A after a test run. This near-maximum value was used as the current would remain within the target current of 2.4 ± 0.02 A if any downward decay in output current occurred during the measurement. Measurements were taken in stacks of four, and a second time window was possible for two of the squares on the flat ground. When the highest elevation square produced very noisy data, no squares were attempted at even higher elevation, as the lateral moraines on the valley sides would have intruded into the loop. One square included part of the camp, but no adverse noise effects from the metal objects in the camp were detected.

3.2.4 Ground-penetrating radar

Both 25 and 50 MHz antennae were tested for the ground-penetrating radar (GPR) survey. The larger and consequently more awkward 25 MHz antennae were to be used only if the 50 MHz did not reach comparable depths. This was tested through a common-mid-point (CMP) survey (§ A.3) 36 m long, run along the transect line on the flat polygons near camp using both the 25 and 50 MHz antennas. As the 25 MHz reached a return time of 1200 ns, approximately twice the apparent time of the 50 MHz and corresponding to a greater probed depth, the GPRsurvey was made using the larger antennas. This did result in some logistical issues when manoeuvring on the rocky terrain, as the 25 MHz were just

under 4 m in length.

Measurements were made at 1 m spatial intervals, with an antenna separation of 4 m and a sampling interval of 3200 ps, with 64 stacks for each trace to improve the signal-to-noise ratio (§ A.3). Difficulties included frequent poor ground contact on the rocky moraine ground. On occasion the antennas were 30 cm off the ground when balanced on two rocks. However, the antennas were always much closer than the maximum air distance of 1/10 of the 12 m wavelength. External interference was absent, once the hand-held VHF safety radio was switched off. Light snow created interference on the first day of the GPR survey, particularly in the first 300 m of the transect at the south-west end (Fig. 3.5(a)).

3.2.5 Magnetic survey

From 11 December, magnetometer measurements were made in the morning for ten minutes at one-minute intervals. This was combined with a daily morning report on the space weather supplied by Scott Base. The K-index recorded at Australia's Casey Base was used to decide whether a survey should be made. Rapid diurnal changes prevent the instrument's normal precision of measurement of 0.1 nT, and the magnetometer reverts to ± 1 nT (EG&G Geometrics, 1992). This was a good indicator of poor surveying conditions.

For the subsequent week, solar flares and high solar activity was sufficient to disrupt HF communication and produced days of severe to moderate magnetic field activity. This halted the magnetic survey. By December 18, the K-index had dropped to 2, and it was found that the magnetometer could be set to take readings automatically at set time intervals. At a sampling time of 2 minutes, a near-continuous record of the total field was taken, at a location 15 m from camp (similar to Fig 3.3.4).

A preliminary walk made to the top of the very rounded ridgeline showed bedrock outcrops, probably of Precambrian gneiss (§ 2.2.2). This investigation prompted extension of the planned magnetic survey to more than halfway up the side of the mountain, considerably beyond the resistivity and ground-penetrating radar lines.

On the morning of December 24, with limited time left in Victoria Valley, the magnetic variability was checked and found to be adequate if not ideal to survey. The sampling interval was set to every five steps, approximately three metres. From the base station at camp, six substations were marked at roughly 20-reading intervals out to the north-east until the survey reached to the end of the GPRmeasurements. To the south-west, seven substations were initially established but several more were set up as the survey was continued late in the day far up the side of the ridge past the beginning of the GPR. The surveying procedure was to sequentially move out to each substation in turn, then return to the base station, then survey out to the next substation, return to base, and walk out again. In this way, each segment between substations was surveyed three times. The constant return visits to the base station were necessary to provide continued points on the background variation curve, for later fitting and subtraction. The full 2 km of magnetic survey measurements was eventually completed just before 11 pm that evening.

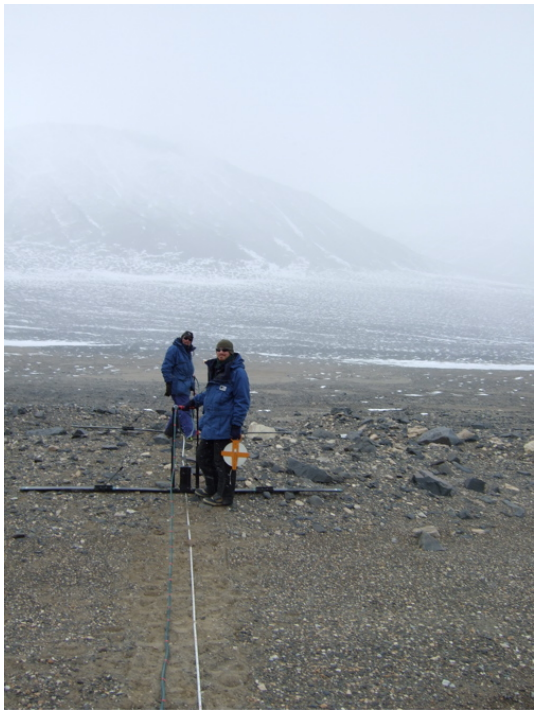

(a) 25 MHz ground-penetrating radar, as photographed by the console wearer.

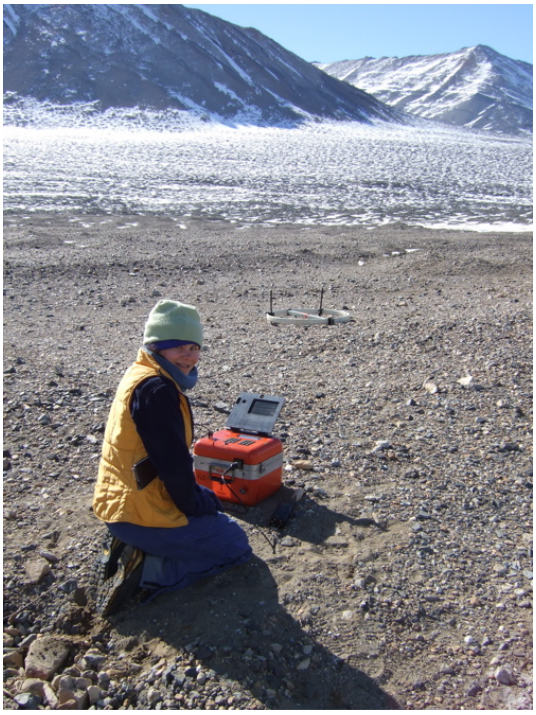

(b) Time-domain electromagnetism in operation. The levelled receiver is in the background.

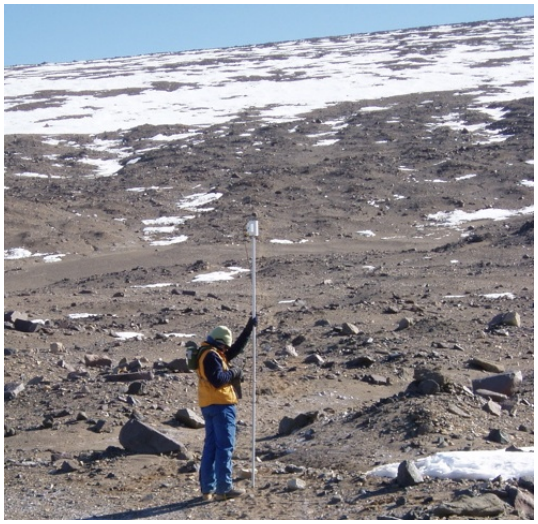

(c) Bedrock survey in Victoria Valley, using a single sensor on top of the pole, connected by cable to the chest-mounted, manually operated magnetometer (Photo: M. Godfrey).

(d) The console, battery and recording laptop for the two-dimensional resistivity tomography.

Figure 3.5: The geophysical methods in use at the Victoria Valley field site.

(a) Looking east along the transect towards the end of the ridge off Slump Mountain. The yellow resistivity cable is at the lower left.

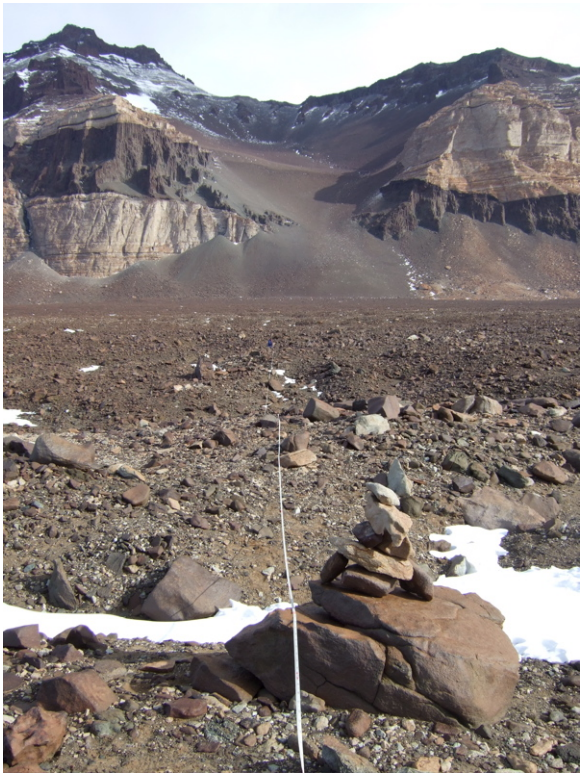

(b) Looking west along the transect towards Mt Weller, at left. The white line in the centre is a tape measure laid for the GPR.

Figure 3.6: The Beacon Valley transect.

3.3 Beacon Valley

Compared to Victoria Valley, the ground was much more heavily armoured with large boulders, presenting greater logistical difficulties. The orientation of the transect was perpendicular to the valley (Fig. 3.1(c)), as in Victoria, placing it almost due east-west (Fig. 3.6). Its starting point was on the lateral moraine on the eastern side of the valley at S 77° 51.094', E 160° 37.112'. This moraine showed a clear visual distinction from the valley floor. It was light tan with an armouring of small well-developed ventifacts, abundant scattered granite boulders, and gentle and even in slope. Some thirty to forty metres west there was a gradual transition to much larger rocks, predominantly weathered red-brown basalt with scattered sandstones, which marked the material of the valley floor. Crossing to the west the transect passed through six evenly spaced and roughly bowl-shaped sinkholes of between forty and a hundred metres across and between ten and thirty metres depth, before passing into flattish terrain at about 850 m. This continued until a gentle shallow sloping depression (3 m deep) at the end of the transect, S 77° 50.851', E 160° 34.428'. The total length of the transect was 1.3 km.

3.3.1 Topographic measurements

Topographic surveying was made using the resistivity electrodes at 5 m spaced data points. However, before the surveying was finished, the resistivity electrodes had to be removed so that the ground-penetrating radar could be done without interference. Small rock cairns were built at all the remaining points to be surveyed, and the rocks replaced in their natural locations on the survey's completion.

3.3.2 Resistivity tomography

It was possible to lay and run three 128-electrode lines in the space of four days. This was due to good weather and a lot of hard work. This produced a profile with a total length of 1280 m across the valley. Lines were run with electrodes at the maximum 5 m spacing. The contact resistances were all comparatively low (below 30 kΩ), and there were no electrode errors on any of the three lines. Additionally, it was found possible to set the software running without interrupts, making continuous surveillance unnecessary. These factors decreased the measurement time to 7 hours.

3.3.3 Ground-penetrating radar

GPR measurements using the 50 MHz antennas with a 2 m separation were made at 0.5 m spatial intervals over the same transect as defined by the resistivity, but extended 40 m further to complete a full 1.30 km of readings. As before, a stack of 64 per trace was used, but the new sampling interval was 1600 ps. As it was recorded, the data showed strong chaotic reflections and diffractions due to reflections from the boulder layer on the surface. Data were recorded in 100 m sections with a half-metre overlap on the files in case of unexpected antenna battery failure from the cold. The 1.8 m long 50 MHz antennas were reasonably manageable on the very rocky and highly undulating terrain. They were used as the 25 MHz antennas would not have been manageable and were unlikely to produce significantly more information. The fibre optics were protected from snagging on rocks by housing in a garden hose pipe, which worked well, with the minor inconvenience of the hose pipe becoming nearly inflexible due to the cold. Prolonged exposure to low temperatures had also made the plastic sheathing of the fibre optic lines quite brittle, and repairs were required after small fragments cracked and flaked from the glass fibre near the connectors on several occasions.

3.3.4 Magnetometer base station

The sedimentary basement (§ 2.2.3) made the area less suitable for a magnetic survey of bedrock, as the expected response would be smaller and have greater variability. Instead measurements were made of the diurnal variation. This record was not as successful as in Victoria Valley, due to intermittent problems with constant operation of the instrument after a wire short. This caused numerous gaps in the later part of the record, and the magnetometer ceased functioning altogether on January 20. Several periods of solar flare activity produced notable fluctuations in the local field. One in particular

Figure 3.7: Magnetometer base station in Beacon Valley, 25 m from the camp. The white-painted sensor is to the left of centre.

on January 15 caused a six-hour dip of several hundred nT in the magnetic field, nearly six times the normal diurnal drop.

3.3.5 Time-domain (transient) electromagnetism

The time-domain electromagnetism technique was not used in Beacon Valley. The initial reconnaissance showed that the topographic variation was between 1.5 and 3 m on the polygon sides and over 10 m into the large bowl-shaped sinkholes. The steep relief of the surface profile of the central Beacon polygons has long been noted (Ugolini et al., 1973). Since time-domain electromagnetism works on the principle that the underlying structure is predominantly level layering, and it is difficult to correct for topography, the topographic variation was too severe for TEM to be applied.

Chapter 4

Results and data analysis

In this chapter, the data from the two field sites in the Dry Valleys of Antarctica (Chapter 3) are analyzed. The data were collected using geoelectrical resistivity tomography (§ 4.1), electromagnetic (ground-penetrating radar in § 4.2, time-domain electromagnetism in § 4.3) and magnetic surveys (§ 4.4). This combination of geophysical methods allows conclusions to be drawn about the occurrence and characteristics of ice in the ground, and its influence on the surface morphologies of patterned ground. The results of the individual data sets are synthesized (§ 4.5) — with separate consideration of the two field sites of Victoria Valley (§ 4.5.1) and Beacon Valley (§ 4.5.2). This is used to show the relationships between the buried ice, the subsurface topography and the surface expression of patterned ground (§ 1.4).

On frozen ground, electric, electromagnetic (induction or radar) and refraction seismic methods are the preferred non-intrusive methods for studying subsurface strata (McGinnis et al., 1973; Guglielmin et al., 1997; Moorman et al., 2003; Hauck et al., 2007). The results from the application of a single geophysical method to a particular situation can be ambiguous. This is because the conclusions about the properties of the subsurface material have to be made from experience and analogy, unless direct ground comparison evidence, such as cores, are available. Using a combination of different methods reduces this ambiguity.

4.1 Resistivity tomography

Geoelectrical resistivity measurements provide information about the electrical resistivity of subsurface material. At the freezing point of water, there is a marked increase in the electrical resistivity of a material. This makes electrical geophysical methods suitable to detect, locate and characterize ground containing frozen material. These methods have been applied in numerous permafrost studies (Haeberli, 1985; Hauck et al., 2003).

The tomographic variant of the electrical method is widely used (Hauck et al., 2007). It overcomes limitations inherent in the other method, vertical electrical sounding (VES), which is one-dimensional and assumes a horizontally homogeneous subsurface. Lateral variations due to heterogeneous ground

along a survey line can significantly influence results, obscuring individual features. Resistivity tomography is two-dimensional and can therefore avoid this problem (Hauck et al., 2007).

Resistivity tomography assumes that the variation in resistivity is two-dimensional, in vertically stacked zones that have boundaries perpendicular to the profile. The lateral extent of the zones is assumed to be sufficiently large that no boundaries that are parallel to the profile will induce effects. This assumption is not always valid. It means a subsurface body in the shape of a cube will introduce three-dimensional effects to the results, which are harder to model and may produce artefacts. For example, high-resistivity bodies can be surrounded by small, low resistivity "haloes" (Dahlin et al., 2007). An empirical guideline is that a lateral width of five times the profile length of the zone will normally produce two-dimensional geology.

The resistivity of ground material is influenced by both temperature and lithology. Differences in resistivity between the frozen and unfrozen states of a material can reach up to two orders of magnitude (Haeberli, 1985). Intrinsic variability of the resistivity of sediments due to lithology can be about an order of magnitude (Haeberli, 1985). For frozen ground in general, resistivity increases with decreasing subzero temperature and increasing ice content, with a slight influence from lithology.

The main influence on the resistivity of ice-rock mixtures is the unfrozen water content. As electric currents are transported by ionic conduction in the liquid phase of water, geoelectric methods are particularly sensitive to changes in the unfrozen water content of the ground. High specific resistivities therefore suggest an absence of ionic conduction, and the presence of ice. Unfortunately, since both air and ice-filled pore spaces have high resistivities, resistivity tomography is unsuited to distinguish between ground that is dry and unfrozen, and frozen ground (Hauck et al., 2007). For example, a frozen silt can have a lower resistivity than an unfrozen sand.

Distinguishing between bodies of ice and ground containing ice can be more feasible. Frozen sediments and glacier ice are difficult to mistake as the difference between the two materials is at least an order of magnitude (Haeberli, 1985). The electrical DC resistivity of polar ice is in the tens of $\mathrm{M\Omega \cdot m}$. However, the resistivities of extremely ice-rich permafrost and buried snowbank ice may approach each other. Perennial snowbank ice has slightly lower values of 1–10 $\mathrm{M\Omega \cdot m}$ from laboratory studies (Haeberli, 1985). If pure ice occurs at the surface, it may cause problems with the detection of underlying lower-resistivity frozen ground.

Resistivity data presents an inverse problem. This inversion can be made using a standard algorithm (Loke and Barker, 1995), which is implemented in the Geotomo RES2DINV program. This determines a two-dimensional resistivity model for the subsurface through a non-linear least-squares optimization technique. The resistivity model obtained is not unique and therefore its interpretation is ambiguous, though the major features of models from different inversions should be similar. This problem is shared with most geophysical techniques (Hauck et al., 2007). The model depends on data quality, measurement geometry and the choice of inversion parameters (Hauck et al., 2003). Iterations of the model were set to stop when the change in RMS error went below 0.5%.

The Wenner array used in this study (§ 3.2.2, § 3.3.2, § A.1) produces data sets with a characteristic

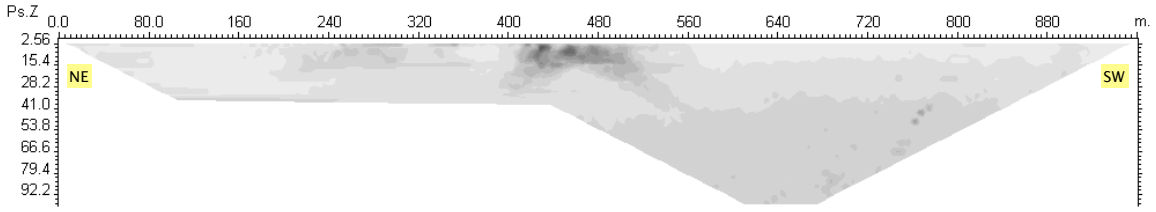

Figure 4.1: The apparent resistivity measurements for the Victoria transect shown in a pseudosection. One partial (left side) and one complete data set have been combined.

triangular profile. At the edges of the data set there are fewer measurement points than in the centre, and this lack of data can create anomalous features. As a result, the bottom corners and regions close to the subsurface sides will have larger uncertainties. The resolution of features in the centre is dependent on the current flow path coverage. Uncertainty in the centre can be ascertained by considering the point-to-point uncertainty and sensitivity of the profile.

The slack in the resistivity cables needed to allow for rises and dips of the ground decreased the electrode spacing from the nominal spacing of 5 m by up to 0.3 m. Electrode placement alteration from the theoretical profile used by the modelling may introduce noise and false anomalies to the subsurface model (Szalai et al., 2007). This possibility is increased in regions of high rockiness and undulating terrain like the two field sites (Szalai et al., 2007). However, this risk was reduced by the large electrode spacing used in the fieldwork, which reduces the percentage positioning error of the electrodes. In Victoria Valley, the positional inaccuracies could slightly displace the modelled features from the true terrain features, as the recorded terrain was measured independently of the electrodes (§ 3.2.1). The topography measurements were aligned with the electrodes in Beacon Valley (§ 3.3.1).

4.1.1 Victoria Valley

The combination of an incomplete and a complete data set (Fig. 4.1) made the inversion problem more difficult. The assumption of moderately damped topographic influence was made for the modelling. Fig. B.1 in § B.1 indicates that poor sensitivity, where present, is at and close to the surface. This is as expected from the difficulties found with contact resistances in the field (§ 3.2.2).

The modelled subsurface structure (Fig. 4.2) is displayed over two scales to highlight different features at different depths. Note that subsurface resistivities in the Dry Valleys were found to be extremely high, much more so than typical measurements in temperate areas, where the range is from tens to several hundred $\Omega \cdot$ m. However, because of the enhanced salt content, the resistivity values in the Arctic and Antarctic lowlands are in general reduced from the corresponding resistivity values in mountain regions (Guglielmin et al., 1997). Discussion here of “high” and “low” resistivity is therefore in relation to the range of resistivities seen in the subsurface. Since this transect covers 960 m, “small” is also considered to be at the minimum resolution of the data, dictated by the 5 m electrode spacing interval.

The geophysical tomogram Fig. 4.2(a) shows that the very top of the surface is moderately re-

sistive, and the shallow subsurface has substantially lower resistivity. Low resistivity values could indicate a low ice content (Hauck et al., 2003). However, an enhanced salt content, possibly in combination with a high unfrozen water content, could obscure the presence of significant amounts of ice in the soil (Guglielmin et al., 1997). This would also produce the low resistivities that form a consistent subsurface zone across the entire profile between depths of $\sim$ 60–80 m. This zone is particularly distinct in the north-east half of the tomogram.

There are also clear markings near the surface to the south-west of the 560 m mark, semi-regularly spaced vertical zones of alternating higher and lower resistivities. As these are five to ten metres wide, they are at the limit of spatial resolution. Their vertical extent varies slightly, but is about ten metres. Polygons in this area are still ten to twenty metres in size, so these vertical zones are about half a polygon in size.

The most interesting features of Fig. 4.2(b) are the discrete regions of very high resistivity (greater than 240 k$\Omega \cdot$m). These concentrated objects are in the shallow subsurface, beginning from two to ten metres below the surface and extending down no further than twenty-five metres. They vary in lateral extent from ten to eighty metres. There are also more tenuous, smaller high-resistivity areas near the stream. The small area of flatter polygonal ground halfway up the hill appears to correlate well with a very small high-resistivity region just below the surface, at $\sim$ 2 m depth, at the 815 m mark.

There are three candidates for the material of these regions, and all explicitly involve ice. Ice-cemented masses of clasts, perhaps of different material to the surrounding deposits, with a very high ice content, would have different resistivities to the surrounding sediments. However, even a high content of segregated ice would probably not produce resistivities of the magnitude measured. Glacial moraines are frequently ice-cored, and the position of these objects in the centre of the valley floor is not inconsistent with the site of a small terminal moraine that has been subsequently overridden, although only hummocky moraine is visible on the surface. Buried bodies of massive ice from the lake that overlay the area or left from the retreat of the Victoria Upper Glacier are also a possible explanation of these measurements. The burial mechanisms for such glacial ice are well understood. Either a buried ice lens or an ice-cored moraine is probably the most feasible explanation, as only the resistivities of massive ice would be sufficiently high.

Shallow-depth, high-resistivity anomalies in Antarctic permafrost have been identified before. Hauck et al. (2007) interpreted a body at 2 m depth of 7 k$\Omega \cdot$m in an otherwise homogeneous substrate of 2–3 k$\Omega \cdot$m at Refugio de Motos, Livingston Island[1], as permafrost with a higher ice content than elsewhere. Resistivity tomography by Hauck et al. (2007) of an ice-cored moraine at Caleta Argentina on Livingston Island showed the core to have a resistivity of 7–14 k$\Omega \cdot$m and unfrozen moraine material within the 2–3 m thick active layer to be 1.3–2 k$\Omega \cdot$m (Hauck et al., 2007). The core of the similar moraine in Caleta Española had higher specific resistivities, 25–40 k$\Omega \cdot$m, possibly indicative of higher ice content or less unfrozen water. These resistivities are an order of magnitude lower than that of the objects found in this study.

[1]Livingston Island is one of the maritime Antarctic South Shetland Islands.

In comparison, ice-cored moraines in the European Alps have core resistivity values of several hundred k$\Omega \cdot$m, and unfrozen debris resistivities are 10–50 k$\Omega \cdot$m (Hauck et al., 2003). These values are much closer to those found here.

The electrical and seismic properties of rock, water and soil samples from the Dry Valleys of Antarctica have been measured through a range of temperatures (-76°C to $+24^{\circ}$C) (McGinnis et al., 1973). At 0°C, saturated porous soils and rocks had resistivities less than 700 $\Omega \cdot$m, while non-porous rocks had resistivities up to 5 k$\Omega \cdot$m. Indeed, a saturated, saline soil at 20 m depth could have resistivities as low as 10–15 $\Omega \cdot$m, although these resistivities were not observed by this fieldwork at those depths in any detail. This may have been due to the low spatial resolution of the measurements. Some of the resistivities in the near-surface parts of Fig. 4.2(a) do appear sufficiently low.

McGinnis et al. (1973) found that materials with resistivities less than 700 $\Omega \cdot$m could be below -60°C if they had high pore water salinity. The depression of the freezing point by the salts may be sufficient to prevent permafrost from solidifying, permitting the movement of pore fluids. The areas of low resistivity underneath the high-resistivity zones near the surface have resistivities in these ranges (see Fig. 4.2(a)), and may be indicative of such a high-salinity, low-temperature permafrost environment. This might also suggest that the ground is unfrozen (McGinnis et al., 1973). However, a low-temperature ($\sim -18^{\circ}$C), permeable quasi-permafrost soil should have resistivities less than 1 k$\Omega \cdot$m (McGinnis et al., 1973), and this resistivity range is fully consistent with the zone underlying the top $\sim$ 10–15 m of sediments seen in the resistivity profile (Fig. 4.2(a)).

The south-west side of Fig. 4.2(b) shows a gradual increase in resistivity with depth from $\sim$ 70 k$\Omega \cdot$m up to $\sim$ 130 k$\Omega \cdot$m, with some localization into a prominent peak-shaped feature. Correlation with other data is needed to confirm if this high-resistivity feature could be bedrock (see § 4.3, § 4.4). The change in resistivity that appears gradual with increasing depth around the feature would be surprising for an interface between bedrock and valley sedimentary fill. In reality, the resistivity change may be quite sharp, with the gradual appearance due to the volume averaging of the resistivity tomography method. Erosional weathering at the top of the basement that has been overlain by the valley fill is also likely. Bad data points in a linear cluster between 680 m and 780 m do correlate exactly with the "peak" (Fig. 4.1), suggesting that the sharp point of the peak is an artefact.

The resistivities of the gradual increase are somewhat higher than those previously measured for Antarctic bedrock. Frozen quartzite and shale bedrock on maritime Antarctic Livingston Island was found to vary in resistivity between 1.5 and 10 k$\Omega \cdot$m, depending on its unfrozen water or salt content and the bedrock type (Hauck et al., 2007). McGinnis et al. (1973) suggested from comparison of their sample measurements with field geology that resistivities between 1 and 10 k$\Omega \cdot$m indicate bedrock or confining permafrost conditions in unconsolidated material, and resistivities greater than 10 k$\Omega \cdot$m indicated frozen bedrock or glacial debris. The resistivities of bedrock can be above 100 k$\Omega \cdot$m, especially when frozen. With reference to these values, the resistive material at depth in Victoria Valley should be bedrock.

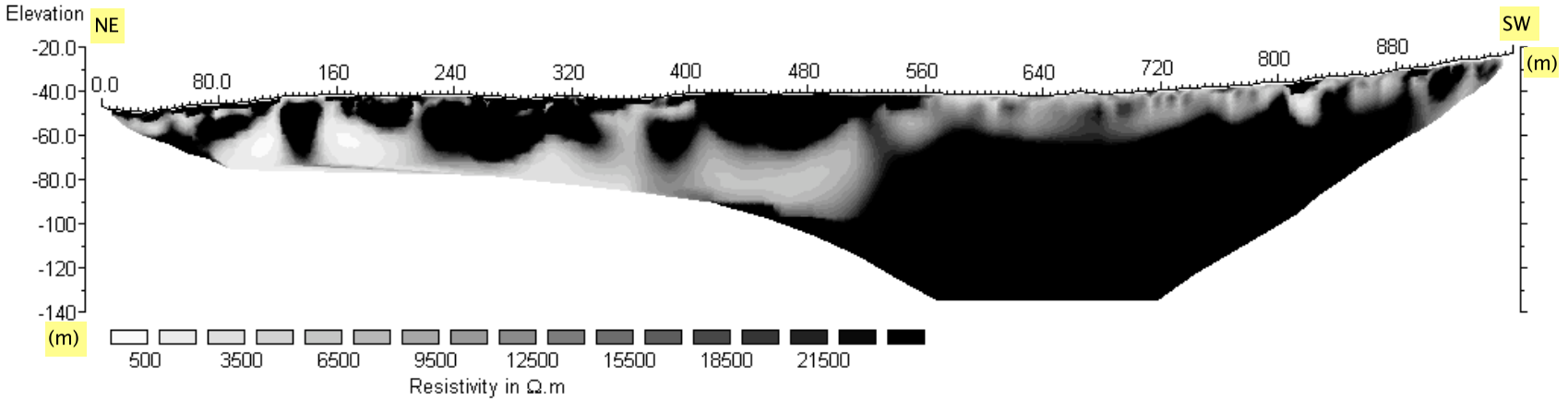

(a) Low-resistivity detail of subsurface, scale from 500 $\Omega \cdot$ m – 24.5 k$\Omega \cdot$ m. See text in § 4.1.1.

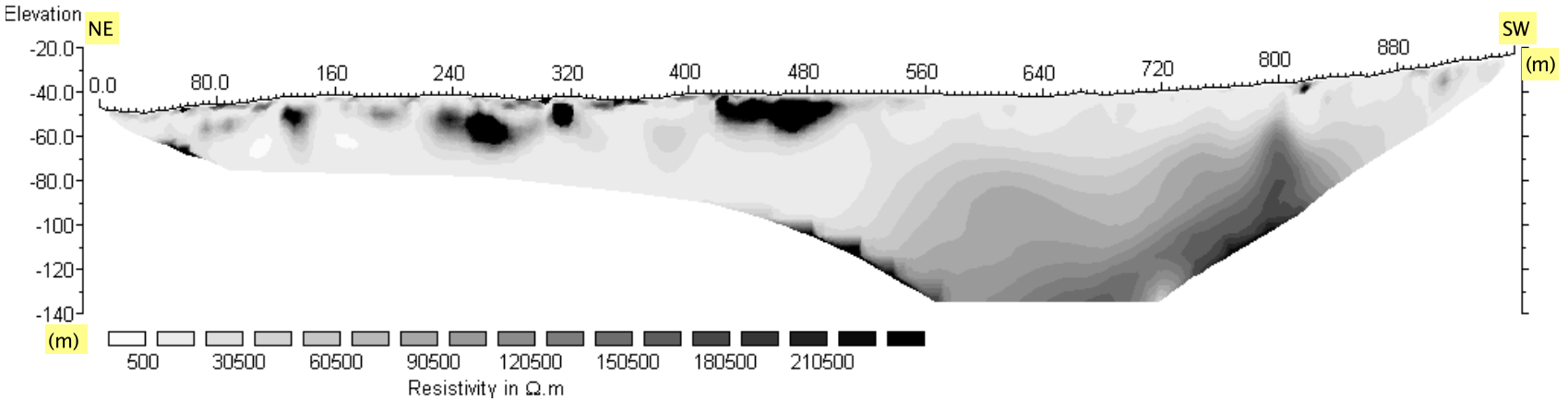

(b) Higher-resistivity detail in subsurface, scale from 500 $\Omega \cdot$ m – 240.5 k$\Omega \cdot$ m. Note the edge effects at the lower levels between 460 m and 560 m, created at the join between complete and incomplete data sets (see § 4.1.1).

Figure 4.2: Victoria transect resistivity model produced with the setting of damped topographic influence (see § 4.1.1). Topographic corrections are from the field measurements (§ 3.2.1).

4.1.2 Beacon Valley

The three complete and error-free data sets obtained could be merged into an extensive tomogram with little trouble, other than that caused by the astonishingly high resistivities (Fig. 4.3). The modelling allows adjustment of the degree of influence that the topography has on the subsurface. The setting of "moderately damped topographic influence" was used. This may have slightly accentuated features in the model. However, the vertical travel in this profile is significantly less than that in Victoria Valley, and the topographic influence is on a complete data set rather than a partial one. The inversion is also acting on measurements that reach to a modelled depth ten times the vertical travel. This means that the influence assumption should be well satisfied.

The area of Beacon Valley profiled in this study is known to be underlain by massive ice (R. Sletten, pers. comm., 2006). Ice is highly resistive, and therefore the large continuous resistive feature across the whole of the modelled profile (Fig. 4.4(a)) is almost certainly the massive ice body. The transition between the moraine on the valley's edge and the valley floor, which is highly distinct visually, is not immediately apparent in Fig. 4.4. It would however lie close to the eastern edge, near the 80 m mark. Possibly biasing the transect further onto the moraine would have helped define this edge, but the data at this end does extend to a depth of thirty metres, so the effect may not be due to the data coverage.

Note that there are edge effects from scarce data points in the bottom corners of the model profile between 240 m and 320 m and between 980 m and 1040 m (Fig. 4.4). These may also be contributing to the extremely high resistivity line-like feature at maximum depth (Fig. 4.4(b)). Since the feature is constructed from inversion of only three data points (Fig 4.3), the base points of the three Wenner triangular measurement distributions, it is more likely to be a modelling artefact. This means that it is very unlikely that the base of the massive ice has been resolved by this data set. However, it does provide a minimum thickness for the ice. This minimum thickness of greater than 110 m is far greater than the $\sim$ 20 m thickness that had been suggested for the ice (R. Sletten, pers. comm., 2006). It raises perplexing questions about the origin of the ice. A body of such thickness would certainly have to be glacial in origin, especially since the ice is agreed in the literature to be massive (Sugden et al., 1995; Marchant et al., 2002).

The way in which the large sinkholes correspond with vertical variation in the upper surface of the ice body is important, as the sinkholes could be produced by sublimation of the ice (Sugden et al., 1995). When excavation pits are dug, the ice generally appears to be close to the surface, half a metre or so below the glacial till (R. Sletten, pers. comm., 2006). The small undulations in the lines of constant resistivity (isograms) at the surface do reflect the local topography, though more closely in some parts than in others (Fig. 4.4(a)). In the central section, the resistivities greater than $10^6\ \Omega \cdot \mathrm{m}$ closely approach the surface, and here the near-surface isogram variation correlates very well with the local topography. At very small scales in the near surface zones, there are fine vertical structures in the zone of $10^4\ \Omega \cdot \mathrm{m}$ that are formed by intrusions of $10^5\ \Omega \cdot \mathrm{m}$ material, apparently linked to the massive high-resistivity body beneath. These features have a size and a spacing that is of the order of

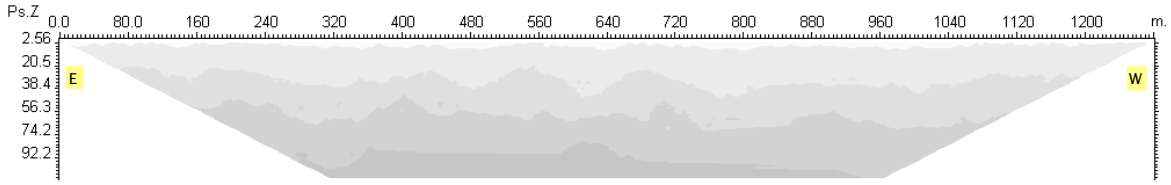

Figure 4.3: The apparent resistivity measurements for the Beacon transect. Three individual overlapping measurements have been combined into a complete data set, shown as an apparent resistivity pseudosection. The small number of bad data points appear as tiny dots of different resistivity within the zones of even resistivity.

individual polygons. They are visible across almost the entire profile.

There are also pronounced dips in the isograms at both the eastern and western ends of the profile that may or may not be artefacts. The dip at the western end correlates well with a change to flatter ground and significantly shallower polygon troughs. The eastern dip has no such relation to a surface change and is in fact the site of at least two prominent sinkholes. It is unlikely that they are artefacts as they are almost directly in the centre of the data sets obtained at those ends of the transect and therefore have good measurement coverage. This implies that the obvious ground variation at the edges of the valley does not directly correlate with the presence of subsurface massive ice.

In the tomogram highlighting the high-resistivity end of the measurement scale (Fig. 4.4(b)), the only distinct feature is narrow in lateral extent, some 60–80 m wide, but extends the full depth of the profile. It is located near to a zone of overlap of two of the data sets, and is therefore probably not an artefact. It is not clear how much variation in resistivity there can be within a massive ice body, or for that matter its significance, but the resistivity of this feature appears to exceed 10 $\mathrm{M\Omega \cdot m}$, a value that can only be found in glacier ice. Lower-scale localized variations do occur to the west of this feature. They correlate with the closest approaches of the isograms to the surface, and their contours with the surface dips. This might suggest that several large semi-vertical fractures run through the ice body and correlate with the surface dips.

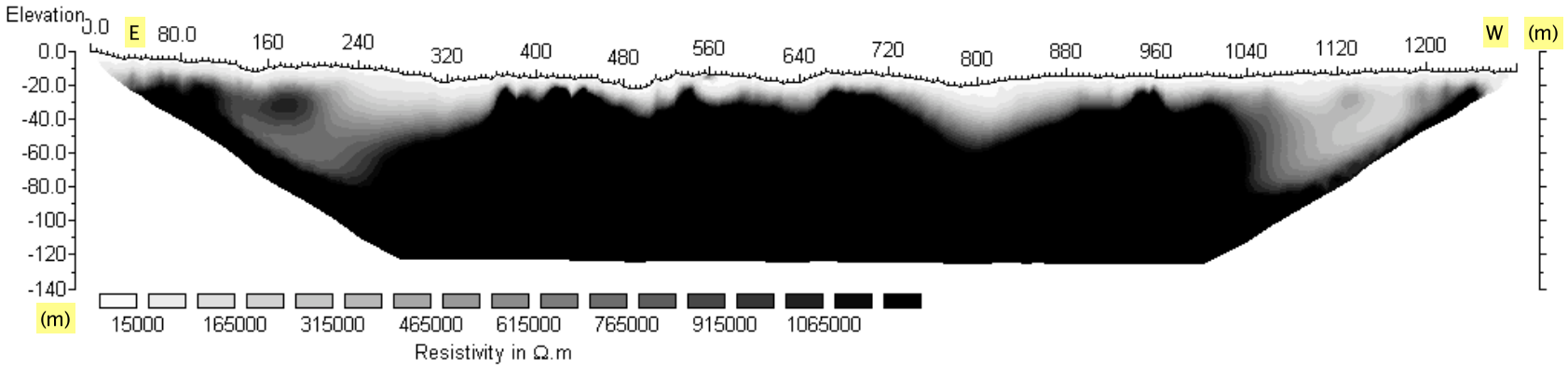

(a) Low-resistivity detail in upper subsurface, scale from 15 kΩ · m – 1 MΩm.

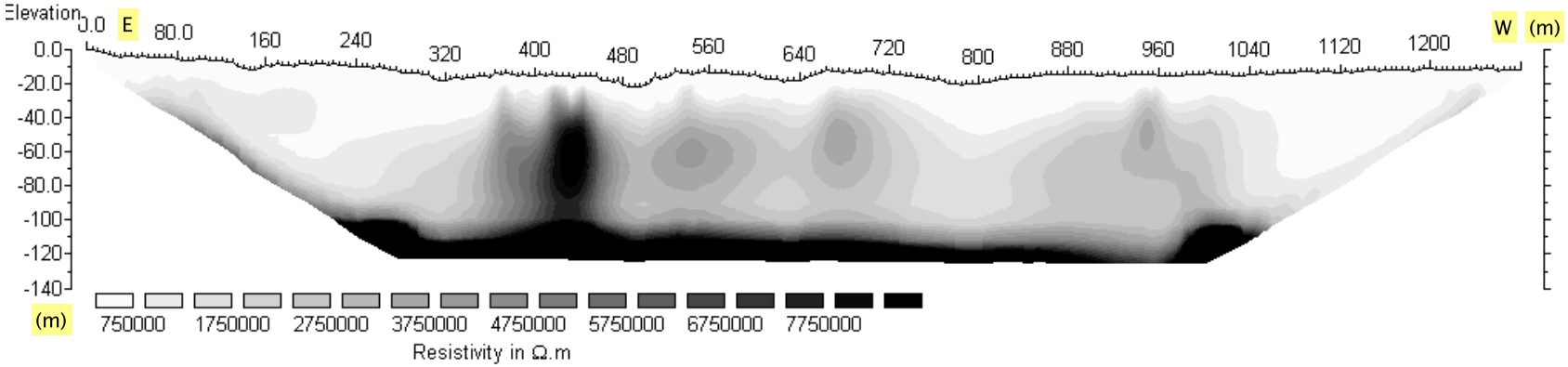

(b) High-resistivity detail in lower subsurface, scale from 0.75 – –7.75 MΩ · m.

Figure 4.4: The model of the Beacon resistivity tomography results processed with the setting of damped topographic influence. Topographic corrections are from the field measurements (§ 3.3.1).

4.2 Ground-penetrating radar

Propagation of electromagnetic waves is more complicated in ice-rock mixtures than in pure ice. Strong attenuation can reduce the penetration depth to a few tens of centimetres, with specific absorption up to an order of magnitude higher in permafrost than in pure ice (Haeberli, 1985). Attenuation is also severe in such fine-grained sediments as clays and silts. Variability of the electrical properties of permafrost material results in a variable wave velocity, the crucial property used to process the radar data.

Part of the ground-penetrating radar signal emitted as a focussed electromagnetic impulse is reflected at boundaries where the electrical properties of the subsurface material changes. The relative dielectric permittivity of materials is primarily determined by their unfrozen water content and partly by lithology. In frozen sands and gravels, the unfrozen water content is about 5–10% by volume in the active layer, asymptotically increasing to $\sim 15\%$ above the base of the permafrost zone (Haeberli, 1985). Well-frozen sands with some excess ice have dielectric coefficients that are little different from pure ice, while dry or frozen sands have dielectric coefficients in the range of 2 to 5. Pure ice in temperate regions has a dielectric coefficient of 3.2 and an attenuation of ~ 0.1 dBm^{-1}. Polar ice generally has even less attenuation.

Penetration depth in ice is a function of the strength of the impulse emitted and the ice thickness, in situations where the background noise is low (Haeberli, 1985). Changes in attenuation, scattering and reflection coefficient can be used to observe changes in the type of subsurface ice (Haeberli, 1985).

Processing of the ground-penetrating radar data used the pulseEKKO v.4.32 software (Sensors and Software, 1996). This processing was iterative, with multiple readjustments of the processing parameters needed to best remove noise and bring out the main features of the data. Filtering to remove noise spikes was more successful on the Beacon data set than on the noisier Victoria set. The cause of the greater noise in Victoria Valley is unknown. A temporal α filter (median filter) with width of 9 traces averaged to 3 points best removed the noise. The merged and filtered file was then processed ("migrated") using a standard Fast Fourier Transform (FFT) to collapse the diffraction curves (details in § B.2). A FFT was used as the alternative method, synthetic aperture migration, can produce more artifacts.

Successful processing is dependent on finding the right electromagnetic wave propagation velocity. This was determined by a common mid point survey (CMP) (§ A.3) in Victoria Valley, which gave a value of 0.13 ns·m^{-1}. Since the terrain precluded measurement of a CMP in Beacon, the closest velocity was found by trial and error, using the Victoria velocity as a starting point. Comparison of the Victoria migrations at velocities from 0.07 to 0.17 ns in steps of 0.02 ns can be seen in § B.2, Fig. B.4.

Correct processing collapses the diffraction curves back to points, while over-migration converts the diffraction curves into upturned parabolas. This is a check on the CMP velocity. Thick upturned parabolas are generated by natural features, and thin, line-like parabolas are produced by noise.

4.2.1 Victoria Valley

The prominent features of the GPR profile across Victoria Valley (Fig. 4.5) are the roughly continuous linear reflectors at a depth of $\sim$ 20 m. The reflectors are mainly parallel to the surface. The most prominent of these features is between the 135 m and 555 m marks. Its position correlates partly with the large area of very flat low-relief polygonal ground. It correlates very roughly with the increase in resistivity at a depth of $\sim$ 20 m seen in the resistivity tomography (Fig. 4.2(a)), and could be indicative of a change in the properties of the high-salinity permafrost suggested by those measurements. It can be traced with decreasing strength back to the edge of the moraines high up on the hill. There are some small, short and closely stacked reflectors in the approximate location of the buried ice bodies identified in the resistivity tomography (§ 4.1.1). To the north-east of this, the rock-rich hummocky moraine landscape has created too many diffractions to provide clear signals, although a slight continuation of the earlier linear reflector, at almost the same depth, can be seen.

Haeberli (1985) suggests that a permafrost basal zone of increasing liquid water content may be typical. It would increase scattering and reduce the reflection coefficient as the dielectric constant smoothly increases. However, the base of permafrost in Antarctica is likely to be at least several tens of metres deep (McGinnis et al., 1973; Haeberli, 1985), and the other methods (§ 4.1.1, § 4.3) suggest that the bedrock base is considerably deeper than the 40 m depth reached by the GPR. The near-surface, roughly parallel reflectors may indicate sediment layering.

4.2.2 Beacon Valley

The ground-penetrating radar in Beacon Valley was not overly affected by the abundant rock cover of the surface. However, very few clear linear reflectors could be determined, and much of the profile (Fig. 4.6) appears filled with indistinct features that are roughly parallel, but chaotic. The clearest feature is a linear reflector between the 540 m and 620 m marks, with an eastward apparent dip. It could indicate a boundary within the ice, correlating to ice of different ages. This possible boundary could also be generated by aggradational ice forming on massive glacial ice, although given the dry environment of Beacon Valley, this would be unlikely. It is unlikely to be related to the polygons above due to its size, though it does appear to reach the surface. A shorter reflector dipping at the same apparent angle sits near the surface, underneath a sinkhole, between the 630 m and 660 m marks. Other, smaller, reflectors are likely to be prone to "pattern recognition" errors in identification.

Debris-covered glaciers have provided radio-echo sounding signal returns from depths near 100 m. In contrast, the returned radio-echo signal diminished by an order of magnitude in periglacial rock glacier soundings, indicating stronger absorption and scattering (Haeberli, 1985). Surface debris does not seem to have caused much attenuation here, possibly supporting a glacial origin model for the Beacon Valley ice. In contrast to the basal permafrost liquid water boundary, glacial ice has no major transition at the glacial bed (Haeberli, 1985), so even if linear reflectors at that depth were visible, this method would not be more effective than the resistivity tomography for finding the depth of the ice-bedrock interface.

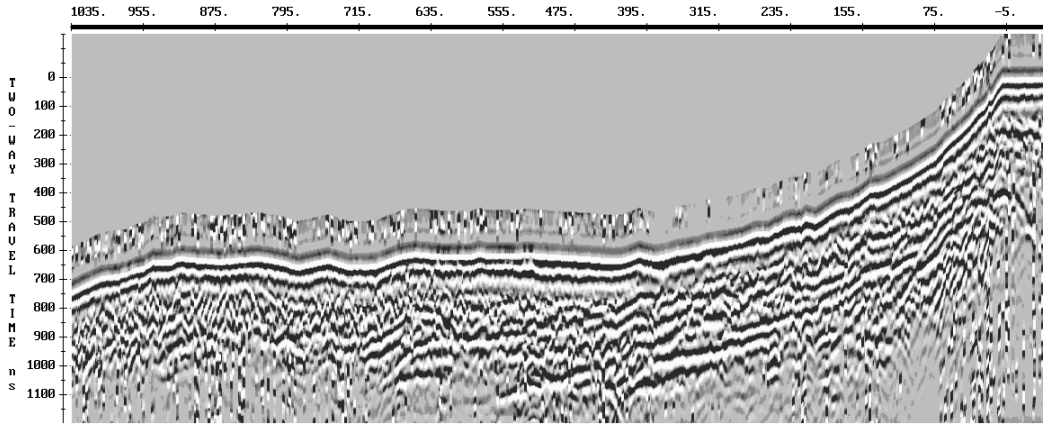

(a) Clipped profile filtered with a temporal 9-point alpha filter, with topographic correction from the field measurements (§ 3.2.1).

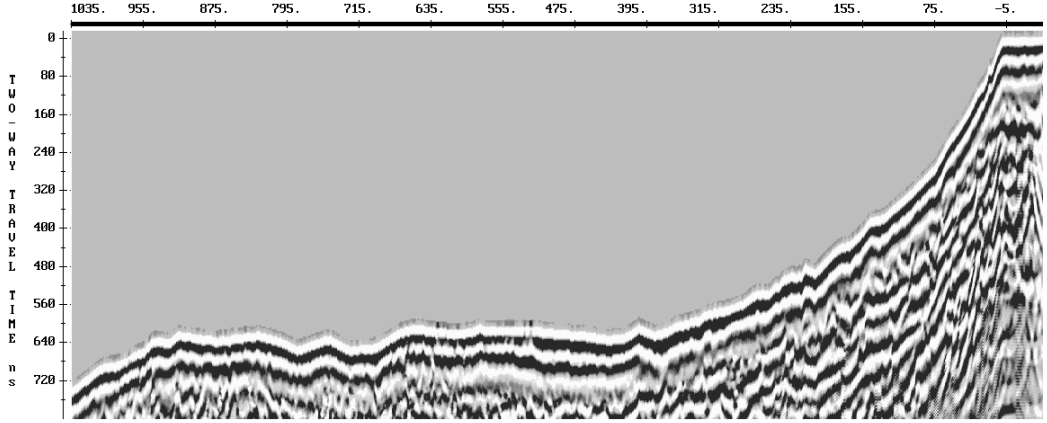

(b) Migration of the profile in Fig. 4.5(a), at a velocity of 0.13 ns·m^{-1}, with topographic correction from the field measurements (§ 3.3.1).

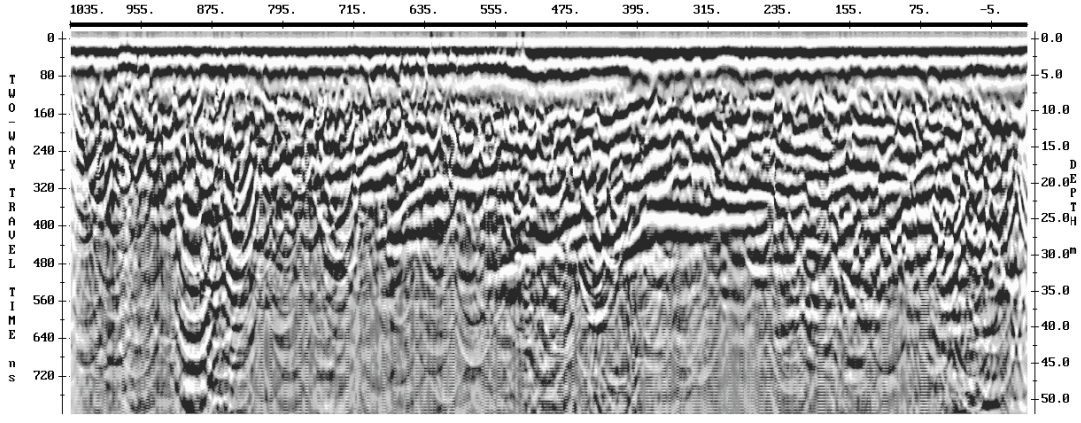

(c) Migrated transect, ns·m^{-1}, without topographic correction.

Figure 4.5: Unprocessed and processed ground-penetrating radar profiles, Victoria Valley. Both the topography-corrected and uncorrected processed profiles are included to more clearly show the features after migration. The small "step" at the south-west end of the profiles is a topography correction artefact. As with the other profiles, north-east is at the left, but here the distance scale has its zero point at the south-west end.

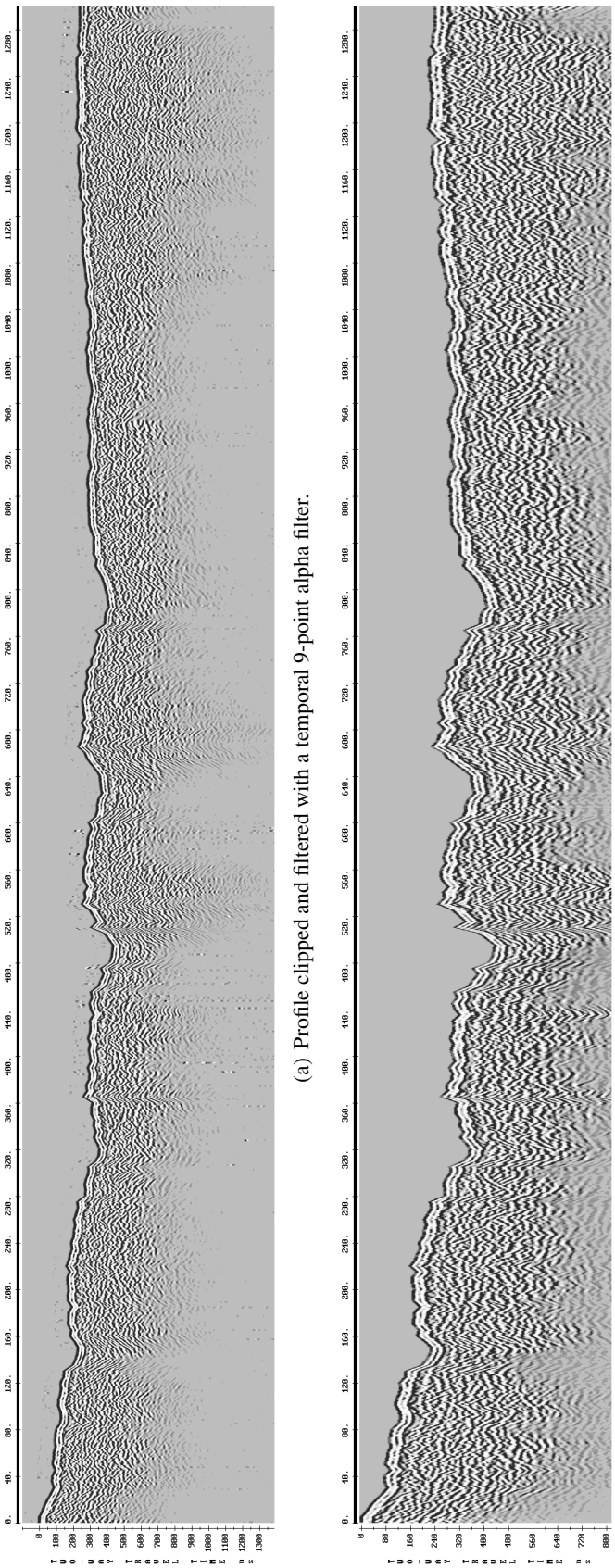

(a) Profile clipped and filtered with a temporal 9-point alpha filter.

(b) Profile processed with a resampling frequency of 3200, a rescaled window of 512 points, and a velocity of 0.10 ns.

Figure 4.6: Ground-penetrating radar profiles with topographic correction, Beacon Valley.

4.3 Time-domain (transient) electromagnetism

This method is sensitive to subsurface vertical layering (stratified sediments). Transient electromagnetism (TEM) decays quickly to an asymptotical value, so the resistivities and depths of the upper subsurface layers are those best constrained by modelling of the data. Transient EM sounding methods are designed to be interpreted with a layered earth solution. If the subsurface is laterally inhomogeneous, the modelling results may not relate to the actual subsurface structure (Interpex Ltd., 1993).

Modelling was made using the Interpex TEMIX-GL v.3.24 DOS-based software, which is designed to interpret transient electromagnetic sounding data taken by the commercial Geonics PROTEM instruments. This software fits a one-dimensional layered earth model to the sounding curves of the measured ground response, calculating a synthetic electromagnetic sounding curve.

Data sets of four measurements were loaded from the file recorded by the instrument. Points were masked from consideration by the fitting from the point where the decay curve degenerated into noise. If a point appeared to continue the curve, but was within the noise regime as defined by its surrounding points, it was eliminated.

The smooth models of the data (Appendix B.3.1) use constant thickness layers to approximate a quasi-continuous model. An inversion using resistivity as the only parameter, the smooth model can be used to guide construction of the layered model. It is also a check on the layered model — if features not present in the smooth model appear in the layered model, the layered model may be overly complex.

The layered models were created through defining the thickness and resistivity of several ground layers, according to the smoothed models. This creates a geological model with physical properties that have a response approximating that of the observed data set, and displays a synthetic curve with a percentage fitting error. TEMIX converts between measurement time and physical depth using the model's mean conductivity and the diffusion depth formula. The thickness and resistivity of each layer were then adjusted, refining the model. In general it seemed best to apply Occam's razor and use the fewest possible layers. When a model that had a very low error was found, a full least-squares inversion using ridge regression was made. This provided the best estimate of the model's fit.

The final step required equivalence analysis to generate a set of equivalent models. The parameter resolution matrices were calculated to determine the unknown linear combinations of model parameters and the allowable range of each parameter (Appendix B.3.3). These matrices are important as they provide information on whether each parameter is separately resolved, or if the parameters are only resolved in combination. A uniquely resolved parameter has a value in the matrix close to 1. The deviation of the equivalent models from the best-fit model is limited by the data, and so provides a measure of the uncertainty in the best-fit model. Two equivalent models were generated for each parameter of the model (resistivity, thickness, conductance), with an error limit for the models of 1.2% of the best-fit error.

The modelling was successful for at least four of the seven field measurements made. However, having a second measurement time window at some of the sites did not seem to improve the fit at

those locations. Only one or at most two of the data points within the second time window were usable due to increased noise in that regime. That a second window could be taken at all did indicate high accuracy from good signal strength in the first time window. Overall, the models appear to be useful to a depth of at least one to two hundred metres, but their reliability will decrease below that depth. However, this still extends the depth range covered by the set of methods.

Additionally, the `plot linear` command can be used to determine if a conductor is confined or infinite: lithological layers can be treated as infinite, while mineralized bodies are finite. Finite conductors have transients that decay exponentially, so their late-time normalized voltages become linear (Interpex Ltd., 1993). This can be used as a check for three-dimensional effects on any ambiguous data.

The data from the Victoria Valley sites began on the slope of the hill (Fig. 4.7(a), 4.7(b)) and then moved onto the valley floor (Fig. 4.7(c), 4.8(a), 4.8(b), 4.8(c)). One was adjacent to the stream (Fig. 4.9(a)). The most interesting layer appears at the second site down the hill, site 6, and is also present at sites 5 and 4, with a possible appearance at site 7 (Fig. 4.9(a), 4.8(c), 4.7(b), 4.7(a)). It is a layer with exceptionally low resistivity. In all well-defined cases its resistivity less than 30 $\Omega \cdot$ m, and is also only two to five metres thick. It is very thin in comparison with all other features modelled by the TEM. The smooth models support its existence (§ B.3.1). Since these sites as a group cover the full transect, with sites 7 and 6 adjacent and sites 5 and 4 only separated by a hundred metres, continuity of the layer between sites will map its progression across the full profile, assuming it is a linear subsurface feature.

The first site up on the hill (Fig. 4.7(a)) does not precisely show the linear spike seen in the other models, but has the same 50 m thick "wedge" of decreasing resistivities displayed around the spike by the other sites, though it is poorly resolved. The centre of this wedge could be used to infer a projected spike depth of $\sim$ 170 m. Site 7 has lower subsurface resistivities than the other sites that feature the spike, with a modelled near-surface layer of well resolved 2 k$\Omega \cdot$ m resistivity and thickness and an unresolved below-wedge resistivity of 45 k$\Omega \cdot$ m.

The second site (Site 6), immediately adjacent to the first and on visually identical terrain slightly down the slope of the hill, is the first to clearly show the spike feature (Fig. 4.7(b)) at a depth of 120–150 m. It sits below a layer of highly resolved resistivity and thickness. Site 6 has a very high-resistivity layer of unresolved thickness within 20 m of the surface, which is consistent with the depth of the boundary to resistivity that was detected by the resistivity tomography (Fig. 4.2(a)). The uncertainty may be more influenced by the broad scatter of some of the data, as shown by the masked points on the data plot (Fig. 4.7(b)).

Site 1, the first site on the flat area of the former lake delta, shows a data set that appears poor and shows little of the expected profile of a good decay curve. Nonetheless, a one-dimensional layered model of great simplicity could be fitted to it with surprisingly little uncertainty, providing very good constraints on the subsurface structure. This model shows an absence of subsurface variation, with an intriguingly low resistivity of 600 $\Omega \cdot$ m that is several hundred $\Omega \cdot$ m less than found at these depths

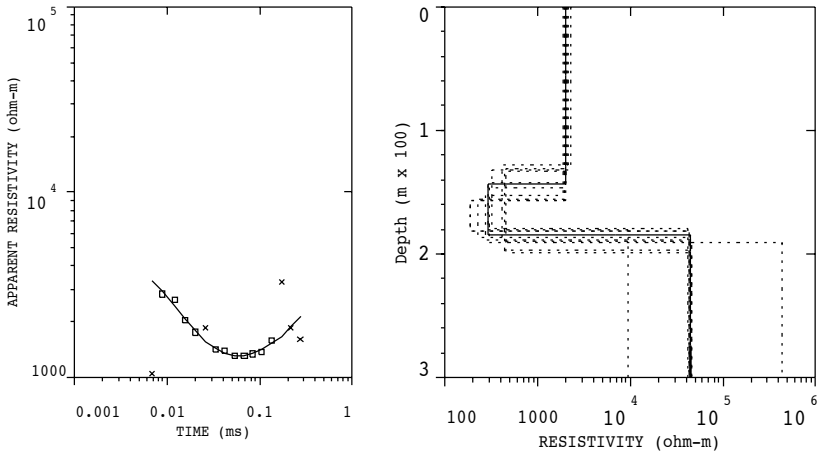

(a) High on hill slope (Site 7). Fitting error 4.4%.

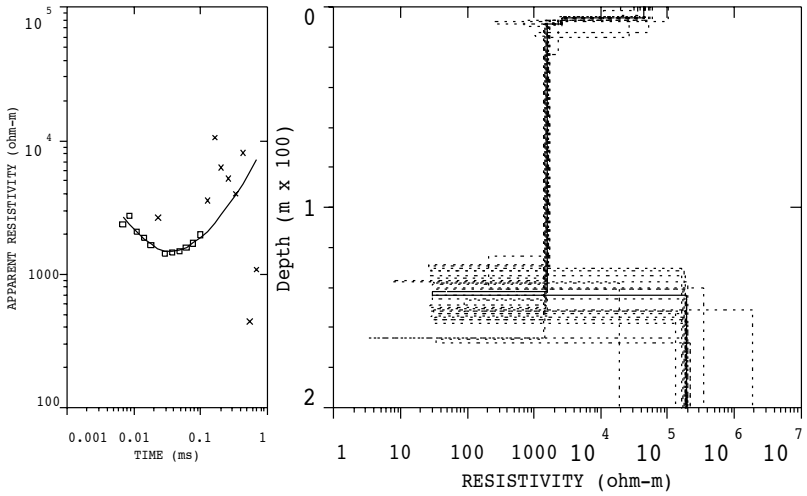

(b) On moraine material on hill slope (Site 6). Fitting error 10.0%.

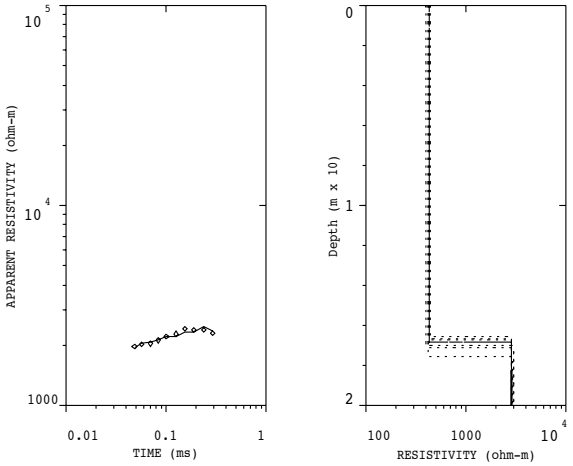

(c) On the young, flat, patterned ground (Site 1). Fitting error 3.2%.

Figure 4.7: Time-domain electromagnetism data sets from Victoria Valley with synthetic curve (left), and resulting one-dimensional layered earth model (solid line) with equivalent models for uncertainty (dashed line) (right). Data points masked from the modelling are indicated by crosses. Site locations are shown in Chapter 3 in Fig. 3.4.

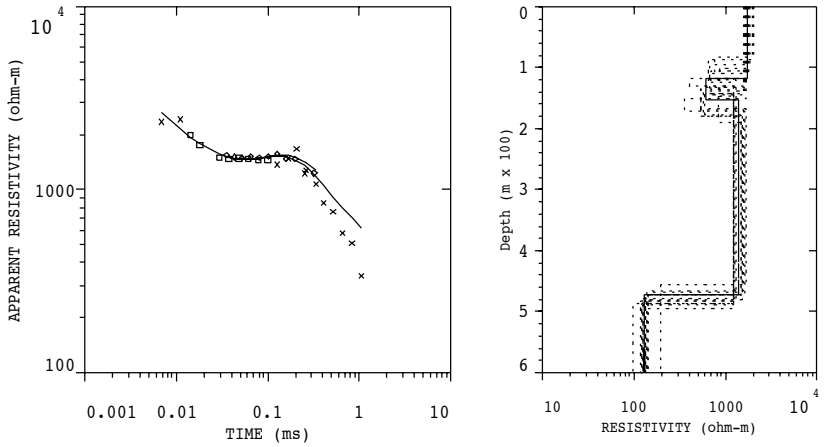

(a) Very flat polygons (Site 2). Fitting error 3.4%.

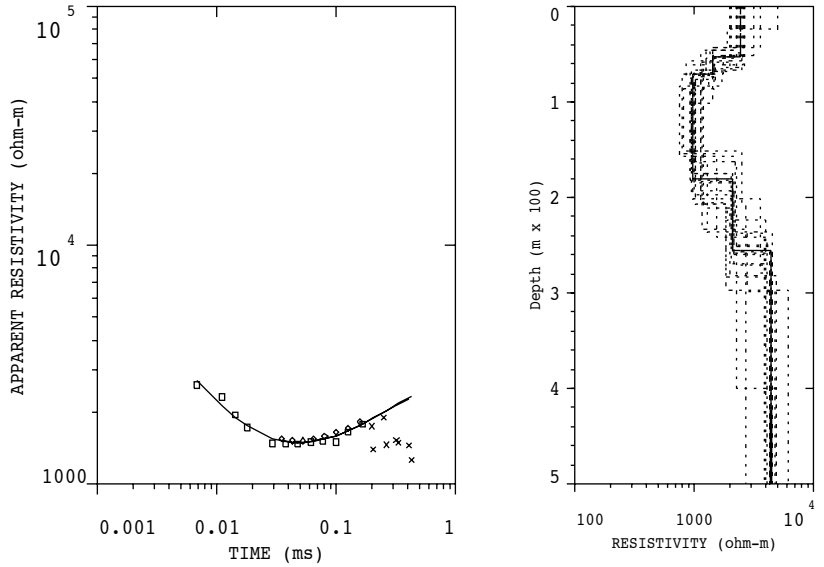

(b) Very flat polygons close to camp (Site 3). Overlaps Site 2 by 25%. Fitting error 5.2%.

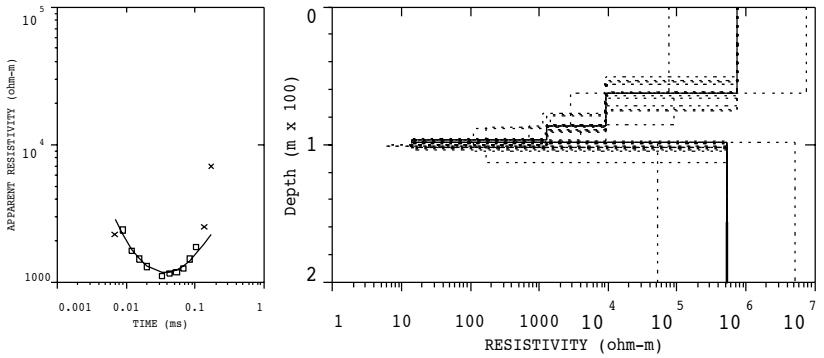

(c) Slightly raised polygons close to camp (Site 5). Fitting error 8.7%.

Figure 4.8: As for Fig. 4.7, for sites 2, 3 and 5 (locations in Fig. 3.4).

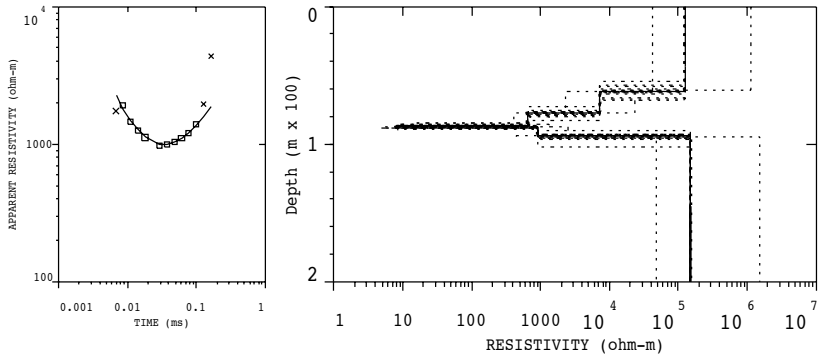

(a) Undulating moraine with polygons, bordered by the lake shore (Site 4). Fitting error 3.4%.

Figure 4.9: As for Fig. 4.7, for site 4 (locations in Fig. 3.4).

in the previous sites, until a depth of 170 m is reached and the resistivity escalates to a more standard 3 k$\Omega \cdot$m. This resistivity is well resolved (§ B.3.3). The extreme simplicity of this model in a region well defined by the resistivity tomography may suggest some modifying three dimensional effects, although it could be due to the change in slope angle that began at the south-west side of the loop.

Site 2 shows an excellent decay curve with a clear and expected shape. It could be modelled with good constraints. In the first hundred metres it is well resolved in thickness and resistivity. The resistivity is consistent with two of the three previous sites. The $\sim$ 40 m thick layer of unresolved thickness (§ B.3.3) that shows a slight drop of a few hundred $\Omega \cdot$m may be a modelling artifact, though its existence is suggested by the smooth model (§ B.3.1, Fig. B.6(a)). The great depth reached in subsequent layers is not entirely convincing, although the order-of-magnitude similarity of resistivity to the layers above is at least consistent, and is well resolved (§ B.3.3). However, the decline in resistivity at these depths could be a manifestation of the increased noise at later return times.

A second model with more layers was created for the data from Site 2 to show the effects of adding more layers and obtaining a fit with similar fitting error (3.6% for this model) (Fig. B.8(a)). This model had an extra layer, but examination of the resolution matrix shows that it is not resolved, and therefore little different to the layer above it. It has also reduced the resolution of the first layer. The first model (Fig. 4.8(a)) is therefore the one used in the interpretation.

Two model suites were plotted to show the effects of varying the model parameters. The first was a variation on the thickness of each layer in steps of 10 m from 10 to 70 m (Fig. B.8(b)). The second varied resistivities in the third layer from the surface by steps of 100 $\Omega \cdot$m from 700 to 1300 $\Omega \cdot$m (Fig B.8(c)).

Site 3 and Site 5 both sit adjacent to the transect on the wide area of flat patterned ground. Site 3 has data with some noise, and when modelled a fit with a reasonably small error could only be obtained by a more complex model with six layers. This model could not be simplified without immediately increasing the uncertainty of the fit to over twenty per cent. Near-surface resistivities remain around 2–4 k$\Omega \cdot$m, and show more complexity than in the same depth range of Site 2 (Fig 4.8(a)). There

is a moderately well constrained less resistive 1 k$\Omega \cdot$m layer from 70 to 180 m depth. The thinner layers either side of this less resistive layer are not resolved. Below this the resistivity is resolved and does increase, but remains below 6 k$\Omega \cdot$m. This is not consistent with the resistivity tomography measurements over the same area. Site 5 shows the spike feature (Fig. 4.8(c)) at a depth of 100 m. The relatively high uncertainty from the modelling of site 5 may be due to the difficulty of fitting a model to the pronounced parabolic curve of the data, possibly indicating three-dimensional effects. Very little of the model is resolved at all (§ B.3.3), only the thickness of the first layer.

If the spike feature is taken to have lateral continuity, the models show a gradual but slight progression of it towards the surface with increasing distance across the valley. At Site 4 (Fig. 4.9(a)) it is at 85–90 m. Site 4 is otherwise very similar to Site 5 (Fig 4.8(c)), and has an almost identical parameter resolution matrix (§ B.3.3). This is interesting to consider as they lie on visually different polygonal terrain. The resistivities of the layers surrounding the spike are uniformly of order 10^5 $\Omega \cdot$m for Sites 6, 5, and 4, consistent with the resistivity tomography measurements.

There are several possible explanations for the nature of the spike feature. The possibility that it is an artifact of the data is decreased by its appearance on multiple data sets at different locations, and its lack of appearance on all the data sets. If it were a systematic effect, it would be expected to be consistent, but it varies considerably in its properties between data sets. It is also well fitted by most of the models that reveal it, although some models do have very tentative layer resolutions. The model with the poorest fit has an uncertainty of 10%, most of which is the uncertainty in the exact depth of the feature rather than in its existence. TEM as a method most effectively sees conductive layers, so is likely to detect such layers that are present. The possibility that the layer is bedrock is unlikely, as there are signals of some detail returned from depths below it. One explanation is that it is a layer of clay or clay till, which have comparably low resistivities. The multiple glaciations in the valley would be likely to have deposited such till layers.

The most probable explanation is that it represents the signal from a layer or lens of liquid water. This water is not fresh and may be brackish. This is likely considering the close proximity of the lake, which, like other lakes in the Dry Valleys, is briny at depth (De Carlo and Green, 2002). The freezing point of water is determined by its chemistry, and dissolved salts from the highly salty soils of the Dry Valleys would depress the freezing temperature of briny water. It is possible that the layer of water is resting on the bedrock. However, this does not explain its decreasing depth further out into the valley, a behaviour contrary to that expected from the slope of the bedrock in a typical U-shaped glacial valley. Its depth is beyond the reach of the resistivity measurements, so it cannot be confirmed with that geophysical method, but the magnetic survey (§ 4.4) may provide correlative information.

4.4 Magnetic survey and magnetometer base station

Separation and matching of the data from the magnetic survey (§ 3.2.5) presented difficulties. The record of measurements only provided the time of each measurement and the field strength. The

spatial location of each measurement was recorded as its position relative to marker stations at set locations. However, there were frequent reversals of direction during the walking of the survey. Data processing involved the derivation of the physical location of each measurement from the continuous record, correcting for the reversals in direction. The $\sim$ 60 m spacing of the marker stations provided an upper limit on the matching of the measurements at any given point between its traversal in alternating directions. This matching varied between transect legs, caused by the differences in gait from traversing the undulating and sloping terrain in different directions, and was ± 2 measurements (Fig. 4.10(a)).

Alignment of the data from the outward and return to base station legs was assisted by observed underlying lateral changes in the field. These were most distinct on the south-west leg, a pattern significant if the basement gradually approached the surface in that area as might be expected in a glacial U-shaped valley.

The terrestrial magnetic field goes through a regular diurnal variation. Solar outbursts significantly affect the Earth's magnetic field, causing additional field variation superimposed on the diurnal variation (Gonzalez et al., 1994). Such solar outbursts occurred around the time of the survey. On December 24, the minute-to-minute field variation was much greater than would be considered acceptable for a survey in a non-polar location, where the variation would normally need to be much less for a survey to be considered acceptable.

The diurnal background variation during the time of the survey measurements was measured by intermittent data points at the base station. These were fitted by a linear model (Fig. B.9(a)) and then with a more accurate polynomial model (Fig. 4.10(b)). Fitting was made through the MATLAB `polyfit` function. The high order of the polynomial required to fit the scarce base station data points may suggest that the high field variation has adversely affected the data quality. It can be seen from Fig. 4.11(a) at the time of transect measurement and also from the superimposed measurements of Fig 4.11(b) that the day of the full survey was typical. This improves the likelihood of a valid model fit. Comparison with the previous day for segmentation of the day into parts for modelling was also helpful to confirm that the scattered data points accurately represented the expected diurnal change in that time period (Fig. B.9(b)). However, far fewer base station measurements were made during the survey of the first part of the south-west leg on December 22, 2006, and the modelling that resulted was significantly less accurate. The measurements from December 24 should be considered as closer to fully corrected.

The results of the magnetic survey are a little inconclusive due to the uneven results of the correction for diurnal effects, probably due to the outburst-created field variation. Fig. 4.10(b) shows a constant value of $\sim$ 63 mT in the part of the survey overlying the flank of Nickell Peak. This consistently drops until a point midway across the flat area of polygonal ground, where it sharply climbs. This turnaround does appear to be real as it occurs on the south-west data sets from both days, but its magnitude may be partly be an artefact. The data to the north-east across the hummocky moraine and past the stream then approximates the original constant value.

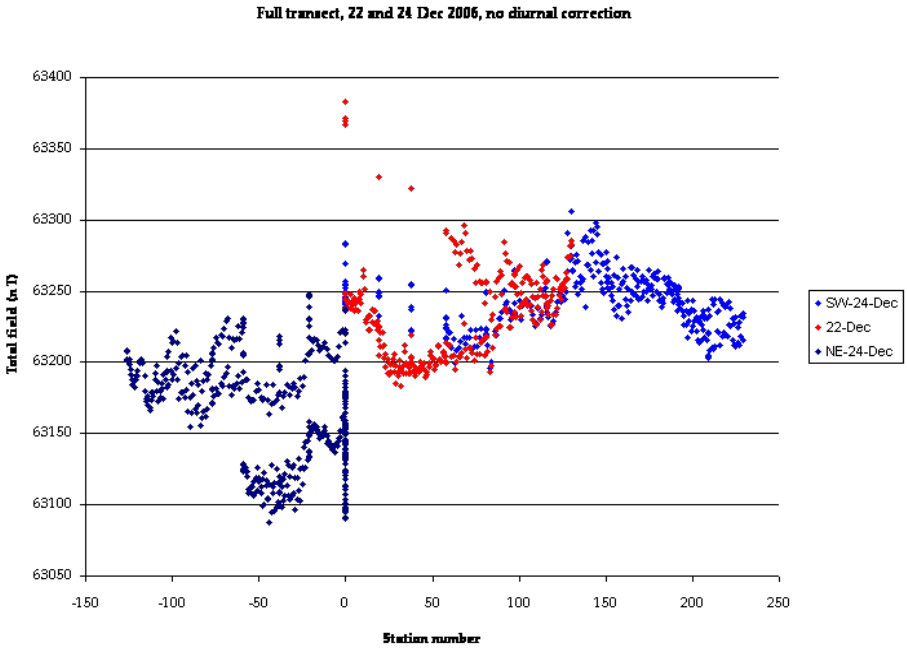

(a) Data uncorrected for diurnal variation during the transect measurements.

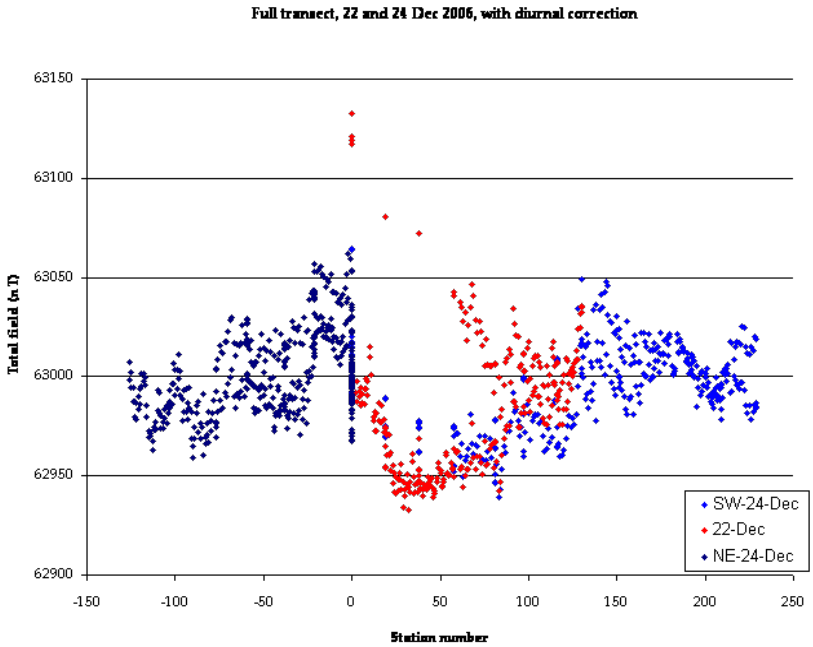

(b) Data corrected for diurnal variation by a 13th-order polynomial model.

Figure 4.10: Total magnetic field measurements over the Victoria Valley transect, with stations at ~ 3 m spacing. This profile extends ~ 500 m further to the south-west than the profiles measured by the other geophysical methods. Zero station number corresponds with the base camp. Station number -130 corresponds with the north-east end of the GPR transect.

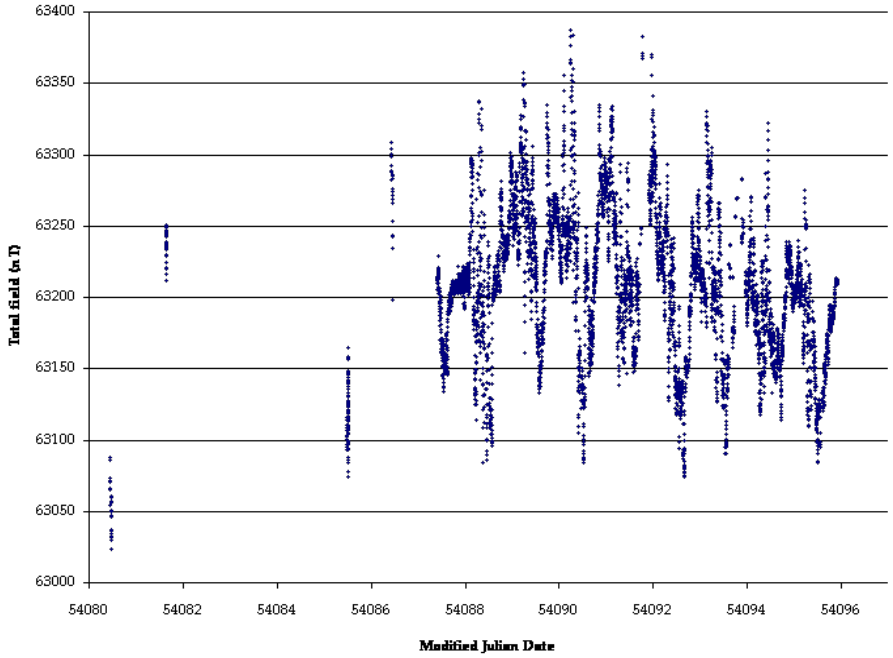

(a) Background record through time, 11–27 December 2006.

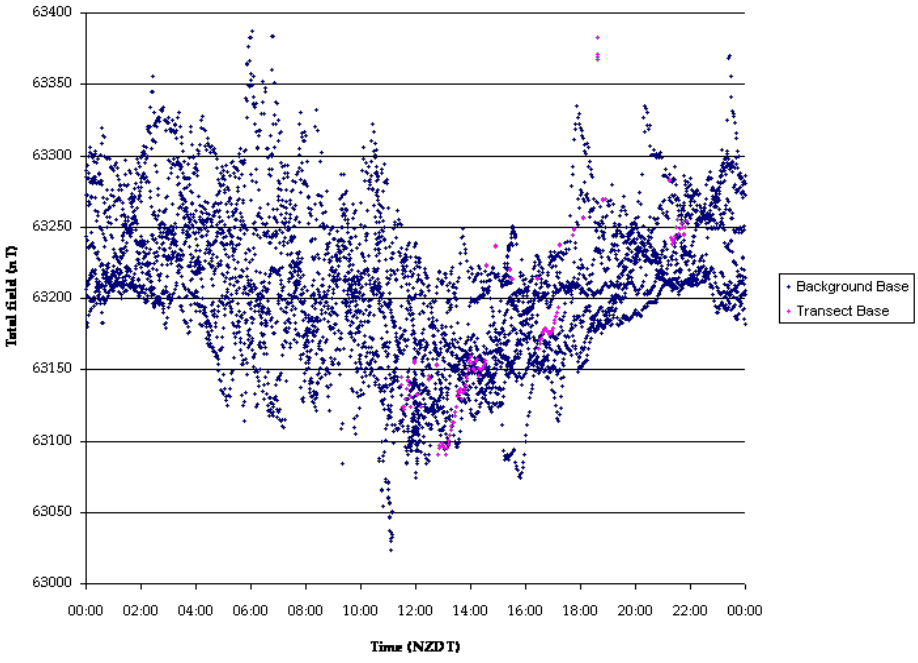

(b) Diurnal variation from all background measurements. The short-term sharp variations correspond to solar flares. The peak-to-peak variations at a given time of day are $\sim$ 100 nT and the diurnal variation is $\sim$ 300 nT.

Figure 4.11: Measurements made at the base station in Victoria Valley.

The strong dip in the field may indicate an asymmetry in the topography of the valley basement. Such asymmetry is known to occur in glacial valleys, but has not previously been considered for Victoria Valley. This low point on the magnetic profile does not coincide with the current low point in the sedimentary fill of the valley, where the lake is located, and is several hundred metres to the south-west. Lakes in glacial valleys do generally form at the low point of the trough, possibly arguing against this interpretation. An alternative interpretation is that the low point corresponds to a crosscutting dike in the predominantly igneous basement. The numerous dikes in the area (§ 2.2.2) have not all been mapped for continuity or extension from the St. Johns Range in the north-east across to Nickell Peak in the south-west (Turnbull et al., 1994). Although the trend of these dikes is almost parallel to the transect, the end of a dike could match the dip in the transect, assuming a homogeneous basement.

The record of the background measurements made in Beacon Valley can be found in Appendix B.4.

4.5 Synthesis

4.5.1 Victoria Valley

The profile of Victoria Valley provided by the electrical resistivity tomography suggests a permafrost in the glacial valley sediments that is dissected by polygons to a significant depth of over 10 m. This permafrost contains multiple lenses of massive ice that may indicate ice-cored moraines or pieces of solid buried glacial ice.

Electrical resistivity measurements at nearby Lake Vida, at the eastern end of Victoria Valley, showed confining permafrost to exist from a depth of 10 cm to greater than 200 m, and possibly as much as 1 km. This thick and extensive permafrost is in keeping with a normal continental-geothermal gradient of $18^{\circ}\mathrm{C} \cdot \mathrm{km}^{-1}$ (McGinnis et al., 1973). In contrast, Taylor and Wright Valleys have permafrost layers that are in parts thin given the present climate. These layers are underlain by saturated and unfrozen sediment that may form a continuous hydrogeological system (McGinnis et al., 1973).

The measurements at Vida were interpreted as a subsurface environment of thick ice lenses layered with a frozen, 40% sand/gravel outwash plain, with frozen crystalline basement at $\sim$ 80 m depth and the western end of the lake overlying frozen glacier debris (McGinnis et al., 1973). A layer of low resistivity, less than $10^3\ \Omega \cdot \mathrm{m}$, at depths below 100 m under the centre of the lake was interpreted as possible unfrozen brine or low-resistivity sediments. The multiple massive ice lenses in Victoria Valley are similar to the lenses found at Lake Vida by McGinnis et al. (1973).

The polygons in places provide a link between a highly resistive, active layer zone near the surface and a zone of low resistivity that could be unfrozen, permeable, high-salinity sediments. This zone is abruptly stopped at a depth of 20 m by a return to high resistivity (Fig 4.2(a)), which on examination in Fig. 4.2(b) shows a gradation from 10^4 to $10^5\ \Omega \cdot \mathrm{m}$. While this has a resistivity suggestive of bedrock, particularly frozen bedrock, its depth and subsurface topography is not supported by the TEM data. However, the resistivity tomography profile is incomplete in the spatial ranges that would indicate whether it did support the TEM measurements. The time-domain electromagnetism suggests a

subsurface that is relatively electrically homogenous in the first 100 m. This is particularly supported by the very well resolved resistivities and thickness of the single layer down to $\sim$ 120 m measured in the first several hundred metres of transect at the southwestern end. A sharp and moderately resolved layer only several metres in thickness appears at about the $\sim$ 720 m mark and ascends in depth from $\sim$ 170 m to $\sim$ 85 m by the 160 m mark. This very low-resistivity layer is indicative of a layer or lens of brackish water overlying the bedrock interface. It is possible that it was so thin that the resistivity tomography did not have sufficient resolution to detect it. The existence of a liquid layer at depth would be in line with the results found by McGinnis et al. (1973) in Taylor and Wright Valleys. The magnetic survey suggests that the valley floor may exhibit asymmetry, although the location of its low point does not coincide with the location of the lake. Alternatively, the low point found in the magnetic profile may indicate that a crosscutting dike underlies that part of the transect. The ground-penetrating radar indicates the existence of strong reflectors in the upper 30 m of the subsurface. Since the former lake delta extended over much of the valley floor of Upper Victoria Valley, these are probably related to sediment deposition. The strongest part of these reflectors is related to the flat polygonal ground, but this has developed on the former delta.

The relationship between individual polygons in the flat area and the subsurface ice-cemented layers may be clearly seen in Fig. 4.12(a). The vertical line-like features at a 10–15 m spacing are of significantly lower resistivity than the surrounding sediments. They are stalactite-shaped, extending downwards from the surface, and also frequently topped by a small cap of very high resistivity. Since the limit of resolution of the resistivity tomography is determined by the spacing of its electrodes, 5 m, the width of these features is questionable. Future work resampling the data to provide higher resolution over a small area would resolve this issue. Further fieldwork with electrodes at 2–3 m spacing would help to confirm such data reanalysis. However, their spacing relative to the observed size of the polygons in that part of the transect strongly suggests a correlation to the polygon contraction cracks. The small cap of high resistivity would then be due to the uncemented and air-filled material in the upper part of the wedge. Their depth, in contrast, is greater than that thought to be formed by contraction cracks, but no crack in the area has been excavated to its full depth. The resistive effect caused by a crack is probably due to its loose and slightly ice-cemented wedge of sand, less indurated than the surrounding permafrost. Additionally, the alteration zone of ground resistivity created by a crack might extend further than the physical extent of the crack.

4.5.2 Beacon Valley

The resistivity tomography has identified the buried ice with the possibility of some internal complexity. Its thickness, reaching beyond the limits of the measurements at $\sim$ 110 m, is far greater than previously thought, although its full lateral extent may not have been mapped.

Resistivity sounding would not be any more helpful than the tomography method in trying to obtain the base of the ice. Soundings in glacial ice have two problems: the extremely high resistivity of the ice makes penetration to large depths impossible with short arrays, and the similarly high resistivity

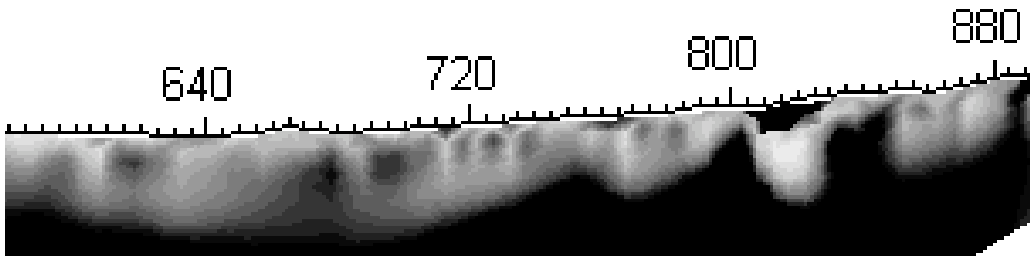

(a) Victoria Valley

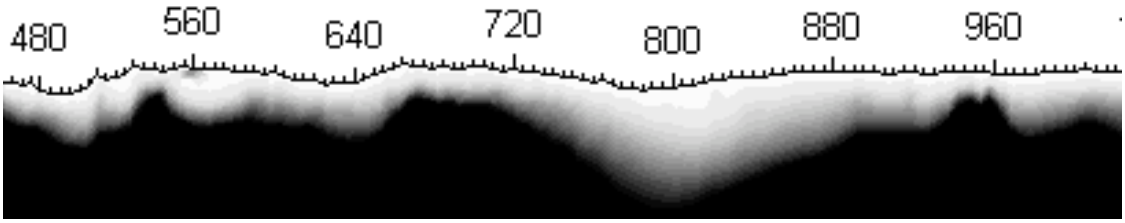

(b) Beacon Valley

Figure 4.12: Comparative examination in close up of the near-surface ice structures found by the resistivity tomography. The spacing of the vertical structures approximately matches the size of the surface expression of polygons.

contrast at the base of the ice introduces large uncertainties in the depth calculation (Röthlisberger, 1967).

The resistivity tomograms show there is a clear link between the subsurface massive ice and the overlying topography in the central part of the transect profile. The underlying ice has generated different subsurface characteristics on the scale of the polygons in Beacon Valley. Sletten et al. (2003) notes that the ice content of the ice-cemented polygon centres are for most examples either at $\sim 10\%$ or $\sim 90\%$ ice. Models of pattern development with age, such as that of Sletten et al. (2003), take into account the effects of varying surface substrate between locations. Fig. 4.12(b) shows features of similar scale to Fig. 4.12(a), in a reversed effect: the thin vertical lines are of higher resistivity than their surrounding substrate. They also have the opposite orientation, with a stalagmite form that reaches towards the surface from the ice mass. Massive ice polygons are surrounded by cracks that aid ground deflation through increased ice sublimation, as well as providing sources of surficial sediments. The polygon centres are known to be much more ice-cemented than the cracks. It is possible that in Beacon Valley the features may be due to the polygon centres, being connected to the subsurface ice mass, rather than the cracks.

Ice-cemented sedimentary polygons are controlled only by net accumulation and recycling of material into their cracks, producing net ground inflation. The depth of cracks in Beacon Valley will not be constant as the surface is deflating unevenly from sublimation (Sletten et al., 2003). The cracks may be increasing in depth. Sletten et al. (2003) notes that patterned ground underlain by spatially nonuniform massive ice in Wright Valley is younger than that in Beacon, and shows a more complex undulating pattern and microtopography than Beacon polygons. Microrelief is thought to be most

affected by the substrate characteristics (Sletten et al., 2003), and is far more pronounced in Beacon Valley.

The ground-penetrating radar adds little to the resistivity tomography, possibly identifying some dipping reflectors of small lateral extent compared to the length of the transect. These could be related to ice of slightly different ages or origins.

The repeatability of the data may be an area of some interest. None of the measurements were able to be repeated due to the large person-hour investment required for each and the limited field season. Zwartz (2005) mentions that their resistivity sounding measurements in Beacon Valley were consistently lower on repetition 6 days after the first measurement. In addition, Clark (1973) found the resistivity of the bedrock in the area to vary strongly with temperature in warm weather. However, general temperature effects are surface effects, mostly affecting the contact resistances. Since these resistances were perfectly adequate for the resistivity tomography measurements in Beacon Valley, it is unlikely to be an issue for concern.

4.5.3 Technique synthesis

The four geophysical methods selected for use in the field sites in the Dry Valleys of Antarctica worked well, with few difficulties in operation (Chapter 3). They provided data of use in understanding the subsurface structure of the permafrost ground in both Victoria Valley and Beacon Valley. Previously unknown detail of the patterned ground and buried ice of the field sites was discovered. Resistivity tomography, ground-penetrating radar and time-domain electromagnetism have provided the most useful data sets. In particular, the time-domain electromagnetism data is considered to be the first from the Dry Valleys, and therefore provide useful information on the applicability of the method to Antarctic permafrost. Many of the layers modelled could be well resolved. This is also the first time that resistivity tomography has been applied to the buried ice in Beacon Valley. It appears to be a method highly suitable for resolution of subsurface buried ice bodies, even when encountering the dry, highly resistive surface soils of the Dry Valleys.

Chapter 5

Implication of Antarctic results for Mars

Geophysical work in the Dry Valleys of Antarctica is useful to our understanding of Mars. It is applicable to the targeting, instrument selection and equipment design of future missions. This chapter expands on the discussion of § 4.5 by extending some of the results from the fieldwork in the Dry Valleys of Antarctica to the periglacial formations seen on Mars (Chapter 2). This is in line with the direction of the research suggested in § 1.4, and is discussed in § 5.1. The suitability and opportunities for current and future application of the geophysical methods used in the Antarctic fieldwork to Mars is presented in § 5.2.

5.1 Polygonal patterned ground and buried ice

It is important to consider that there are real problems associated with transferring the environment of the Dry Valleys of Antarctica to that of Mars. However, such mitigating factors as the high salinity in both locations, the aridity and the geological setting support the comparison. These differences simply need to be recalled and taken into account where relevant. For example, the temperature range is significantly lower. Additionally, the factors controlling the rate of polygon evolution are numerous and not entirely understood. For example, if the ground is dry enough to lack cohesive strength, patterned ground may develop extremely slowly or not at all. The magnitude and frequency of crack opening from thermal forcing, the available amount of æolian sand for wedge formation, the substrate properties and climatic change modifications of the thermal cycle are all controlling parameters. Removal of permafrost can leave fossil patterned ground, as in Utopia Planitia (Klima, 2003). This can at times be difficult to identify from orbital photographs and multi-wavelength data alone. This study dealt with ice-rich active patterned ground. Similar studies of fossil patterned ground on Earth could be useful future work.

It is not yet well understood how the spatial variation in polygon size and microtopography of polygons reflects environmental conditions (Sletten et al., 2003). Surface ages, the presence of near-surface ice and soil properties may all be potentially inferred from patterned ground development. From the resistivity tomogram of Beacon Valley in the Dry Valleys of Antarctica, it is suggested that

there are links between the centres of polygons and underlying massive ice. The polygons in Victoria Valley do not have these connections to buried massive ice, and the discrete lenses of massive ice found in the subsurface permafrost sediments do not show an influence on the surface expression of the patterned ground. The small-scale patterned ground of Mars shows variation in its morphology comparable to that of terrestrial patterned ground (§ 2.3.2, Fig. 2.2). It may therefore be similarly unaffected by the presence of subsurface lenses of ice. These ice-rich areas with subsurface ice lenses may only become evident when cratering occurs, and terrain softening (§ 2.3.2) can develop.

Thin, highly conductive layers of brackish water or clay tills can be found at depth through time-domain electromagnetism. This was found in Victoria Valley. Clay tills are less likely to occur on Mars, due to the lack of chemical weathering necessary for their formation (Kieffer et al., 1992), but brackish or even highly saline water is a definite possibility (Burt and Knauth, 2003). The possibility of "brine sandwiches" between subsurface ice and layered salts, or even bedrock, has been suggested for Mars (Burt and Knauth, 2003). Such layers should therefore be considered likely in the interpretation of Martian data sets.

The resistivity tomography in Beacon Valley has produced data that suggests buried massive ice of glacial origin may be many tens of metres thick in areas adjacent to glacial formations. Such periglacial formations are widespread on Mars. The depth and lateral extent of distinctive buried ice features such as debris aprons and fretted terrain on Mars (§ 2.3.2) are inferred from evidence of visible flow and surface deformation. It is suggested that their extent may therefore be much greater than what is frequently assumed, as there are no surface indications of any such movement and deformation in the Beacon Valley ice. The survival of the internal fabric of the Beacon Valley ice (van der Wateren and Hindmarsh, 1995) may be related to the internal topography that appears to be visible on the resistivity tomograms of the ice mass, and, to a lesser degree, on the ground-penetrating radar profiles. This internal topography supports the idea that the ice mass is stagnant.

The resistivity data from Beacon Valley can be interpreted as preferential retreat of the ice from the surface in areas of ground depression. Whether this evolution is tied to the polygons at the surface was less clear. Modelling of the near-surface Martian ice suggests that if a suddenly opened trench, such as that created by a stress fracture, extends to a depth similar to the level of the ice, the ice retreats to a new stable level below the new topography on a timescale of hours (Kossacki et al., 2001). If the trench extends well below the ice boundary level, the ice level does not alter. This modelled behaviour would produce results similar to that inferred from the Beacon Valley data.

The ice in Beacon Valley has been preserved for extended periods of time. In a relatively stable climate, it has perhaps lost only a few metres of thickness (Sugden et al., 1995) when overlain by a thin layer of sublimation till, small clasts and boulders. The size and extent of the ice imaged by the resistivity tomography, together with the minimum ages for it that have been provided by dating, require at least some explanatory mechanisms for its long-term stability. The feasibility of long-term stability against sublimation of the buried ice over millions of years is an issue relevant to both Earth and Mars. The Martian dust is thought to be an excellent thermal insulator, with a layer of just 5 mm

providing full ice stability if the particles and the pore spaces are 50 μm in diameter (Kossacki et al., 2001). This permits ice to be present up to depths of only a few millimetres below the surface (Skorov et al., 2001). The rate of vapor diffusion through the regolith determines both the survival time of buried ice in a dry climate at instability, and the possibility of ice replenishment from atmospheric vapor (Kossacki et al., 2001). Smaller pores (finer regolith) lead to slower vapor diffusion. However, the ice equilibrium point is determined only by subsurface temperature and atmospheric water content (Hudson et al., 2007). The sublimation till overlying the Beacon Valley ice is coarser, but there may be alternative physical mechanisms due to the different atmospheric moisture content of the Dry Valleys. Meteorological measurements in Beacon Valley suggest that despite the low humidity of the atmosphere, the humidity is equal to the saturation vapor pressure at the surface of the ice (Schorghofer, 2005). Modelling of this factor shows that it slows ice loss to sublimation by a factor of three at the current valley temperatures (Schorghofer, 2005). Sublimation would cease entirely at temperatures 5°C lower. Additionally, the pressure drop caused by the fierce katabatic winds did not have a significant effect on the calculated mean sublimation loss. This is important for Martian buried ice as well, as the wind velocities on Mars can be significantly greater than those in the Dry Valleys, despite the lower atmospheric density.

It is suggested that the links between the subsurface permafrost and the surface expression of polygons inferred in Victoria Valley will be useful for subsequent developments in the understanding of the general Martian polygon systems. The two field sites should be considered as applicable to different types of Martian permafrost and periglacial phenomena. The situation of Victoria Valley is considered to be relevant to areas of terrain softening. The "sublimation" polygons and the buried massive ice in Beacon Valley, will be applicable specifically where lobate debris aprons and viscous debris flows (§ 2.3.2) are present. These features are suitably rich in massive subsurface ice.

5.2 Design and targeting of future Mars missions

Since direct surface imaging of Mars is now well established, there is a growing need to consider the application of other scientific techniques that can provide additional information. Geophysical methods provide subsurface data. Orbital, aerial and ground-based techniques, as used in this study, can all be used in a complementary fashion. However, only a few comparisons of the various geophysical methods and their applicability for Mars have yet been made, (eg. Yoshikawa et al. (2006)), and the current study provides additional data.

All of the geophysical methods applied in the fieldwork of this study would work well in the environment of Mars. The cold and the abrasive dust of the Dry Valleys of Antarctica did not cause any problems that could not be overcome by minor equipment alterations. For example, the fibre-optic sheathing on the ground-penetrating radar cables would need to use plastic that remained ductile in subzero temperatures.

The standard spacecraft instrument constraints of mass, low power requirements, volume and

deployment configurations dictate the design of any geophysical instruments for direct study of Mars. Low data rates and volume are an attractive feature of geophysical instruments, since the satellite downlink requirements can also be an important constraint.

Ground-penetrating radar (GPR) is a method that can quickly and non-intrusively provide valuable information about the subsurface of Mars, with spatial resolution of a few centimetres near the surface and tens of metres at greater depth. The complex dielectric properties of the subsurface are not currently known (Leuschen et al., 2003). They are important in the design of a Martian GPR, requiring it to have a wide range of bandwidths and operating frequencies. The standard trade-off between near-surface resolution and adequate depth penetration must also be considered (Davis and Annan, 1989).

Terrestrial radar applications range from orbital and airborne imaging systems to surface-based ground-penetrating systems. GPR can extend the knowledge of near-surface geology and structure, including dielectric properties, to the regional scale and extensive volume penetration provided by orbital systems (Grant et al., 2003). Orbital systems use radar sounding with wavelengths of metres to hundreds of metres. They have in the past only been used to obtain subsurface data for Earth's moon, where they were used during the Apollo program as the ALSE experiment on Apollo 17 (Phillips et al., 1973). More data is expected from the LRS experiment on the Japanese lunar orbiter SELENE (Ono and Oya, 2000) due to launch in late 2007. In the polar regions of Earth, airborne systems have been used routinely. Airborne systems have been tested in the Dry Valleys of Antarctica for comparison with the Martian radar data. Holt et al. (2006b) used single-pass radar sounding at 52.5–67.5 MHz in Taylor Valley and across the Taylor Glacier, attempting to isolate surface clutter from varying topography so that subsurface echoes could be identified.

The radar systems currently orbiting Mars are MARSIS and SHARAD (§ 1.1). The returns from MARSIS are likely to be at spatial resolutions greater than can reasonably be compared with the data collected in this project. That which will be obtained by SHARAD is more comparable, as it should be able to resolve liquid water or ice bodies several tens to several hundred metres thick. The ground-penetrating radar profiles made in this fieldwork, albeit at different wavelengths to MARSIS and SHARAD, suggest that shallow subsurface lenses of massive ice in Mars-like environments will not always be clearly visible.

Though orbital systems are currently providing subsurface information on Mars, the application of ground-penetrating radar to a surface role has been considered (Grant et al., 2003; Leuschen et al., 2003). One of these systems, a sled design that operates from 5 to 120 MHz, has had prototype testing in the Alaskan Arctic (Leuschen et al., 2003), while a rover-mounted unit has been tested in the Californian desert (Grant et al., 2003). Target and expected operational depths for such rover-mounted GPR are generally 10–30 m. This is sufficient to delineate stratigraphy and structure from a tenth of a metre to one metre in scale.

Rover-mounted units do have difficulties accommodating antennæ of the size required to broadcast and receive at the required low frequencies. For example, the antennae design of Leuschen et al.

(2003) operating from 10 to 120 MHz was 3.75 m long, similar to that used with some difficulty in Victoria Valley for a 25 MHz profile. This is still prohibitive for a mobile rover. There is the possibility of placing the transmitting antenna on a stationary lander and a more compact receiver on a mobile rover (Leuschen et al., 2003). A flexible line 100 MHz design that can be reeled onto the ground or deployed as a telescoping/extendable rod has been tested (Grant et al., 2003). Such a ground line would work in rocky terrain like Victoria and Beacon Valleys only as long as the line direction was never changed. From the Antarctic field experience, a ground line would be quite impractical.

The experiments of Leuschen et al. (2003) tested how their GPR could differentiate between subsurface ice deposits and ice-cemented soils. Although their dielectric boundaries had resolution of a metre, they had difficulty determining the geology (Leuschen et al., 2003). This difficulty in making an unambiguous detection of water is known, but if liquid water is present in the subsurface, it will provide a sharp and detectable dielectric contrast (Grant et al., 2003). However, knowledge of the stratigraphy and setting can help in determining past aqueous involvement. For example, the ground-penetrating radar profile made in the Victoria Valley fieldwork of this study supports the existence of a lake delta overlying the transect. It shows layered linear reflectors that lie parallel to the ground surface.

The surface rock clutter expected of most Martian environments may be a problem for GPR. This would depend on their size and distribution. It may be possible to model and remove such effects (Holt et al., 2006b). Substrates with significant iron-bearing minerals such as magnetite can produce losses due to magnetic absorption (Cereti et al., 2007; Cassidy, 2007). They are likely to be abundant at many Martian localities, but can hopefully be avoided in the landing site selection process. Both of these problems were experienced to some degree in Beacon Valley. However, it was possible to obtain some subsurface information from the ground-penetrating radar profile. Abundant fine-grained Martian regolith material, including weathering by-products, salts and fine-grained magnetite will increase the attenuation (Cereti et al., 2007). The dry conditions should partly alleviate this effect (Grant et al., 2003). Brine layers near the surface will attenuate radar signals (Yoshikawa et al., 2006), although the thin brackish layer detected at depth in Victoria Valley did not affect the radar results. This is because it was much deeper than the radar return depth.

Dielectric contrasts between water and surrounding rock or sediments found through the use of GPR are not always sufficiently high to unambiguously identify the presence of water. Low-frequency electromagnetic (EM) methods, which utilize induction rather than wave propagation, are sensitive to electrical conductivity rather than permittivity. At times they can be more appropriate than GPR for water detection, as material conductivities range over many orders of magnitude, and both fresh and saline water have conductivity values quite different to their surroundings (Grimm, 2003b). For these reasons, low-frequency electromagnetic methods including TEM have been successfully used in terrestrial situations for groundwater detection (McNeill, 1990; Danielsen et al., 2003). The low frequencies of these methods allow greater depth penetration than that reached by radar. For example, the modelled depths at which the TEM was still providing well-resolved information approached 200

m in some parts of the transect in Victoria Valley, while the radar reached less than 40 m. Their diffuse signals are also little affected by small-scale subsurface features, where radar can encounter adverse scattering.

The possibility of applying TEM to the Martian environment was initially suggested in Russian research in the 1980s. A lightweight TEM system with a 20–30 m loop that was to be laid out by a rover was developed for the subsequently cancelled Mars 94 mission (Grimm, 2002). This possibility has been reconsidered in the last five years (Grimm, 2002, 2003a). Inductive electromagnetism has otherwise not been widely considered as a planetary science technique in the past. Its only applications have been to the Moon and the moons of Jupiter, where it was used for global sounding in conjunction with an external magnetic field (Grimm, 2002). Inductive EM has the advantages of greater geoelectrical sensitivity, particularly useful in the detection of water, but with the disadvantage of lower resolution. This is due to the logarithmic resolution with distance of inductive/diffusion methods and the linear resolution with distance of wave methods (Grimm, 2002). Additionally, active TEM methods of the type applied in the current Antarctic study are generally more massive and require more power than GPR (Grimm, 2003b).

The most useful design for an active TEM for a Martian mission would mount the equipment on an unmanned aerial vehicle. The depth attainable would be dependent on the transmission loop size. An airborne system of several kilograms would be able to detect water at a depth of several hundred metres, and a fixed-loop system of several tens of kilograms would reach depths of several kilometres (Grimm, 2002).

There are a few interpretation issues with the application of the method to Mars. The great sensitivity of textscem methods could detect electrically conductive, supercooled thin films of water produced by adsorption as easily as aquifers (Grimm, 2002, 2003a). Conductive, strataform geological formations are hypothesized. Such formations are visible on the surface, for example the hematite exposures of Sinus Meridiani (Grimm, 2003a). Either of these situations have the potential to be confused with aquifers. A thin adsorption film of water is an alternative explanation for the low-resistivity feature found by the TEM in Victoria Valley. However, the other explanations are more likely, as the adjacent lake will have saline water at depth (De Carlo and Green, 2002), and a layer of glacial till could have formed easily in the past (§ 4.3).

Modelling of the time-domain and frequency-domain electromagnetic responses from the likely ice and rock mixtures in the Martian subsurface suggests that detection of ice would be difficult unless it was massively segregated (Grimm, 2002). Any liquid water would however be very easily detected. Saline water appears to have been detected clearly by the TEM applied here in Victoria Valley, Antarctica, which offers a good model and supportive evidence for TEM application to Mars. Further TEM use in the Dry Valleys of Antarctica could offer strong support for the inclusion of a TEM instrument on future Mars missions.

The nuclear magnetic resonance imaging technique, more commonly used in proton-precession magnetometers like those used in this fieldwork (§ A.4), may also be useful as a Martian geophysical

method as it is sensitive to hydrogen and therefore to water (Grimm, 2003a). It has been used in a terrestrial context on pingos near Fairbanks, Alaska to successfully resolve aquifers beneath massive ice, but could not resolve the surrounding frozen silt (Yoshikawa et al., 2006).

Resistivity tomography is not feasible at this time for a Martian mission, partly due to the mass and large bulk of the equipment, and its long-duration moderate power requirements. The equipment used in Antarctica had a total mass of nearly two hundred kilograms. Although the method has been shown to work without difficulty in arid and subzero environments, the difficulties involved in sufficiently miniaturizing it for the deployment of the long cables, and its subsequent recovery and redeployment, may be considerable. The very high contact impedances due to the hyper-arid Martian ground may also make the method impractical. Once sufficiently detailed large-scale, low-resolution data has been obtained for the Martian subsurface, it may be reconsidered, as it could resolve the form and dimensions of the subsurface ice found in Antarctica.

The subsurface ice features found in Victoria Valley are examples of the types of ice lenses that could be found in the Martian permafrost sediments. Their lateral extent is up to 80 m, four times too small to be resolved by MARSIS. Their vertical extent of 10–20 m is also far below the resolution of the ground-penetrating radar instruments currently in use on two Martian missions (Picardi et al., 2004; Seu et al., 2007). These ice lenses were not well defined by the GPR used in this study. This suggests that future higher-resolution ground-penetrating radars on Martian missions may produce less informative results about very near-surface buried ice masses than has been envisaged by the current MARSIS and SHARAD instruments (Ori and Ogliani, 1996; Picardi et al., 2004; Farrell et al., 2004; Seu et al., 2007). Information of great use in characterizing the subsurface of the planet (eg. Watters et al. (2006)) will still undoubtedly be obtained.

Chapter 6

Conclusion

The hydrosphere of Mars is thought to be almost entirely within the cryosphere. It is expressed in complex periglacial and glacial forms across the planetary surface. Ice is dominant in shaping the present landscape. This cold, windswept world can be difficult to understand simply from aerial photography. The Antarctic Dry Valleys, which offer a dry, cold, windy, Mars-like environment where features of known origin can be studied, are frequently used for comparison to tie Martian landforms to more specific periglacial and glacial origins.

Patterned ground is an important indicator of subsurface permafrost conditions, and will potentially be useful to infer environmental changes. In this study, 1.3 km long profiles of the patterned ground in Victoria Valley and Beacon Valley of the McMurdo Dry Valleys, Antarctica, were created using four geophysical methods. Two-dimensional resistivity tomography, 25 MHz ground-penetrating radar, time-domain electromagnetism and a field-magnitude magnetic survey were undertaken in Victoria Valley. In Beacon Valley the geophysical methods used were resistivity tomography and 50 MHz ground-penetrating radar.

The resistivity tomography at both locations is significant. It provides the first imaging of the spatial extent of the massive buried ice in Beacon Valley, and resolves previously unknown near-surface lenses of massive buried ice in Victoria Valley. The buried ice in Beacon Valley extended to a depth of greater than 110 m, below the range of the geoelectrical method. The buried ice lenses in Victoria Valley are also tens of metres in spatial extent and 10–20 m thick. They are inferred to be of glacial origin.

The resistivity tomograms from Victoria Valley and Beacon Valley had sufficient near-surface resolution to identify features related to the surface expression of polygons. In Victoria Valley, regularly spaced, near-surface features on the tomogram were interpreted as showing the sand wedges that delineate the polygons. The cracks appear to extend further (up to 10 m) into the subsurface than was previously thought from excavation. These cracks may connect with the zone of unfrozen, permeable, high-salinity sediments that underlies much of the polygonal patterned ground of the area. In Beacon Valley, the regularly spaced, near-surface features were interpreted as showing connections from the ice-cemented centres of the polygons to the buried massive ice beneath. These differences suggest

that there is fundamentally different polygon development in Victoria Valley compared to Beacon Valley. It is suggested that this is due to the Beacon Valley polygons developing on massive ice with a "sublimation" origin, and the Victoria Valley polygons developing in deep, continuous permafrost sediments.

The TEM data from Victoria Valley also provides a data set of which no previous examples appear to exist in the literature. This may be relevant to future applications of TEM to Mars. It shows that low-resistivity features, such as a low-salinity water layer, can be detected at depths below a hundred metres in permafrost ground. This layer is suggested to overlie bedrock. Although it is deeper than the high-resistivity material identified as bedrock in the resistivity tomograms, the TEM data is preferred, as the resistivity measurements are incomplete at that depth across the full transect.

The fieldwork and the data analysis suggest that ground-penetrating radar and TEM are suitable methods for use on Mars missions. Although resistivity tomography has provided some of the most useful results in this study, and those most relevant to interpretation of future Martian data, its equipment requirements prohibit its use on near-future Mars missions. As TEM has not yet been used on a Mars mission, based on the results in the Antarctic environment, its selection should be given serious consideration on future missions.

6.1 Future work in the Dry Valleys of Antarctica

Determining the extent and depth of the ice in Beacon Valley is an important scientific goal, and further research in this area is necessary. It would best be done with resistivity tomography, but to obtain greater depth, a larger array would be required. Cables are commercially available that have 10 m electrode spacing, but this would cause a decrease in resolution. However, the extra depth that would be gained would be more important, as it would hopefully allow measurement of the thickness of the ice. Additionally, testing a prototype larger array in Beacon Valley would be informative for a future resistivity tomography array for Mars exploration.

More transects in Beacon Valley are needed. A more extensive resistivity transect extending across the full width of the valley would confirm the extent of the buried ice. The location of further transverse transects is also crucial, as this transect was placed on the boundary between the furthest incursion of the Taylor Glacier and the furthest down-valley extent of the Mullins Glacier. It raises the question of the origin of the buried ice.

Longitudinal transects would resolve the question of origin. A 3 km transect is the longest that can be made without a camp move, due to the weight of commercially available resistivity equipment. Careful logistics planning could allow more than one section of longitudinal transect. Due to the often rapid advance of inclement weather in Beacon Valley, it would not be advisable to try for distances much longer than 3 km for safety reasons. A longitudinal transect would begin up on the rocks of the Mullins Glacier, proceed over the debris fan at its base, and extend down the valley, perhaps 2-3 km past the location of this fieldwork, towards the Taylor Glacier. This transect would also answer

unresolved questions about the ice of the Mullins Glacier.

The magnetic data could be useful in studies of field variation. Event K069, from the University of Newcastle, NSW, were using the Arrival Heights magnetometer during January as part of a magnetosphere dynamic variation study. Contact was made with them to discuss an exchange of data, and incorporation of their field measurements could provide further comparative information.

Comparison of the topographic data collected with the high-resolution (2 m data point spacing) LIDAR data available for the two field sites was attempted but was unsuccessful due to technical problems. The LIDAR data forms a digital elevation model, which could be used to create a simulation of the expected radar return, possibly in combination with the topographic data. This could be used to isolate the surface effects and more accurately determine the measured subsurface structures when compared to the radar data (Holt et al., 2006b).

Further resistivity tomography imaging in Victoria Valley is strongly suggested. Determining the full spatial extent of the ice lenses is important. The best way would be to take a series of parallel profiles across the flat area of polygonal ground adjacent to the K054 camp, probably at a 2.5 m electrode spacing for greater near-surface resolution. These would be combined into a 3D resistivity model. Such a model would also reduce uncertainties from the 2D modelling of possible 3D structure that has been made in this study.

A core of the ice lenses in Victoria Valley would allow dating of the age of the ice, and also allow examination of the ice fabric. This would help to determine the origin of the ice, and whether the glacial origin suggested here is correct. Coring in Victoria Valley would be feasible as the ice lenses are in places within ten metres of the surface, and their lateral extent of several tens of metres means that precision location of the drilling rig should not be necessary to strike part of the buried ice. However, further resistivity tomography work would help locate the best sites for drilling a core of maximum scientific value.

6.2 Acknowledgements

I would like to sincerely thank my supervisors, Dr David Nobes and Associate Professor Peter Cottrell, of the Department of Geological Sciences and of the Department of Physics and Astronomy, respectively. Their assistance and advice at all stages of this project was invaluable. In particular, thanks to David Nobes for his initial proposal of the opportunity for this fieldwork, and to Peter Cottrell for agreeing to help, and providing enthusiastic astronomy support to this planetary science project.

Funding for the Antarctic fieldwork was generously provided by the Department of Physics and Astronomy of the University of Canterbury and by the Brian Mason Scientific and Technical Trust.

Myfanwy Godfrey, Jon Lapwood and David Nobes provided help with the data collection, and nine weeks of good company, in Antarctica. Ron Sletten of the University of Washington in Seattle gave insight and helpful discussion in the field at both sites, and provided helicopter support for the K054 reconnaissance to Beacon Valley. Logistical support for Event K054 was supplied in an outstanding manner by Antarctica New Zealand and Helicopters New Zealand. An optical level from the University of Auckland was provided on loan by Event K015.

Warren Dickinson of Victoria University of Wellington provided comments on the resistivity data and the loan of the LIDAR data CD. Jamie Shulmeister sparked the research into Martian rock glaciers and debris aprons. Margaret Bradshaw gave advice on Antarctic fieldwork, and loaned her geological map of Beacon Valley. Michael JasonSmith provided helpful comments on LaTeX.

Sue and Michael Bannister, my parents — thank you.

This project is dedicated to the men and women of the first manned mission to Mars.
May their geophysical investigations be successful.

Appendix A

Geophysical techniques

A.1 Two-dimensional resistivity tomography

This technique injects a low amperage current into the ground through an electrode, sinking the current into a distant electrode, and measures the voltage drop across the known separation distance through two intervening additional electrodes (Fig. A.1). This allows the resistivity of the subsurface volume to be calculated. Since the subsurface is not generally homogeneous, any zones of varying resistivity can be found through increasing the electrode spacing, creating a hemisphere of increasing volume that intersects successive zones. Interfaces between zones modify the shape of the volume, and further affect the flow of current. This varying interaction with electrode separation means the measurement is apparent and not true resistivity, but by sampling at multiple locations and with multiple electrode separations, a profile of apparent resistivity with depth and position can be created (Geotomo Software, 2004). The electrode array used has 128 electrodes, arranged in four "strings" of 32-wire cables with contacts for electrodes, with the Tigre console, 12 V battery power source, and recording laptop located centrally and in a protective plastic case (Fig. 3.5(d)). The outer strings were linked to the console by extension cables. Connections to the ground are made by hammering in the electrodes, slim

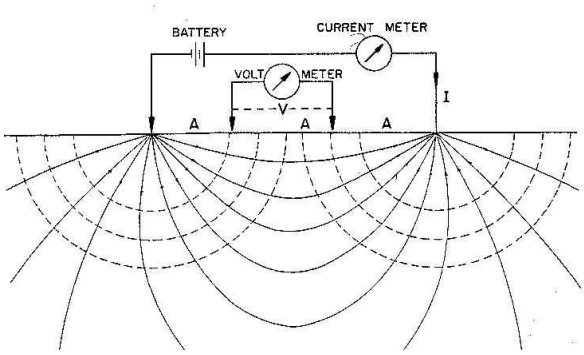

Figure A.1: Physical layout of resistivity tomography.

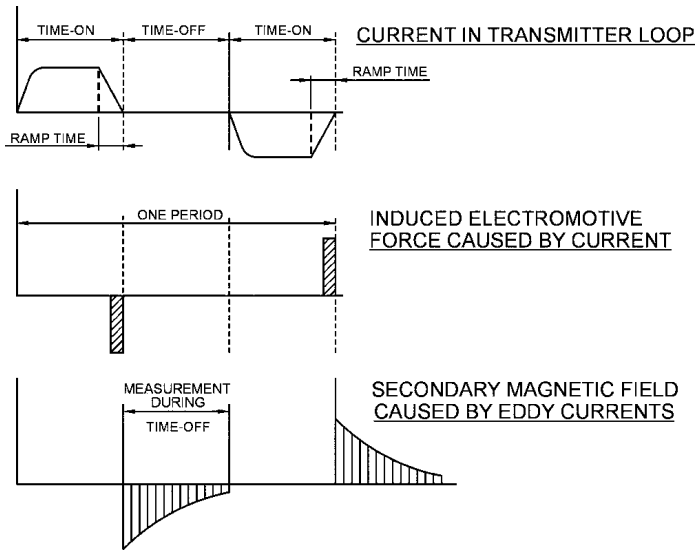

Figure A.2: Principles of the time-domain electromagnetic method. After McNeill (1990).

steel pegs that clip to the cables. The survey design was a Wenner array, a two-dimensional layout that constructs a triangular profile of apparent resistivity values, as the number of possible readings reduces with increasing electrode separation.

A.2 Time-domain (transient) electromagnetism

Time-domain electromagnetism (TEM) can reach greater depths than electrical resistivity tomography. The layout consists of a very large square loop of electrical cable connected to the transmitter, the circular wire coil of the receiver in the centre of the loop, and a console for recording the data nearby (Fig. 3.5(b)). In this study the instrument was the Geonics PROTEM EM47. A current is run through the transmitter loop, creating a primary magnetic field, and abruptly switched off, producing "smoke-rings" of eddy currents propagating out from the loop down into the ground (Nabighian, 1979). These induced currents generate secondary magnetic fields, which cause a measurable current to flow in the receiver coils. The ground response decays exponentially over time, with the last measurements from the deepest layers, and dependent upon the resistivity (Fig. A.2). The method is suited to finding conductive layers, which have a longer passage time and greater induced current for the loops, and so produce a more informative signal.

A.3 Ground-penetrating radar

Ground-penetrating radar (GPR) transmits shaped pulses of radio waves into the ground, where some of the radiation is reflected if a dielectric interface boundary between regions of different permittivity

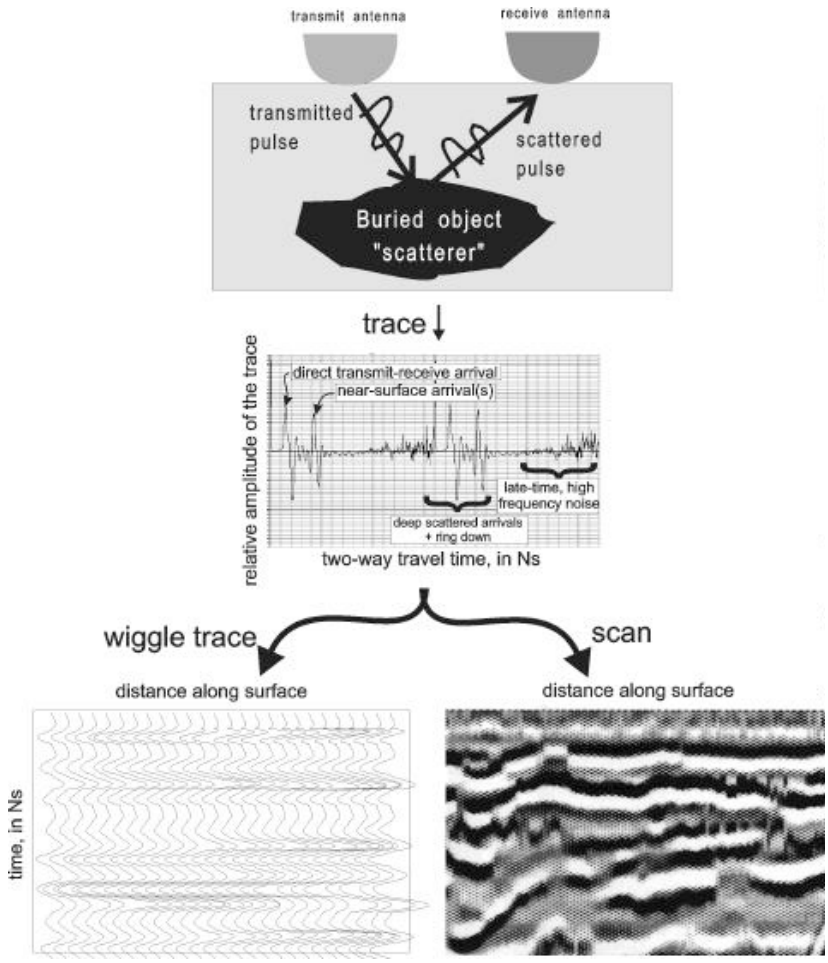

Figure A.3: Principles and application of ground-penetrating radar. After Daniels (2000).

ε_r is encountered (Davis and Annan, 1989). The rest of the radiation continues to propagate. A large difference in relative permittivity creates a strong reflection, which registers prominently on the return profile (Fig. A.3). Travel time from the transmitter to reflector and back to the receiver is used to determine the depth of reflectors, once the wave's velocity in the material is known. Theoretically this is reduced from c by one over the square root of the relative permittivity, but it is practically found by a common mid-point (CMP) survey across the field site, which systematically increases the symmetric offset distance of the antennae about a central point and measures the variation in travel time with increasing distance (Davis and Annan, 1989). Subsurface velocities are generally given in $\mathrm{m.ns}^{-1}$. The penetration capacity of the radar waves is affected by their frequency and by attenuation due to electric currents being induced in the conductive ground. Attenuation increases with frequency, so a longer wavelength increases the depth that can be probed. The resolution has two components. Vertical resolution differentiates signals adjacent in time, which is a function of frequency and so decreases with depth. Lateral resolution differentiates horizontally adjacent objects, and is dependent

on the beam size of the energy cone at a given depth, going to $\lambda/4$ at the surface.

The equipment was a Sensors and Software pulseEKKO 100 A system. It comprised two antennas connected by fibre optics to a backpack-mounted radar console unit and 12 V battery, operated by a laptop (Fig. 3.5(a)).

Some GPR definitions are given here, as they are only used in Chapter 3 and Chapter 4.

Time window: the time in ns for which radio wave reflections will be recorded in a given measurement. Lower frequencies equal longer return times from a greater depth of penetration, which equal a longer window.

Trace: the information recorded at one point on a survey line. Multiple readings are generally taken, since the time window for each reading is very short, and integrated or "stacked" to produce a trace.

Sampling intervals: both temporal and spatial. The frequency of the readings is not to exceed the period of the centre of the antennae frequency operation range, and the maximum spatial step of antennae movement is set by the Nyquist interval, one over the sampling frequency.

A.4 Magnetic surveys and the proton-precession magnetometer

The proton-precession magnetometer can be used to measure fluctuations in the local magnetic field. By running a strong current through a hydrogen-rich liquid, the magnetic moments of the protons are removed from alignment with the Earth's magnetic field. Switching off the current allows the magnetic field to exert a force on the nuclei, which causes them to precess. The frequency of precession is proportional to the magnitude of the field (Milsom, 2003).

The EG&G Geometrics G-856 magnetometer was operated as a single-measurement instrument recording the magnitude of the magnetic field. This was due to only the top one of the two decane-filled sensors functioning, but was adequate to survey a profile (Fig 3.5(c)). During operation the sensor was oriented north, placing the coil axis perpendicular to the magnetic field to produce an optimum signal (EG&G Geometrics, 1992). Surveys of the topography of the bedrock can be made when the bedrock is known to be igneous, as such rocks contain magnetic minerals which amplify the field.

Base station measurements (Fig 3.3.4) must be made during the course of a survey, to be able to correct for diurnal variation in the local magnetic field. These diurnal changes are primarily due to the changing exposure of the local ionosphere to the solar wind as the Earth rotates. Superimposed on this are more unpredictable changes produced by variations in the solar wind. Therefore, for greater accuracy base station measurements should also be made for some days either side of the survey to establish the diurnal variation.

A.5 Notes on conventions

Compass directions in this report are New Zealand/Pacific as used in Antarctica.

Times of field season measurements are in New Zealand Daylight Time (NZDT), thirteen hours in advance of UTC.

The Julian Date used in the magnetometer data processing is the number of fractional days since 12 noon UT on 1 January, 4713 BC, in the proleptic Julian calendar. The Modified Julian Date is formed from the Julian Date by truncating the first two digits, and setting the day to begin at midnight UT, so that MJD = JD - 2400000.5.

Appendix B

Additional data

B.1 Resistivity tomography uncertainties

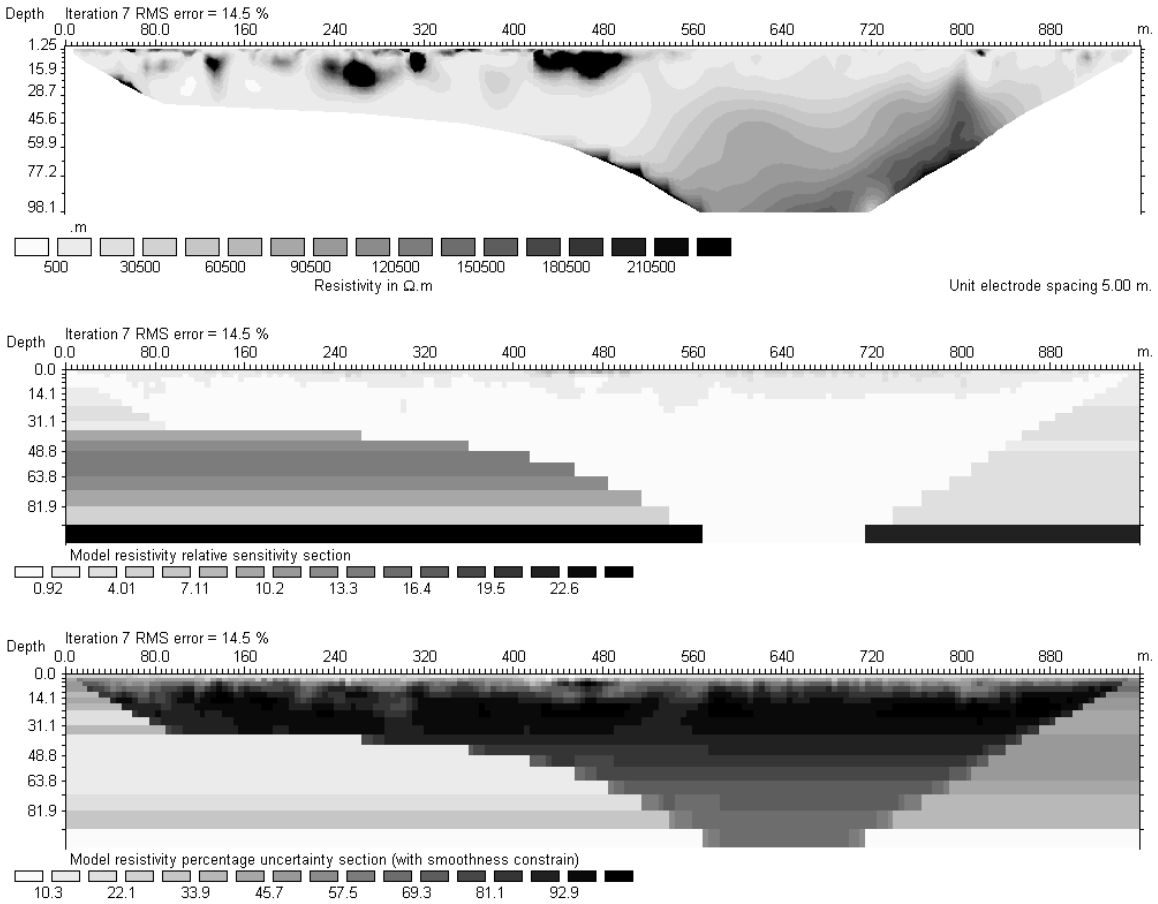

Figure B.1: The resistivity tomography transect model for the Victoria Valley data in comparison with sensitivity and uncertainty plots. Both vertical and horizontal scales are in metres.

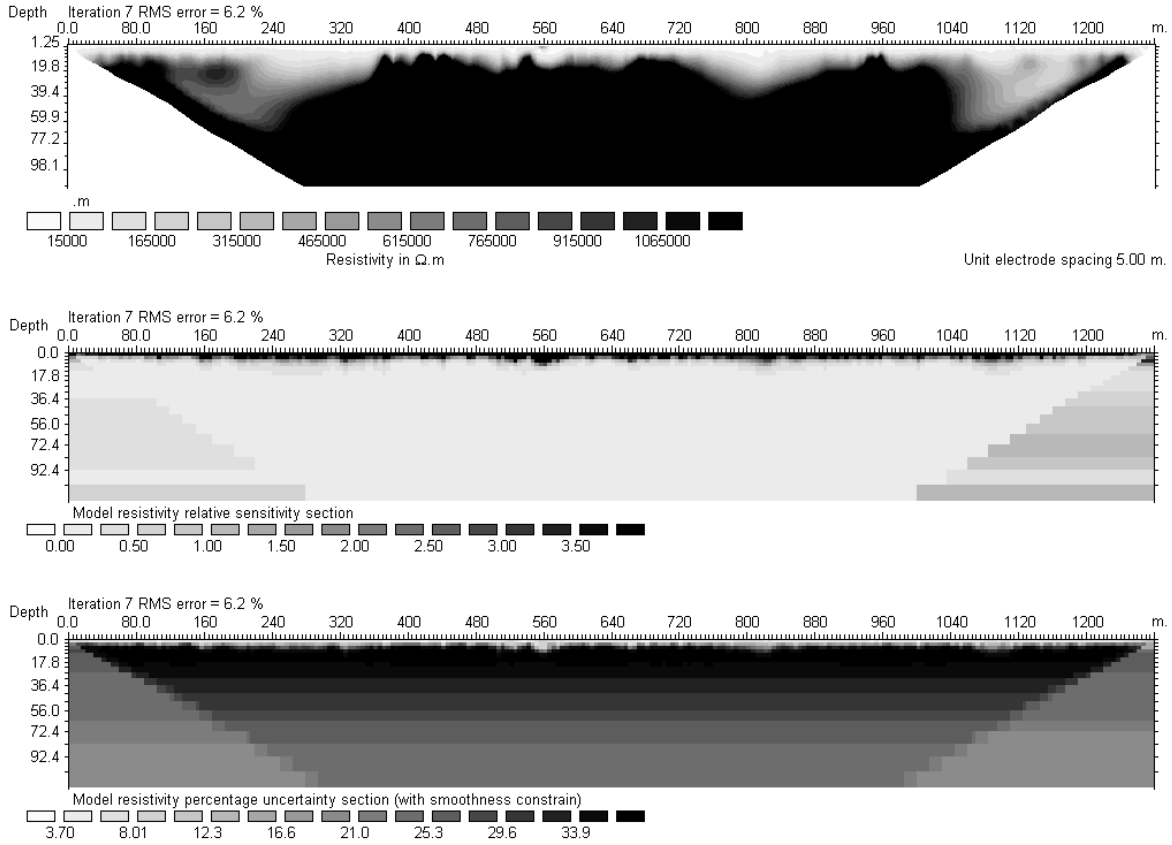

Figure B.2: The resistivity tomography transect model for the Beacon Valley data in comparison with the sensitivity and the uncertainty of the model.

B.2 Ground-penetrating radar: effects of processing

The individual measurement files were checked and the time zero made consistent for each data set. These files were then merged into a single long profile using the EKKO_Tools library's `merge` function, which successively overlaps files based on the start and end locations given in their headers. Topography was added as a two-column ASCII file of distance and elevation using `topo_add`. The topography-corrected file was slightly clipped to an appropriate time scale using `chopdata`.

Migration collapses diffraction curves formed by the combination of the slow lateral progression of the antennae over point reflectors in the ground and the outward propagation of the transmitted pulses. Standard migration (Fast Fourier Transform) was used, with some alteration from default parameters: `skip x`, the overlap for the taper, was set from 10 to 30, providing a 50% overlap, and `taper x` was set from 10 to 15, to help stop the "leak" of the Fourier transform (the Gibbs effect).

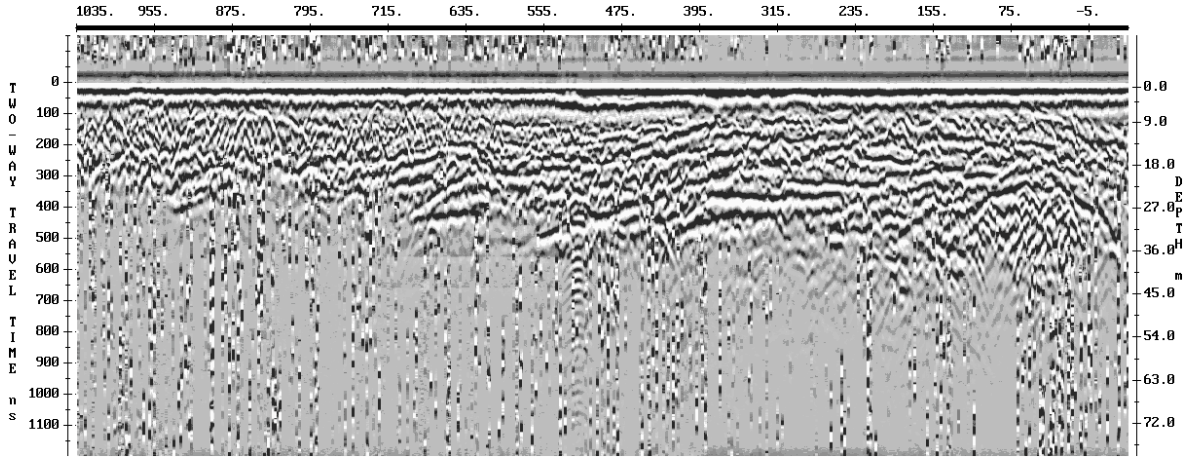

(a) Raw unfiltered transect profile.

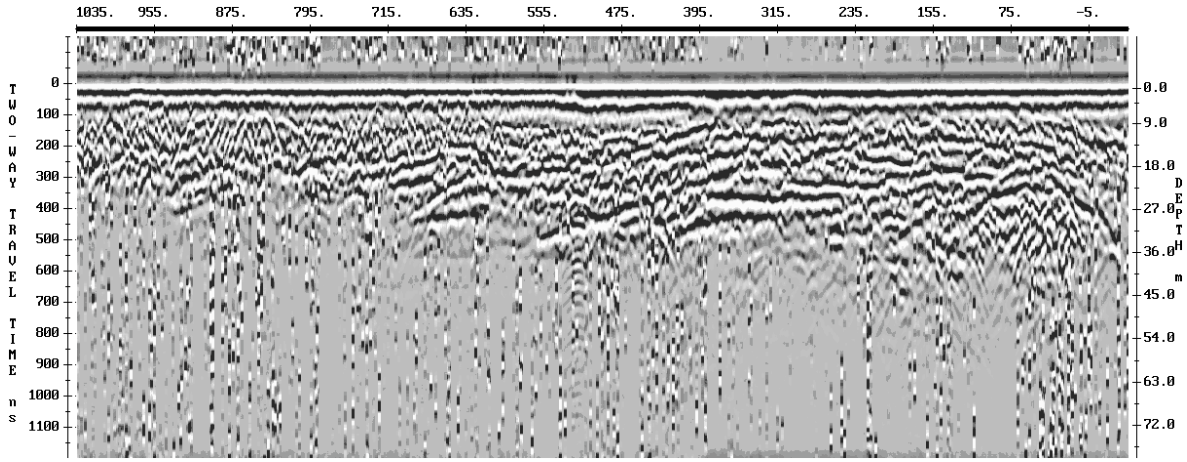

(b) Clipped profile filtered with a temporal 7-point alpha filter.

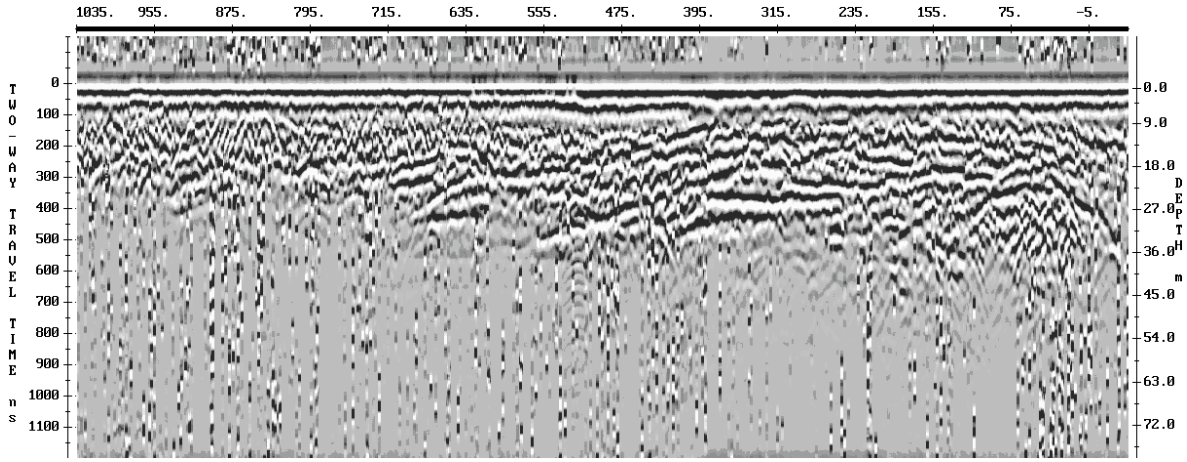

(c) Clipped profile filtered with a temporal 9-point alpha filter.

Figure B.3: Ground-penetrating radar profiles without topographic correction, showing the effects of filters, Victoria Valley. North-east, as before, is at left.

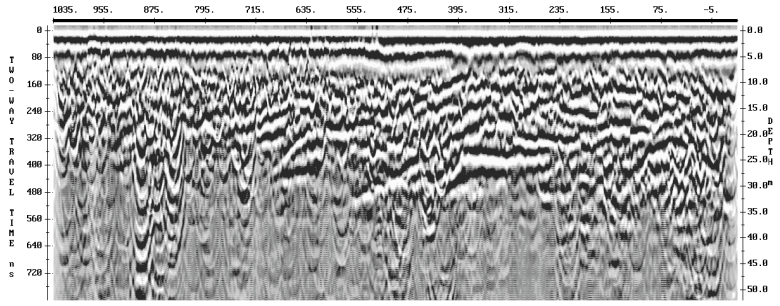

(a) Migration of filtered profile with velocity = 0.09 ns.

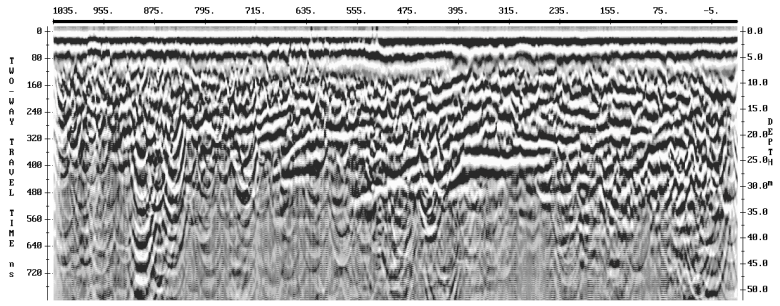

(b) Migration of filtered profile with velocity = 0.11 ns.

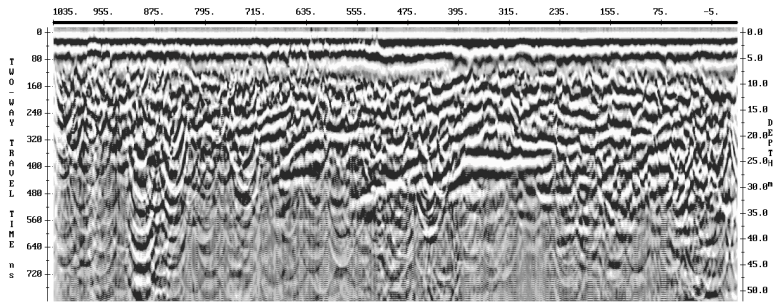

(c) Migration of filtered profile with velocity = 0.13 ns, as found by the CMP.

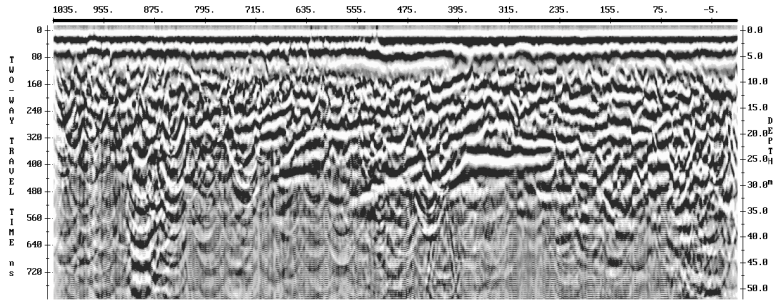

(d) Migration of filtered profile with velocity = 0.15 ns.

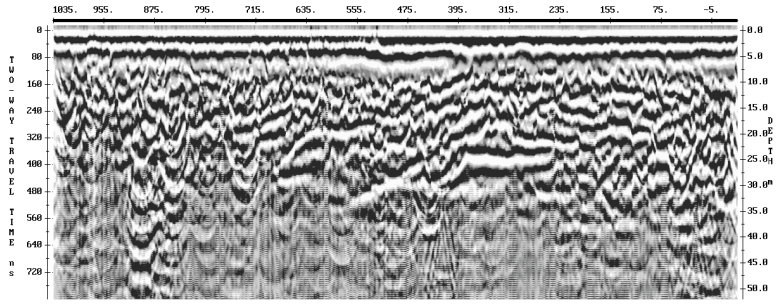

(e) Migration of filtered profile with velocity = 0.17 ns.

Figure B.4: Ground-penetrating radar profiles processed with different velocities, Victoria Valley.

B.3 Time-domain (transient) electromagnetism models

B.3.1 Smooth models

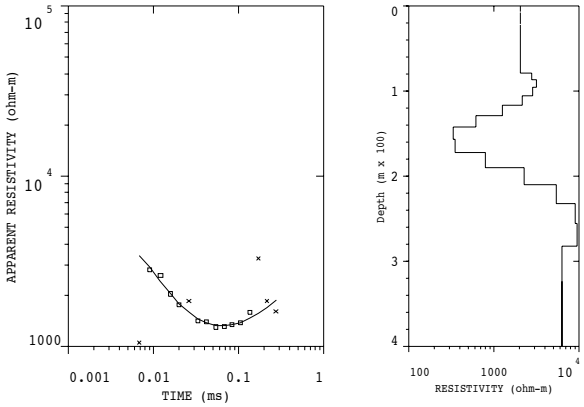

(a) High on hill slope (Site 7).

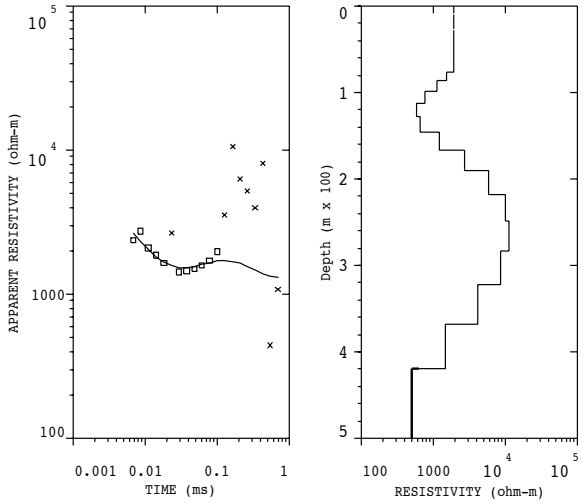

(b) On moraine material on hill slope (Site 6).

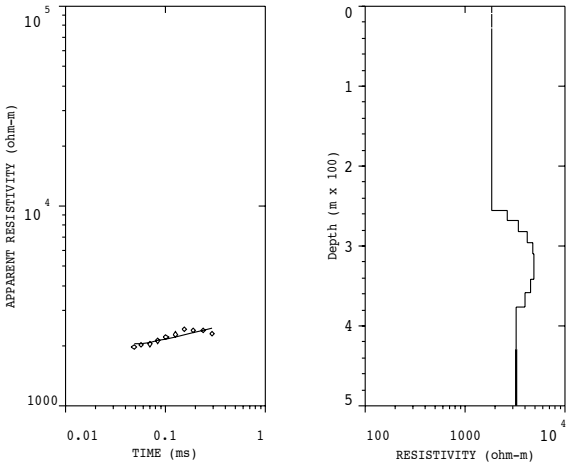

(c) On the young, flat, patterned ground (Site 1).

Figure B.5: Time-domain electromagnetism data sets from Victoria Valley with synthetic curve (left), and resulting one-dimensional layered earth smooth model (right). Data points masked from the modelling are indicated by crosses. Site locations are shown in Chapter 3 in Fig. 3.4.

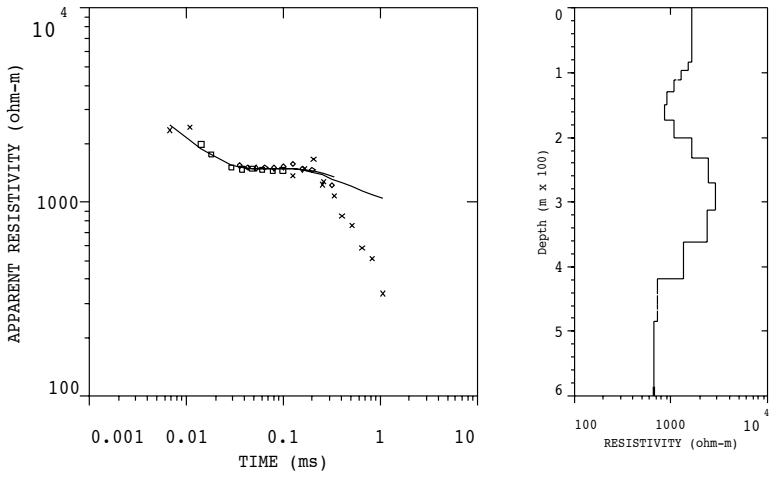

(a) Very flat polygons (Site 2).

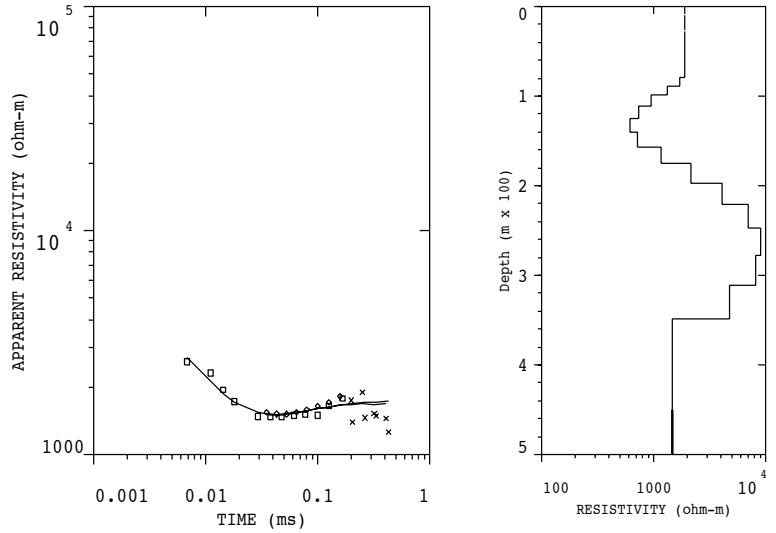

(b) Very flat polygons close to camp (Site 3). Overlaps Site 2 by 25%.

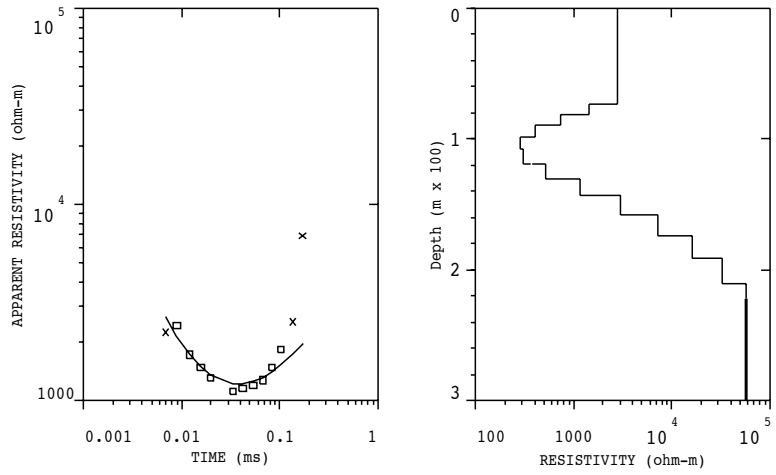

(c) Slightly raised polygons close to camp (Site 5).

Figure B.6: As for Fig. B.5, for sites 2, 3 and 5 (locations in Fig. 3.4).

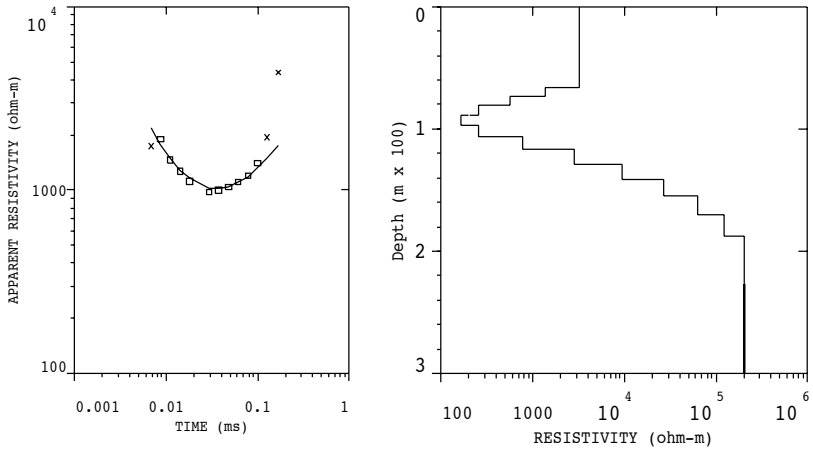

(a) Undulating moraine with polygons, bordered by the lake shore (Site 4).

Figure B.7: As for Fig. B.5, for site 4 (locations in Fig. 3.4).

The first step in the modelling was the calculation and viewing of the smooth model of the data. This approximate quasi-continuous model, produced by the `estimate (smooth model)` command, is an inversion using resistivity as the only parameter.

Layered models were chosen by defining the thickness (depth) and resistivity of several layers in the `interpret (interactive graphics)` data view. Forward modelling and single inversion iterations were made. Full inversion of satisfactory models was made using `invert`.

Equivalence analysis was then made using `equivalence`, which uses the parameter resolution matrix, `show resolution (matrix)`. These matrices are given in § B.3.3.

B.3.2 Model suite comparisons

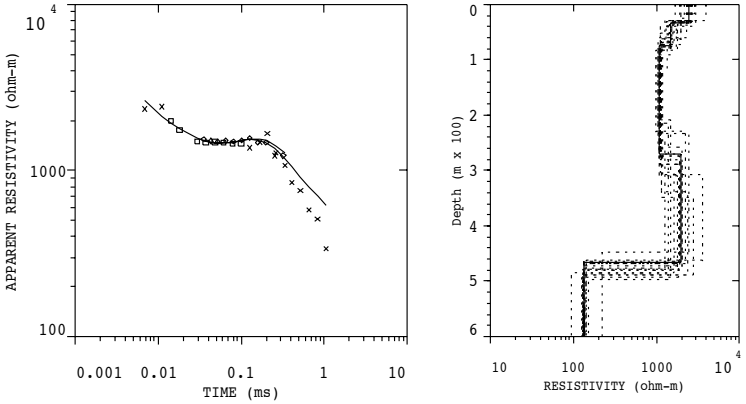

(a) Second modelling of location 2 for comparison. Crosses indicate masked data points. Fitting error 5.2%.

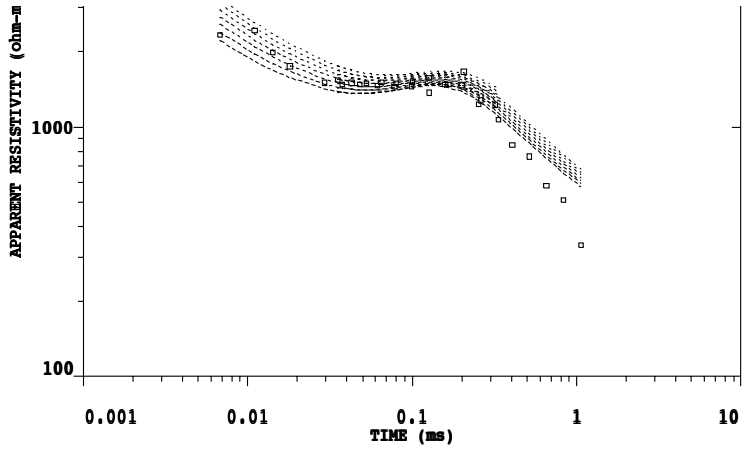

(b) Thickness of the layer closest to the surface varied by 10 m per step.

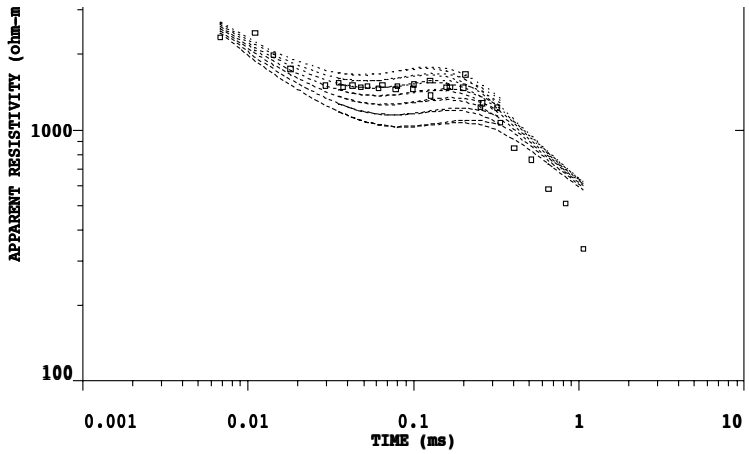

(c) Resistivity of the third layer varied by $100\Omega \cdot$ m per step.

Figure B.8: Comparison of model effectiveness with parameter variation. Time-domain electromagnetism data sets from Victoria Valley, location 2, with suites of synthetic curves indicated by dashed lines. The descent of the synthetic curve into the noise regime and the consequent loss of validity of the model with extreme parameter variation is apparent.

B.3.3 Models and their associated parameter resolution matrices

Layer	Resistivity ($\Omega \cdot$m)	Thickness (m)
1	424.9	16.8
2	2886.9	—

Table B.1: Model parameters, time-domain electromagnetism measurements, Site 1. Fitting error 3.2%.

	p1	p2	t1
p1	0.43		
p2	0.26	0.70	
t1	0.11	-0.18	0.56

Table B.2: Parameter resolution matrix, time-domain electromagnetism measurements, Site 1.

Layer	Resistivity ($\Omega \cdot$m)	Thickness (m)
1	1722.0	118.1
2	603.4	34.2
3	1408.5	319.6
4	132.7	—

Table B.3: Model parameters, time-domain electromagnetism measurements, Site 2, first model. Fitting error 3.4%.

	p1	p2	p3	p4	t1	t2	t3
p1	0.95						
p2	-0.02	0.59					
p3	0.02	0.11	0.88				
p4	0.01	0.05	-0.08	0.82			
t1	0.10	0.18	-0.10	-0.04	0.71		
t2	0.02	-0.33	-0.10	-0.05	0.00	0.22	
t3	-0.04	-0.05	0.07	0.04	0.12	0.10	0.93

Table B.4: Parameter resolution matrix, time-domain electromagnetism measurements, Site 2, first model.

Layer	Resistivity ($\Omega \cdot$ m)	Thickness (m)
1	2455.1	32.4
2	1495.0	41.9
3	1087.5	195.8
4	1960.6	195.4
5	134.0	—

Table B.5: Model parameters, time-domain electromagnetism measurements, Site 2, second model. Fitting error 3.6%.

	p1	p2	p3	p4	p5	t1	t2	t3	t4
p1	0.27								
p2	0.28	0.55							
p3	-0.02	0.03	0.98						
p4	0.03	-0.02	0.02	0.26					
p5	0.02	-0.02	0.01	-0.08	0.84				
t1	0.20	0.31	0.01	-0.02	0.00	0.24			
t2	0.05	0.15	0.03	-0.05	-0.02	0.12	0.10		
t3	-0.05	-0.01	-0.05	-0.20	0.08	0.09	0.16	0.66	
t4	0.00	-0.06	0.03	0.27	-0.03	0.02	0.03	0.26	0.73

Table B.6: Parameter resolution matrix for time-domain electromagnetism measurements, Site 2, second model.

Layer	Resistivity ($\Omega \cdot$ m)	Thickness (m)
1	2446.2	52.7
2	1446.0	18.4
3	979.1	109.2
4	2098.0	74.9
5	4422.9	—

Table B.7: Model parameters, time-domain electromagnetism measurements, Site 3. Fitting uncertainty 5.2%.

	p1	p2	p3	p4	p5	t1	t2	t3	t4
p1	0.31								
p2	0.12	0.15							
p3	0.03	0.07	0.90						
p4	0.04	-0.01	0.03	0.12					
p5	0.06	0.05	-0.05	0.04	0.88				
t1	0.35	0.13	0.07	-0.06	-0.01	0.60			
t2	0.04	0.01	0.02	-0.03	0.01	0.11	0.07		
t3	-0.06	0.01	-0.15	-0.25	-0.07	0.19	0.11	0.59	
t4	-0.04	-0.01	0.03	-0.07	-0.08	0.01	0.02	0.13	0.05

Table B.8: Parameter resolution matrix, time-domain electromagnetism measurements, Site 3.

Layer	Resistivity ($\Omega \cdot$m)	Thickness (m)
1	124617.0	61.8
2	7258.8	15.6
3	661.4	8.9
4	8.2	1.1
5	896.5	6.6
6	151866.0	—

Table B.9: Model parameters, time-domain electromagnetism measurements, Site 4. Fitting error 3.4%.

	p1	p2	p3	p4	p5	p6	t1	t2	t3	t4	t5
p1	0.16										
p2	-0.01	0.00									
p3	0.00	0.00	0.00								
p4	0.00	0.01	0.04	0.50							
p5	0.00	0.00	0.00	0.02	0.00						
p6	-0.01	0.00	0.00	0.00	0.00	0.00					
t1	0.01	0.00	0.01	0.03	0.00	0.00	0.92				
t2	-0.01	0.00	0.00	0.00	0.00	0.00	0.23	0.06			
t3	0.00	0.00	0.00	-0.04	0.00	0.00	0.12	0.03	0.02		
t4	0.00	-0.01	-0.04	-0.49	-0.02	0.00	0.01	0.01	0.05	0.50	
t5	0.00	0.00	0.00	-0.02	0.00	0.00	0.00	0.00	0.00	0.03	0.00

Table B.10: Parameter resolution matrix, time-domain electromagnetism measurements, Site 4.

Layer	Resistivity ($\Omega \cdot$ m)	Thickness (m)
1	758505.0	62.4
2	9138.4	23.7
3	1267.8	10.5
4	14.0	2.0
5	524837.0	—

Table B.11: Model parameters, time-domain electromagnetism measurements, Site 5. Fitting error 8.7%.

	p1	p2	p3	p4	p5	t1	t2	t3	t4
p1	0.00								
p2	0.00	0.00							
p3	0.00	0.00	0.00						
p4	0.00	0.01	0.03	0.51					
p5	0.00	0.00	0.00	0.00	0.00				
t1	0.00	0.01	0.01	0.03	0.00	0.85			
t2	0.00	0.00	0.00	0.01	0.00	0.31	0.13		
t3	0.00	0.00	0.00	-0.02	0.00	0.13	0.05	0.02	
t4	0.00	-0.01	-0.03	-0.49	0.00	0.02	0.01	0.03	0.50

Table B.12: Parameter resolution matrix, time-domain electromagnetism measurements, Site 5.

Layer	Resistivity ($\Omega \cdot$ m)	Thickness (m)
1	44835.2	5.3
2	2572.3	2.9
3	1547.0	133.8
4	29.8	2.0
5	191898.0	—

Table B.13: Model parameters, time-domain electromagnetism measurements, Site 6. Fitting error 10.0%.

	p1	p2	p3	p4	p5	t1	t2	t3	t4
p1	0.96								
p2	0.12	0.10							
p3	0.00	0.00	0.98						
p4	-0.01	-0.01	0.03	0.47					
p5	-0.01	0.01	0.00	0.02	0.05				
t1	-0.02	0.11	0.00	0.01	0.05	0.09			
t2	0.07	0.06	0.01	-0.01	-0.01	0.05	0.04		
t3	-0.01	0.00	0.02	-0.02	-0.02	0.00	0.03	0.97	
t4	0.00	-0.01	-0.02	-0.46	0.02	0.00	-0.01	0.03	0.51

Table B.14: Parameter resolution matrix, time-domain electromagnetism measurements, Site 6.

Layer	Resistivity ($\Omega \cdot$m)	Thickness (m)
1	2010.8	143.7
2	291.7	40.7
3	43987.0	—

Table B.15: Model parameters, time-domain electromagnetism measurements, Site 7. Fitting error 4.4%.

	p1	p2	p3	t1	t2
p1	0.99				
p2	-0.01	0.58			
p3	0.01	-0.01	0.03		
t1	0.01	0.08	-0.01	0.97	
t2	-0.02	-0.46	-0.03	0.09	0.48

Table B.16: Parameter resolution matrix, time-domain electromagnetism measurements, Site 7.

B.4 Magnetometer measurements and modelling

B.4.1 Victoria Valley modelling

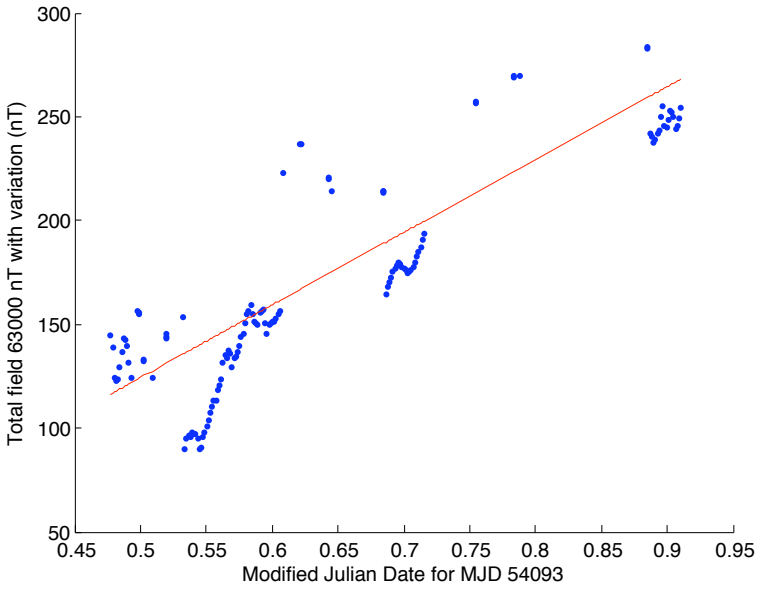

(a) Fitting of a linear model to base station data recorded on December 24, 2006, over the interval of the magnetometer survey.

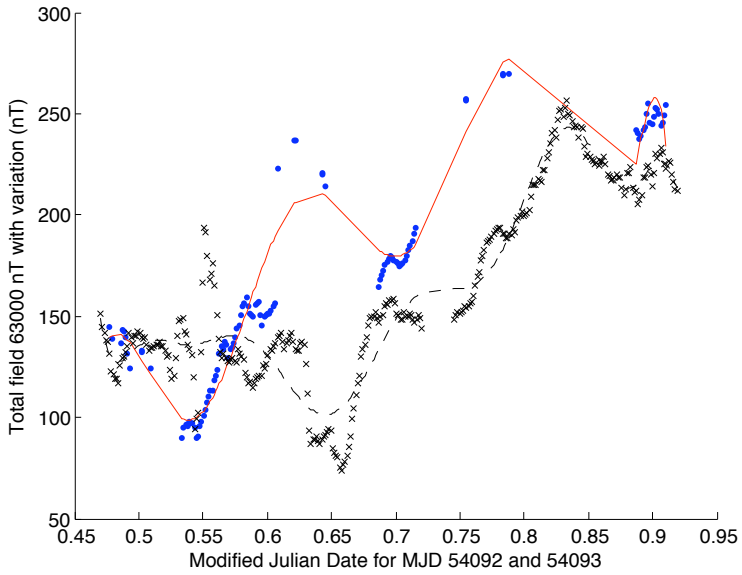

(b) Comparison of base station data recorded on December 24, 2006, over the interval of the magnetometer survey (dots) and over the same time period on the previous day, December 23 (crosses). A 13th-order polynomial modelling function is fitted to each data set.

Figure B.9: Modelling of Victoria Valley base station magnetometer data.

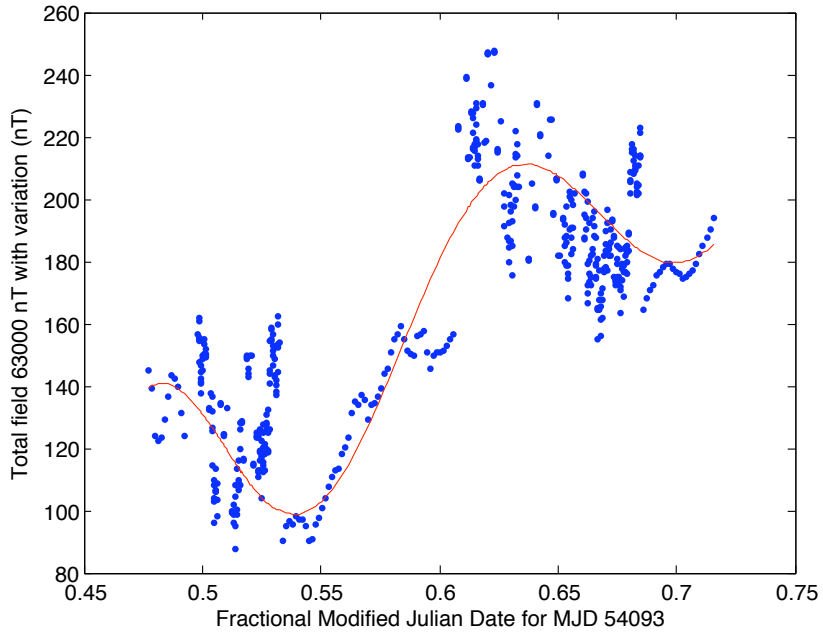

(a) The north-east leg of the transect.

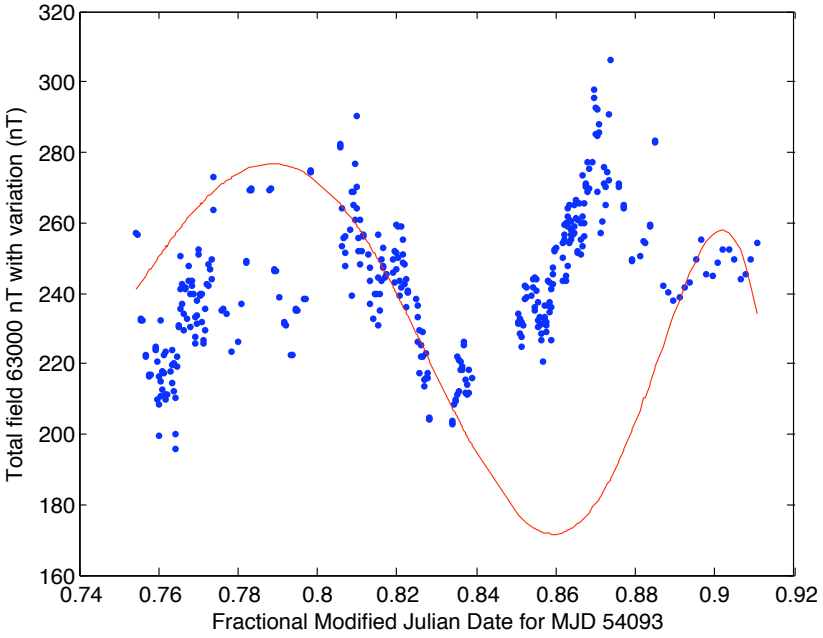

(b) The south-west leg of the transect.

Figure B.10: Model produced from base station measurements in comparison to survey data on December 24, 2006 in Victoria Valley.

B.4.2 Beacon Valley measurements

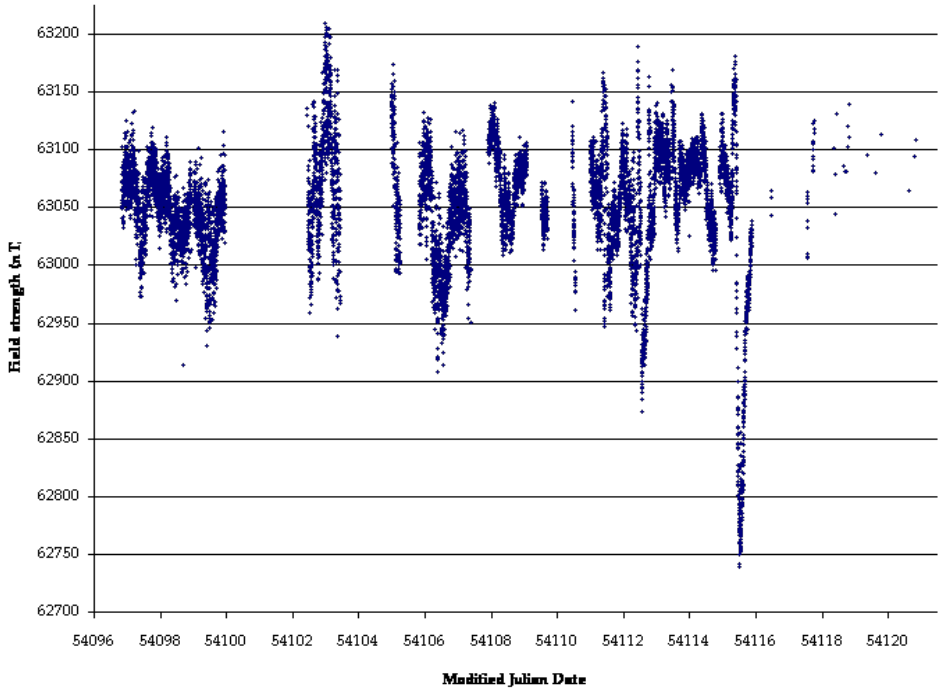

(a) Background record through time, 27 December 2006–20 January 2007.

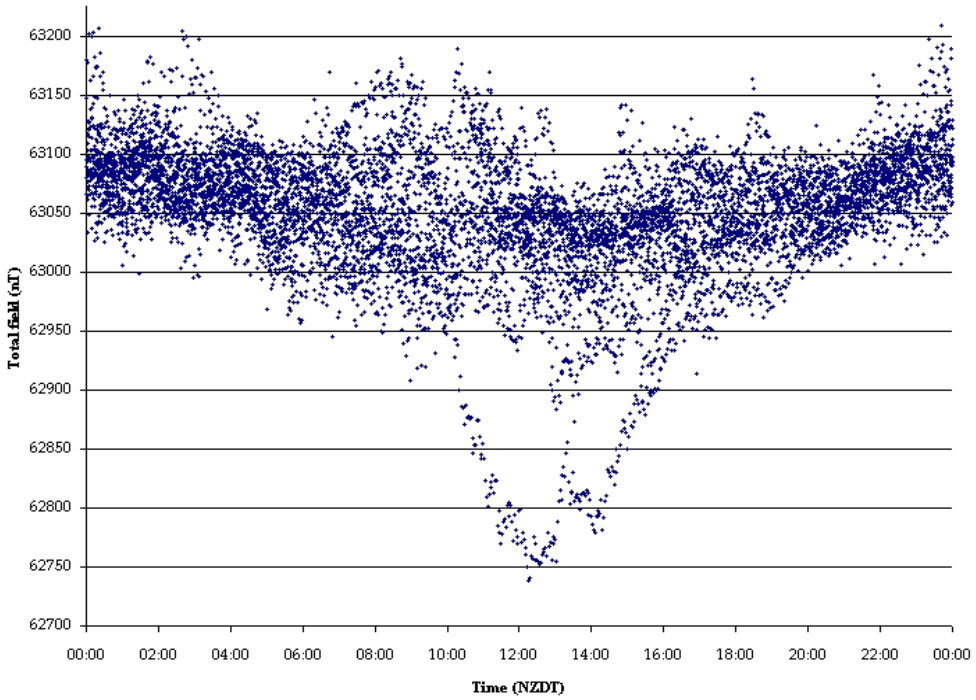

(b) Diurnal variation from all background measurements. The single severe dip corresponds to a solar flare, which is clearly visible as a spike of decrease in the field strength in Fig. B.11(a).

Figure B.11: Measurements made at the base station in Beacon Valley.

References

Allen, C. C., Morris, R. V., Lindstrom, D. J., Lindstrom, M. M., and Lockwood, J. P. (1997). JSC Mars-1 - Martian regolith simulant. In *Lunar and Planetary Institute Conference Abstracts*, volume 28 of *29th Annual Lunar and Planetary Institute Conference*, page 27. Abstract 1797.

Bandfield, J. L. (2007). High-resolution subsurface water-ice distributions on Mars. *Nature*, 447:64–67.

Belcher, D., Veverka, J., and Sagan, C. (1971). Mariner photography of Mars and aerial photography of Earth: Some analogies. *Icarus*, 15:241–252.

Berg, T. E. and Black, R. F. (1966). Preliminary measurements of growth of nonsorted polygons, Victoria Land, Antarctica. In Tedrow, J., editor, *Antarctic soils and soil forming processes*, volume 8 of *Antarctic Research Series*, pages 61–108. American Geophysical Union.

Berkley, J. L. and Drake, M. J. (1981). Weathering of Mars: Antarctic analog studies. *Icarus*, 45(1):231–249.

Black, R. F. (1973). Growth of patterned ground in Victoria Land, Antarctica. In *Permafrost: North American Contribution [to the] Second International Conference on Permafrost, Yakutsk,* U.S.S.R., pages 193–203, 2101 Constitution Avenue, Washington D.C., USA. National Academy of Sciences.

Black, R. F. (1982). Patterned-ground studies in Victoria Land. *Antarctic Journal of the United States*, 17:53–54.

Black, R. F. and Berg, T. E. (1963). Hydrothermal regimen of patterned ground, Victoria Land, Antarctica. Publication 61, International Association of Science, Hydrology Commission of Snow and Ice.

Bondesan, A., Meneghel, M., Salvatore, M., and Stenni, B. (1997). Non sorted polygons in the Terra Nova Bay area (Victoria Land, Antarctica). In Ricci, C. A., editor, *The Antarctic Region: Geological Evolution and Processes*, pages 957–963. Terra Antartica Publication, Siena, Italy.

Boynton, W., Feldman, W., Squyres, S., Prettyman, T., Bruckner, J., Evans, L., Reedy, R., Starr, R., Arnold, J., Drake, D., et al. (2002). Distribution of hydrogen in the near surface of Mars: Evidence for subsurface ice deposits. *Science*, 297(5578):81–85.

Bozzo, E. and Meloni, A. (1992). Geomagnetic anomaly maps of Central Victoria Land (East Antarctica) from ground measurements. *Tectonophysics*, 212(1–2):99–108.

Brook, E., Kurz, M., Ackert, J., Denton, G., Brown, E., Raisbeck, G., and Yiou, F. (1993). Chronology of Taylor Glacier advances in Arena Valley, Antarctica, using in situ cosmogenic ^{3}He and ^{10}Be. *Quaternary Research*, 39:11–23.

Bull, C. (1966). Climatological observations in ice free areas of Southern Victoria Land, Antarctica. Studies in Antarctic Meteorology: Antarctic Research Series 9, American Geophysical Union of the National Academy of Sciences – National Research Council.

Burr, D. M., Soare, R. J., Tseung, J.-M. W. B., and Emery, J. P. (2005). Young (late Amazonian), near-surface, ground ice features near the equator, Athabasca Valles, Mars. *Icarus*, 178:56–73.

Burt, D. and Knauth, L. (2003). Electrically conducting, Ca-rich brines, rather than water, expected in the Martian subsurface. *Journal of Geophysical Research*, 108:8026.

Calkin, P. (1964). Geomorphology and glacial geology of the Victoria Valley system, Southern Victoria Land, Antarctica. Report 10, Ohio State University, Institute of Polar Studies.

Carr, M. (1996a). Channels and valleys on Mars. *Planetary and Space Sciences*, 44(11):1411–1423.

Carr, M. and Schaber, G. (1977). Martian permafrost features. *Journal of Geophysical Research*, 28:4039–4054.

Carr, M. H. (1996b). *Water on Mars*. Oxford University Press, New York, New York, USA.

Cassidy, N. (2007). Attenuation and velocity characteristics of nano-to-micro scale magnetite mixtures implications for near-surface GPR. In *Near Surface 2007: Proceedings of the 13th European Meeting of Environmental and Engineering Geophysics*, Istanbul, Turkey. Paper A34.

Cereti, A., Vannaroni, G., Vento, D., and Pettinelli, E. (2007). Electromagnetic measurements on Martian soil analogs: Implications for MARSIS and SHARAD radars in detecting subsoil water. *Planetary and Space Science*, 55(1-2):193–202.

Chamberlain, M. and Boynton, W. (2007). Response of Martian ground ice to orbit-induced climate change. *Journal of Geophysical Research*, 112(E6):009.

Christensen, P., Bandfield, J., Bell III, J., Gorelick, N., Hamilton, V., Ivanov, A., Jakosky, B., Kieffer, H., Lane, M., Malin, M., et al. (2003). Morphology and composition of the surface of Mars: Mars Odyssey THEMIS results. *Science*, 300(5628):2056–2061.

Clark, B. (1979). Chemical and physical microenvironments at the Viking landing sites. *Journal of Molecular Evolution*, 14(1):13–31.

Clark, C. (1973). Geophysical studies of permafrost in the Dry Valleys. Master's thesis, Northern Illinois University.

Craddock, R. and Howard, A. (2002). The case for rainfall on a warm, wet early Mars. *Journal of Geophysical Research*, 107(E11):21.1–21.36.

Dahlin, T., Wisén, R., and Zhang, D. (2007). 3D effects on 2D resistivity imaging — modelling and field surveying results. In *Near Surface 2007: Proceedings of the 13th European Meeting of Environmental and Engineering Geophysics*, Istanbul, Turkey. Paper A15.

Daniels, J. (2000). Ground penetrating radar fundamentals. Appendix to a report to the US EPA, Region V, Department of Geological Sciences, The Ohio State University, Ohio, USA.

Danielsen, J., Auken, E., Jørgensen, F., Søndergaard, V., and Sørensen, K. (2003). The application of the transient electromagnetic method in hydrogeophysical surveys. *Journal of Applied Geophysics*, 53(4):181–198.

Davis, J. L. and Annan, A. P. (1989). Ground-penetrating radar for high-resolution mapping of soil and rock stratigraphy. *Geophysical Prospecting*, 37:531–551.

Davis, N. T. (2001). *Permafrost: a guide to frozen ground in transition*. University of Alaska Press, Fairbanks, Alaska.

De Carlo, E. and Green, W. (2002). Rare earth elements in the water column of Lake Vanda, McMurdo Dry Valleys, Antarctica. *Geochimica et Cosmochimica Acta*, 66(8):1323–1333.

Denton, G., Armstrong, R., and Stuiver, M. (1971). The late Cenozoic glacial history of Antarctica. In Turekian, K., editor, *The Late Cenozoic Glacial Ages*, pages 267–306. Yale University Press.

Dickinson, W. W. and Rosen, M. R. (2003). Antarctic permafrost: An analogue for water and diagenetic minerals on Mars. *Geology*, 31(3):199–202.

Dickson, J. L., Head, J. W., Kreslavsky, M. A., and Marchant, D. R. (2006). Linear lobate debris aprons, piedmont-like lobes, and crater fill in the Acheron Fossae graben region, Mars: Evidence for debris-covered glacier formation and flow. In Mackwell, S. and Stansbery, E., editors, *37th Annual Lunar and Planetary Science Conference*, page 1321.

Doran, P., McKay, C., Clow, G., Dana, G., Fountain, A., Nylen, T., and Lyons, W. (2002). Valley floor climate observations from the McMurdo dry valleys, Antarctica, 1986–2000. *Journal of Geophysical Research*, 107(D24):4772.

Farrell, W., Plaut, J., Gurnett, D., and Picardi, G. (2004). Mars Express MARSIS radar: A prediction of the effect of overlying ice on detecting polar basal lakes and inter-glacial aquifers. textscnasa Technical Memorandum 212749, NASA STI.

Feldman, W., Boynton, W., Tokar, R., Prettyman, T., Gasnault, O., Squyres, S., Elphic, R., Lawrence, D., Lawson, S., Maurice, S., et al. (2002). Global distribution of neutrons from Mars: results from Mars Odyssey. *Science*, 297(5578):75–78.

French, H. (1996). *The Periglacial Environment*. Addison-Wesley-Longman, Essex, United Kingdom, 2nd edition.

Frolov, A. D. (2003). A review of the nature and geophysical studies of the thick permafrost in Siberia: Relevance to exploration on Mars. *Journal of Geophysical Research*, 108(E4):8039.

Geotomo Software (2004). RES2DINV *v. 3.54: Geoelectrical imaging 2D & 3D*. Allied Associates Geophysical Limited, Dunstable, United Kingdom.

Gibson, E. K., Wentworth, S. J., and McKay, D. S. (1983). Chemical weathering and diagenesis of a cold desert soil from Wright Valley, Antarctica: An analog of martian weathering processes. *Journal of Geophysical Research*, 88:912–928.

Gonzalez, W., Joselyn, J., Kamide, Y., Kroehl, H., Rostoker, G., Tsurutani, B., and Vasyliunas, V. (1994). What is a geomagnetic storm? *Journal of Geophysical Research*, 99(A4):5771–5792.

Grant, J., Schutz, A., and Campbell, B. (2003). Ground penetrating radar as a tool for probing the shallow subsurface of Mars. *Journal of Geophysical Research*, 108(E4):8024–8039.

Greeley, R. (1994). *Planetary landscapes*. Chapman & Hall, New York, New York, USA, 2nd edition.

Greeley, R. and Iversen, J. (1985). *Wind as a geological process on Earth, Mars, Venus and Titan*. Cambridge University Press, Cambridge, United Kingdom.

Greeley, R., Lancaster, N., Lee, S., and Thomas, P. (1992). Martian æolian processes, sediments, and features. In Kieffer, H., Jakosky, B. M., Snyder, C. W., and Matthews, M. S., editors, *Mars*, pages 730–766. University of Arizona Press, Tucson, Arizona, USA.

Grimm, R. (2002). Low-frequency electromagnetic exploration for groundwater on Mars. *Journal of Geophysical Research*, 107(E2):5006–50037.

Grimm, R. (2003a). A comparison of time domain electromagnetic and surface nuclear magnetic resonance sounding for subsurface water on Mars. *Journal of Geophysical Research*, 108(E4):8037.

Grimm, R. (2003b). Comparison of ground-penetrating radar and low-frequency electromagnetic sounding for detection and characterization of groundwater on Mars. *Sixth International Conference on Mars*.

Guglielmin, M., Biasini, A., Dramis, F., and Smiraglia, C. (1997). Detection of permafrost and buried ice in ice-free areas of the Northern Victoria Land (Antarctica) with the Vertical Electrical Soundings (V.E.S). In Ricci, C. A., editor, *The Antarctic Region: Geological Evolution and Processes*, pages 965–971. Terra Antartica Publication, Siena, Italy.

Haeberli, W. (1985). *Creep of mountain permafrost: internal structure and flow of alpine rock glaciers*. Mitteilungen der Versuchsanstalt für Wasserbau, Hydrologie und Glaziologie an der Eidgenossischen Technischen Hochschule, Zürich.

Hartmann, W. and Neukum, G. (2001). Cratering chronology and the evolution of Mars. *Space Science Reviews*, 96(1):165–194.

Hauck, C., Vieira, G., Gruber, S., Blanco, J., and Ramos, M. (2007). Geophysical identification of permafrost in Livingston Island, maritime Antarctica. *Journal of Geophysical Research*, 112(F2):S19.

Hauck, C., Vonder Muhll, D., and Maurer, H. (2003). Using DC resistivity tomography to detect and characterize mountain permafrost. *Geophysical Prospecting*, 51(4):273–284.

Head, J., Marchant, D., Agnew, M., Fassett, C., and Kreslavsky, M. (2006). Extensive valley glacier deposits in the northern mid-latitudes of Mars: Evidence for Late Amazonian obliquity-driven climate change. *Earth and Planetary Science Letters*, 241:663–671.

Head, J., Mustard, J., Kreslavsky, M., Milliken, R., and Marchant, D. (2003). Recent ice ages on Mars. *Nature*, 426:797–802.

Head, J., Neukum, G., Jaumann, R., Hiesinger, H., Hauber, E., Carr, M., Masson, P., Foing, B., Hoffmann, H., Kreslavsky, M., Werner, S., Milkovich, S., van Gasselt, S., and the HRSC Co-Investigator Team (2005). Tropical to mid-latitude snow and ice accumulation, flow and glaciation on Mars. *Nature*, 434:346–351.

Head, J. W. (2001). Mars: Evidence for geologically recent advance of the south polar cap. *Journal of Geophysical Research*, 106(E5):10075–10085.

Helbert, J. and Benkhoff, J. (2006). Digging deep for ice in Isidis Planitia — New constraints on subsurface volatile concentrations from thermal modelling. *Planetary and Space Science*, 54(4):331–336.

Henriksen, M., Mangerud, J., Matiouchkov, A., Paus, A., and Svendsen, J. (2003). Lake stratigraphy implies an 80 000 yr delayed melting of buried dead ice in northern Russia. *Journal of Quaternary Science*, 18(7):663–679.

Holt, J., Blankenship, D., Morse, D., Young, D., Peters, M., Kempf, S., Richter, T., Vaughan, D., and Corr, H. (2006a). New boundary conditions for the West Antarctic Ice Sheet: Subglacial topography of the Thwaites and Smith glacier catchments. *Geophysical Research Letters*, 33(9).

Holt, J., Peters, M., Kempf, S., Morse, D., and Blankenship, D. (2006b). Echo source discrimination in single-pass airborne radar sounding data from the Dry Valleys, Antarctica: Implications for orbital sounding of Mars. *Journal of Geophysical Research*, 111(E6):S24.

Hornig, T., Sokolov, I., and Blumen, A. (1996). Patterns and scaling in surface fragmentation processes. *Physical Review E*, 54:4293–4298.

Hudson, T., Aharonson, O., Schorghofer, N., Farmer, C., Hecht, M., and Bridges, N. (2007). Water vapor diffusion in Mars subsurface environments. *Journal of Geophysical Research*, 112(E5):016.

Hughes, T. (1973). Glacial permafrost and Pleistocene. In *Permafrost: North American Contribution [to the] Second International Conference on Permafrost, Yakutsk,* U.S.S.R., pages 213–223, 2101 Constitution Avenue, Washington D.C., USA. National Academy of Sciences.

Hvidberg, C. S. (2005). Polar caps. In Tokano, T., editor, *Water on Mars and Life*, number 4 in Advances in Astrobiology and Biogeophysics, pages 129–152. Springer-Verlag Berlin Heidelberg, Germany.

Ingólfsson, Ó. and Lokrantz, H. (2003). Massive ground ice body of glacial origin at Yugorski Peninsula, arctic Russia. *Permafrost and Periglacial Processes*, 14(3):199–215.

Interpex Ltd. (1993). TEMIX *v 3.0 User's Manual: Transient Electromagnetic Data Interpretation Software*. Golden, Colorado, USA.

Jakosky, B. and Phillips, R. (2001). Mars' volatile and climate history. *Nature*, 412(6843):237–244.

Kelly, M., Denton, G., and Hall, B. (2002). Late Cenozoic paleoenvironment in southern Victoria Land, Antarctica, based on a polar glaciolacustrine deposit in western Victoria Valley. *Bulletin of the Geological Society of America*, 114:605–618.

Kelly, W. and Zumberge, J. (1961). Weathering of a quartz diorite at Marble Point, McMurdo Sound, Antarctica. *Journal of Geology*, 69:433–446.

Kieffer, H. H., Jakosky, B. M., Snyder, C. W., and Matthews, M. S. (1992). *Mars*. University of Arizona Press, Tucson, Arizona, USA.

Kirk, R., Barrett, J., and Soderblom, L. (2003). Photoclinometry made simple...? In ISPRS-ET *Working Group IV/9 Workshop "Advances in Planetary Mapping 2003"*. International Society for Photogrammetry and Remote Sensing, Houston, Texas, USA.

Klima, R. L. (2003). Distribution and morphology of small-scale patterned ground on Mars. Master's thesis, University of Illinois at Chicago.

Kossacki, K., Markiewicz, W., and Keller, H. (2001). Effect of surface roughness on ice distribution in the south subpolar region of Mars. *Planetary and Space Science*, 49(5):437–445.

Kowalewski, D. E., Marchant, D. R., Levy, J. S., and Head, J. W. (2006). Quantifying low rates of summertime sublimation for buried glacier ice in Beacon Valley, Antarctica. *Antarctic Science*, 18(3):421–428.

Kozhevnikov, N. and Antonov, E. (2006). Fast-decaying IP in frozen unconsolidated rocks and potentialities for its use in permafrost-related TEM studies. *Geophysical Prospecting*, 54(4):383–397.

Kuzmin, R. O. (2005). Ground ice in the Martian regolith. In Tokano, T., editor, *Water on Mars and Life*, number 4 in Advances in Astrobiology and Biogeophysics, pages 155–189. Springer-Verlag Berlin Heidelberg, Germany.

Lachenbruch, A. H. (1962). Mechanics of thermal contraction cracks and ice wedge polygons in permafrost. Special GSA paper 70, U.S. Geological Survey, Menlo Park, California, United States.

Lal, D. (1993). Cosmogenic and nucleogenic isotopic changes on Mars: their rates and implications to the evolutionary history of the Martian surface. *Geochimica et Cosmochimica Acta*, 57:4627–4637.

Lanagan, P., McEwen, A., Keszthelyi, L., and Thordarson, T. (2001). Rootless cones on Mars indicating the presence of shallow equatorial ground ice in recent times. *Geophysical Research Letters*, 28(12):2365–2367.

Laskar, J., Levrand, B., and Mustard, J. (2002). Orbital forcing of the Martian layered polar deposits. *Nature*, 419:375–377.

Leffingwell, E. (1919). The Canning River region, northern Alaska. Professional Paper 109, U.S. Geological Survey.

Leuschen, C., Kanagaratnam, P., Yoshikawa, K., Arcone, S., and Gogineni, P. (2003). Design and field experiments of a ground-penetrating radar for Mars exploration. *Journal of Geophysical Research*, 108:8034.

Levy, J. S., Head, III, J. W., and Marchant, D. R. (2005). The origin and evolution of oriented-network polygonally patterned ground: The Antarctic Dry Valleys as Mars analogue. In Mackwell, S. and Stansbery, E., editors, *36th Annual Lunar and Planetary Science Conference*, volume 36 of *Lunar and Planetary Institute Technical Report*, page 1334.

Loke, M. and Barker, R. (1995). Least-squares deconvolution of apparent resistivity pseudosections. *Geophysics*, 60:1682–1690.

Lucchitta, B. (1987). Valles Marineris, Mars: wet debris flows and ground ice. *Icarus*, 72(2):411–429.

Lucchitta, B. K. (1981). Mars and Earth: Comparison of cold-climate features. *Icarus*, 45(2):264–303.

Mackay, J. (2000). Thermally induced movements in polygons, western arctic coast: A long-term study. *Géographie Physique et Quaternaire*, 54:41–68.

Mackay, J. and Burn, C. (2002). The first 20 years (1978-1979 to 1998-1999) of ice-wedge growth at the Illisarvik experimental drained lake site, western Arctic coast, Canada. *Canadian Journal of Earth Sciences*, 39:95–111.

Malin, M. (1976). *Studies of the surface morphology of Mars*. PhD thesis, California Institute of Technology, Pasadena, California.

Malin, M. C. and Edgett, K. S. (2000a). Evidence for recent groundwater seepages and surface runoff on Mars. *Science*, 288(5475):2330–2335.

Malin, M. C. and Edgett, K. S. (2000b). Sedimentary rocks of early Mars. *Science*, 290:1927–1937.

Malin, M. C. and Rawine, M. (1995). Thirty years of measurements of sand wedge growth in lower Wright, Antarctica. *Antarctic Journal of the United States*, 29:19–20.

Malin Space Science Systems/NASA (1999). South Melea Planum, by the dawn's early light. Press release. MGS MOC Release Number MOC 2-126.

Mangold, N. (2003). Geomorphic analysis of lobate debris aprons on Mars at Mars Orbiter Camera scale: Evidence for ice sublimation initiated by fractures. *Journal of Geophysical Research*, 108(E4):8021.

Mangold, N. (2005). High latitude patterned grounds on Mars: Classification, distribution and climatic control. *Icarus*, 174:336–359.

Mangold, N., Forget, F., Costard, F., and Peulvast, J. (2002). High latitude patterned ground on Mars: Evidence for recent melting of near-surface ground ice. In *33rd Annual Lunar and Planetary Science Conference*. Lunar and Planetary Institute, Houston, USA.

Marchant, D., Lewis, A., Phillips, W., Moore, E., Souchez, R., Denton, G., Sugden, D., Potter Jr., N., and Landis, G. (2002). Formation of patterned ground and sublimation till over Miocene glacial ice in Beacon Valley, southern Victoria land, Antarctica. *Bulletin of the Geological Society of America*, 114(6):718–730.

Marchant, D. R., Head, J. W., and Kreslavsky, M. A. (2003). Tongue-shaped lobes on Mars: Relation to rock glacier deposits and long-term history of emplacement. In Clifford, S., Doran, P., Fisher, D., and Herd, C., editors, *Third International Conference on Mars Polar Science and Exploration*, page 8106.

McElroy, C. and Rose, G. (1987). Geology of the Beacon Heights area, southern Victoria Land, Antarctica, scale 1:50,000. New Zealand Geological Survey miscellaneous series map 15, Department of Scientific and Industrial Research, Wellington, New Zealand.

McGinnis, L. and Jensen, T. (1971). Permafrost-hydrogeologic regimen in two ice-free valleys, Antarctica, from electrical depth sounding. *Quaternary Research*, 1:389–409.

McGinnis, L., Nakao, L., and Clark, C. (1973). Geophysical identification of frozen and unfrozen ground, Antarctica. In *Permafrost: North American Contribution [to the] Second International*

Conference on Permafrost, Yakutsk, U.S.S.R., pages 136–146, 2101 Constitution Avenue, Washington D.C., USA. National Academy of Sciences.

McNeill, J. (1990). Use of electromagnetic methods for groundwater studies. In Ward, S., editor, *Geotechnical and Environmental Geophysics: Review and Tutorial*, volume 1, pages 191–218. The Society of Exploration Geophysicists, Tulsa, Oklahoma, USA.

Mellon, M., Jakosky, B., and Postawko, S. (1997). The persistence of equatorial ground ice on Mars. *Journal of Geophysical Research*, 102(E8):19357–19369.

Milliken, R., Mustard, J., and Goldsby, D. (2003). Viscous flow features on the surface of Mars: Observations from high-resolution Mars Orbiter Camera (MOC) images. *Journal of Geophysical Research*, 108(E6):5057.

Milsom, J. (2003). *Field Geophysics*. The Geological Field Guide Series. John Wiley and Sons, Chichester, United Kingdom, 3rd edition.

Moorman, B. J., Robinson, S. D., and Burgess, M. M. (2003). Imaging periglacial conditions with ground-penetrating radar. *Permafrost and Periglacial Processes*, 14:319–329.

Morris, E., Mutch, T., and Holt, H. (1972). Atlas of geologic features in the Dry Valleys of South Victoria Land, Antarctica: possible analogs of Martian surface features. Interagency Report: Astrogeology 52, United States Department of the Interior Geological Survey, for the National Aeronautics and Space Administration.

Murton, J. and French, H. (1993). Thaw modification of frost-fissure wedges, Richards Island, Pleistocene Mackenzie Delta, western Arctic Canada. *Journal of Quaternary Science*, 8(3):185–196.

Murton, J., Worsley, P., and Gozdzik, J. (2000). Sand veins and wedges in cold æolian environments. *Quaternary Science Reviews*, 19(9):899–922.

Mustard, J., Cooper, C., and Rifkin, M. (2001). Evidence for recent climate change on Mars from the identification of youthful near-surface ground ice. *Nature*, 412(6845):411–414.

Nabighian, M. N. (1979). Quasi-static transient response of a conducting half-space — an approximate representation. *Geophysics*, 44(10):1700–1705.

Neal, J., Langer, A., and Kerr, P. (1968). Giant dessication polygons of great basin playas. *Bulletin of the Geological Society of America*, 79:69–90.

Ng, F., Hallet, B., Sletten, R. S., and Stone, J. O. (2005). Fast-growing till over ancient ice in Beacon Valley, Antarctica. *Geology*, 33(2):121–124.

Ono, T. and Oya, H. (2000). Lunar Radar Sounder (LRS) experiment on-board the SELENE spacecraft. *Earth Planets Space*, 52(9):629–637.

Ori, G. and Ogliani, F. (1996). Potentiality of the ground-penetrating radar for the analysis of the stratigraphy and sedimentology of Mars. *Planetary and Space Science*, 44:1303–1315.

Parsons, R. L. and Head, III, J. W. (2005). Ascraeus Mons fan-shaped deposit, Mars: Geological history and volcano-ice interactions of a cold-based glacier. In Mackwell, S. and Stansbery, E., editors, *36th Annual Lunar and Planetary Science Conference*, page 1139.

Pechmann, J. (1980). The origin of polygonal troughs on the Northern Plains of Mars. *Icarus*, 42:185–210.

Pewe, T. (1974). Geomorphic processes in polar deserts. In Smiley, T. and Zumberge, J., editors, *Polar Deserts and Modern Man*. University of Arizona.

Péwé, T. L. (1959). Sand-wedge polygons (tesselations) in the McMurdo Sound region, Antarctica — A progress report. *American Journal of Sciences*, 257:545–552.

Phillips, R., Adams, G., Brown Jr, W., Eggleton, R., Jackson, P., Jordan, R., Linlor, W., Peeples, W., Porceello, L., Ryu, J., et al. (1973). Apollo lunar sounder experiment. Special Publication: Apollo 17: Preliminary Science Report. 330, NASA, Washington, D.C., USA.

Picardi, G., Biccari, D., Seu, R., Marinangeli, L., Johnson, W., Jordan, R., Plaut, J., Safaenili, A., Gurnett, D., and Ori, G. (2004). Performance and surface scattering models for the Mars Advanced Radar for Subsurface and Ionosphere Sounding(MARSIS). *Planetary and Space Science*, 52(1):149–156.

Pierce, T. L. and Crown, D. A. (2003). Morphologic and topographic analyses of debris aprons in the eastern Hellas region, Mars. *Icarus*, 163:46–65.

Read, P. and Lewis, S. (2004). *The Martian Climate Revisited: atmosphere and environment of a desert planet*. Praxis (Springer), Chichester, United Kingdom.

Robinson, E. (1963). Geophysical investigations in McMurdo Sound, Antarctica. *Journal of Geophysical Research*, 68:257–262.

Rossbacher, L. A. and Judson, S. (1981). Ground ice on Mars: Inventory, distribution and resulting landforms. *Icarus*, 45(1):39–59.

Rossi, A. P., Komatsu, G., and Kargel, J. S. (2000). Rock glacier-like landforms in Valles Marineris, Mars. In *Lunar and Planetary Institute Conference Abstracts*, page 1587.

Röthlisberger, H. (1967). Electrical resistivity measurements and soundings on glaciers: introductory remarks. *Journal of Glaciology*, 6(47):599–606.

Schäfer, J. M., Baur, H., Denton, G. H., Ivy-Ochs, S., Marchant, D. R., Schlüchter, C., and Wieler, R. (2000). The oldest ice on Earth in Beacon Valley, Antarctica: new evidence from surface exposure dating. *Earth and Planetary Science Letters*, 179:91–99.

Schorghofer, N. (2005). A physical mechanism for long-term survival of ground ice in Beacon Valley, Antarctica. *Geophysical Reserve Letters*, 32:L19503.

Schorghofer, N. and Aharonson, O. (2005). Stability and exchange of subsurface ice on Mars. *Journal of Geophysical Research*, 110(E5):3.

Seibert, N. and Kargel, J. (2001). Small-scale Martian polygonal terrain: implications for liquid surface water. *Geophysical Research Letters*, 28(5):899–902.

Sensors and Software (1996). *pulse*EKKO IV *Run Version 4.2: User's Guide*. 1091 Brevik Place, Mississauga, Ontario, Canada. Technical Manual 20.

Seu, R., Phillips, R., Biccari, D., Orosei, R., Masdea, A., Picardi, G., Safaeinili, A., Campbell, B., Plaut, J., Marinangeli, L., et al. (2007). SHARAD sounding radar on the Mars Reconnaissance Orbiter. *Journal of Geophysical Research*, 112(E5).

Skorov, Y., Markiewicz, W., Basilevsky, A., and Keller, H. (2001). Stability of water ice under a porous nonvolatile layer: implications to the south polar layered deposits of Mars. *Planetary and Space Science*, 49(1):59–63.

Sletten, R. S., Hallet, B., and Fletcher, R. C. (2003). Resurfacing time of terrestrial surfaces by the formation and maturation of polygonal patterned ground. *Journal of Geophysical Research*, 108(E4):8044.

Stone, J., Sletten, R. S., and Hallet, B. (2000). Old ice, going fast: cosmogenic isotope measurements on ice beneath the floor of Beacon Valley, Antarctica. In *Eos: Transactions of the American Geophysical Union. Fall Meeting Supplement*, volume 81(48). Abstract H52C–21.

Sugden, D. E., Marchant, D. R., Jr., N. P., Souchez, R. A., Denton, G. H., III, C. C. S., and Tison, J.-L. (1995). Preservation of Miocene glacier ice in East Antarctica. *Nature*, 376:412–414.

Svensson, H., Kallander, H., Maack, A., and Ohrngren, S. (1967). Polygonal ground and solifluction features: photographic interpretation and field studies in Northernmost Scandinavia. Lund Studies in Geography: Series A Physical Geography, No. 40, Department of Geography, the Royal University of Lund, Sweden.

Szalai, S., Koppán, A., and Szarka, L. (2007). Effect of positional inaccuracies on multielectrode results. In *Near Surface 2007: Proceedings of the 13th European Meeting of Environmental and Engineering Geophysics*, Istanbul, Turkey. Paper P28.

Tedrow, J. and Ugolini, F. (1966). Antarctic soils. In Tedrow, J., editor, *Antarctic soils and soil forming processes*, volume 8 of *Antarctic Research Series*, pages 61–108. American Geophysical Union.

EG&G Geometrics (1992). *Model G-856 Proton Precession Magnetometer: Operator's Manual*. EG&G Geometrics, 395 Java Drive, Sunnyvale, California, USA.

Tokano, T. (2005). Water cycle in the atmosphere and shallow subsurface. In Tokano, T., editor, *Water on Mars and Life*, number 4 in Advances in Astrobiology and Biogeophysics, pages 191–216. Springer-Verlag Berlin Heidelberg, Germany.

Turnbull, I., Allibone, A., Forsyth, P., and Heron, D. (1994). Geology of the Bull Pass-St Johns Range area, southern Victoria Land, Antarctica, scale 1:50,000. Institute of Geological and Nuclear Sciences geological map 14, Institute of Geological and Nuclear Sciences, Lower Hutt, New Zealand.

Ugolini, F., Bockheim, J., and Anderson, D. M. (1973). Soil development and patterned ground evolution in Beacon Valley, Antarctica. In *Permafrost: North American Contribution [to the] Second International Conference on Permafrost, Yakutsk,* U.S.S.R., pages 246–254, 2101 Constitution Avenue, Washington D.C., USA. National Academy of Sciences.

van der Wateren, D. and Hindmarsh, R. (1995). Stabilists strike again. *Nature*, 376(6539):389–391.

Wade, F. A. and de Wys, J. N. (1968). Permafrost features on the Martian surface. *Icarus*, 9(1):175–185.

Wall, S. (1981). Analysis of condensates formed at the Viking 2 lander site: the first winter. *Icarus*, 47:173–181.

Washburn, A. (1956). Classifications of patterned ground and review of suggested origins. *Bulletin of the Geological Society of America*, 67:823–866.

Washburn, A. (1973). *Periglacial Processes and Environments*. Edward Arnold Publishers, London, United Kingdom.

Watters, T. R., Leuschen, C. J., Plaut, J. J., Picardi, G., Safaeinili, A., Clifford, S. M., Farrell, W. M., Ivanov, A. B., Phillips, R. J., and Stofan, E. R. (2006). MARSIS radar sounder evidence of buried basins in the northern lowlands of Mars. *Nature*, 444(7121):905–908.

Yoshikawa, K., Leuschen, C., Ikeda, A., Harada, K., Gogineni, P., Hoekstra, P., Hinzman, L., Sawada, Y., and Matsuoka, N. (2006). Comparison of geophysical investigations for detection of massive ground ice (pingo ice). *Journal of Geophysical Research*, 111(E6):S19.

Zwartz, D. (2005). Resistivity soundings in Victoria and Beacon Valleys, Antarctica. Antarctic Data Series No 31, Antarctic Research Centre, Victoria University of Wellington.